

PDF hosted at the Radboud Repository of the Radboud University Nijmegen

The following full text is a publisher's version.

For additional information about this publication click this link.

<http://hdl.handle.net/2066/157655>

Please be advised that this information was generated on 2017-12-05 and may be subject to change.

MRI guided TRUS prostate biopsy – a viable alternative?

Wendy van de Ven

COLOPHON

This book was typeset using L^AT_EX₂ ϵ .

Layout design by Wendy van de Ven, template modified from LaTeXTemplates.com.

Cover design by Rick Wingens (Wingens Webdesign).

Copyright © 2016 by Wendy van de Ven, Nijmegen, The Netherlands. All rights reserved.
No part of this publication may be reproduced or transmitted in any form or by any means, electronic or mechanical, including photocopy, recording, or any information storage and retrieval system, without permission in writing from the author.

ISBN 978-94-028-0172-9

Printed by Ipskamp Drukkers, Nijmegen, The Netherlands.

MRI guided TRUS prostate biopsy – a viable alternative?

PROEFSCHRIFT

TER VERKRIJGING VAN DE GRAAD VAN DOCTOR AAN DE RADBOUD UNIVERSITEIT
NIJMEGEN OP GEZAG VAN DE RECTOR MAGNIFICUS, VOLGENS BESLUIT VAN HET
COLLEGE VAN DECANEN IN HET OPENBAAR TE VERDEDIGEN OP MAANDAG 4 JULI 2016
OM 10.30 UUR PRECIES

DOOR

Wendy Johanna Martina van de Ven

GEBOREN OP 3 JUNI 1987 TE OSS

Promotoren: **Prof. dr. ir. N. Karssemeijer**
Prof. dr. J. O. Barentsz

Copromotor: **Dr. ir. H. J. Huisman**

Manuscriptcommissie: **Prof. dr. P. F. A. Mulders**
Prof. dr. ir. C. H. Slump
Universiteit Twente
Dr. D. M. Somford
Canisius-Wilhelmina Ziekenhuis

The research described in this thesis was carried out at the Diagnostic Image Analysis Group, Radboud University Medical Center (Nijmegen, The Netherlands).
This work was funded by grant **KUN 2007-3971** of the Dutch Cancer Society.

Financial support for publication of this thesis was kindly provided by the department of Radiology and Nuclear Medicine of the Radboud University Medical Center, Nijmegen, The Netherlands.

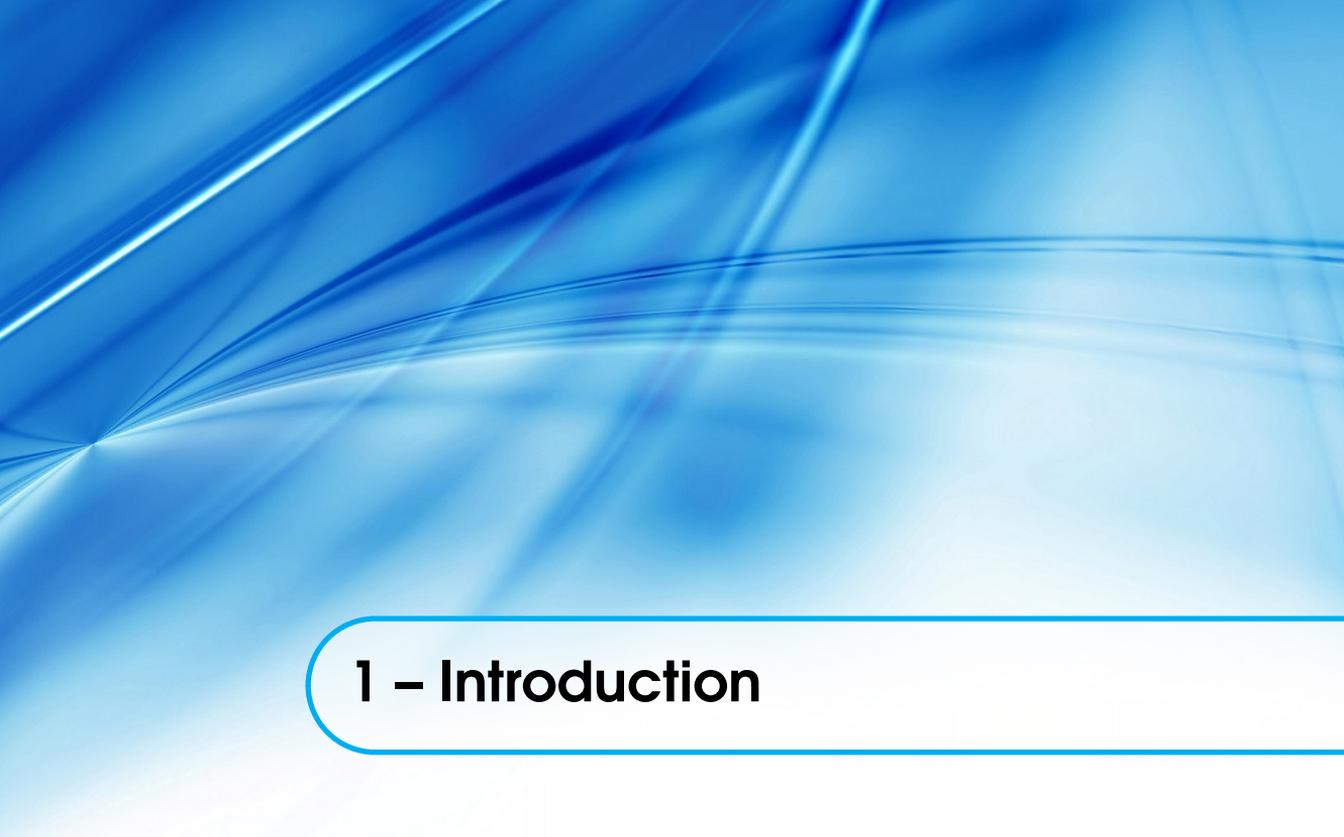


Contents

1	Introduction	1
1.1	Prostate anatomy	3
1.2	Prostate cancer epidemiology	4
1.3	Prostate cancer diagnosis in current clinical practice	4
1.3.1	Ultrasound guided biopsy	6
1.3.2	Gleason grading of prostate cancer	8
1.3.3	Treatment options	10
1.4	Prostate cancer screening	10
1.5	Drawbacks of current practice	11
1.6	MR imaging of the prostate	12
1.6.1	Prostate cancer diagnosis on MRI	14
1.6.2	MR guided biopsy	16
1.7	MR-TRUS fusion	17
1.7.1	Cognitive fusion	17
1.7.2	Computational fusion	17
1.7.3	Clinical MR-TRUS fusion systems	19
1.8	Outline of this thesis	21
2	A viable alternative?	25
3	Required registration accuracy	31
3.1	Introduction	33
3.2	Materials and methods	34
3.2.1	Patients	34
3.2.2	MR imaging protocol	34
3.2.3	Histopathology	35
3.2.4	MR tumour annotation	35
3.2.5	Focal volume segmentation	35
3.2.6	Registration accuracy and hit-rate	37
3.2.7	Statistical analysis	37
3.3	Results	38
3.3.1	Proportion and volume of tumour foci	38
3.3.2	Required registration accuracy	39
3.4	Discussion	40

4	MR-MR registration	43
4.1	Introduction	45
4.2	Methods	45
4.2.1	Patient data	46
4.2.2	Biomechanical modeling	46
4.2.3	Surface-based registration	47
4.2.4	Registration accuracy	48
4.3	Results	48
4.4	Conclusion	48
5	MR-TRUS registration	51
5.1	Introduction	53
5.2	Materials and methods	55
5.2.1	Overview	55
5.2.2	Data collection	56
5.2.3	Segmentation	56
5.2.4	Preprocessing	57
5.2.5	Rigid registration	57
5.2.6	Meshing	57
5.2.7	Radial surface projection	58
5.2.8	Biomechanical modeling	59
5.2.9	Non-rigid surface-based registration	60
5.2.10	Evaluation	60
5.3	Results	62
5.4	Discussion	64
5.5	Conclusions	68
6	Cancer visibility on TRUS	69
6.1	Introduction	71
6.2	Patients and methods	72
6.2.1	Patient selection	72
6.2.2	MR imaging	72
6.2.3	TRUS imaging	72
6.2.4	Histopathology	72
6.2.5	Observer experiment	73
6.2.6	Data analysis	73

6.3	Results	75
6.4	Discussion	77
7	MR-TRUS fusion biopsy	81
7.1	Introduction	83
7.2	Patients and methods	84
7.2.1	Patient population	84
7.2.2	Multi-parametric magnetic resonance imaging	84
7.2.3	Biopsy procedure	84
7.2.4	Histopathology	85
7.2.5	Biopsy evaluation	85
7.2.6	Data analysis	87
7.3	Results	87
7.4	Discussion	89
8	Summary & Discussion	93
8.1	Summary	95
8.2	General discussion	97
8.3	Future perspectives	100
8.4	Closing remarks	101
	APPENDICES	102
	Nederlandse samenvatting	105
	Bibliography	110
	Publications	125
	Dankwoord	131
	Curriculum Vitae	135



1 – Introduction

1.1 Prostate anatomy

The prostate is a small gland situated in the pelvic cavity and is part of the male reproductive system. It is located between the pelvic bones, below the bladder and in front of the rectum (Figure 1.1).¹ In healthy males, the prostate is about the size of a chestnut and somewhat conical in shape. Its body is partly glandular and partly muscular. The gland is perforated by the urethra, originating in the bladder, and the two ejaculatory ducts, originating at the seminal vesicles. The prostate plays a role in normal sexual functioning. It secretes an alkaline fluid, which is added to the spermatozoa and the seminal vesicle fluid, increasing the motility and lifespan of the sperm. Smooth muscles in the prostate help expel semen during ejaculation.

The prostate can be divided into three different anatomical zones: the peripheral zone, transition zone, and central zone (Figure 1.2).² The central zone surrounds the ejaculatory ducts at the base of the prostate and comprises 25% of glandular tissue in a healthy prostate. Approximately 2.5% of prostate cancers originate in this zone.³ The transition zone surrounds the proximal urethra and contains around 5% of the glandular tissue. As individuals age, the transition zone grows substantially in size as the result of benign prostatic hyperplasia (BPH). This is a benign enlargement of the prostate and pushes the central gland away increasing pressure on the urethra. About 10 – 20% of cancers are found here. Lastly, the peripheral zone is located posterolateral and encompasses the majority of prostatic glandular tissue (up to 70% of tissue in a healthy prostate). Approximately 70 – 80% of all prostate cancers arise in this zone. In addition to these glandular zones, the prostate usually contains an area of fibromuscular stroma. This area is usually devoid of glandular components and is composed of only muscle and fibrous tissue.

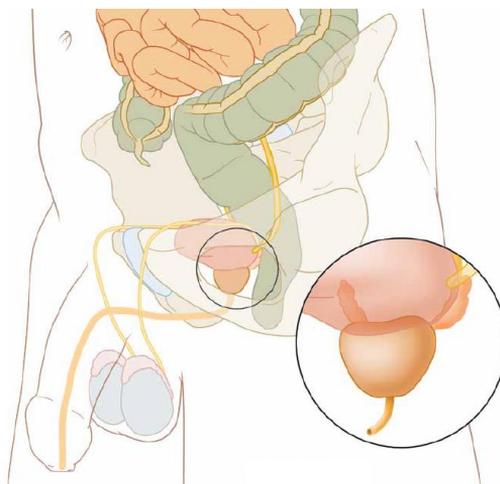


Figure 1.1: Anatomical image of the male pelvis showing the position of the prostate, which is located immediately under the bladder.

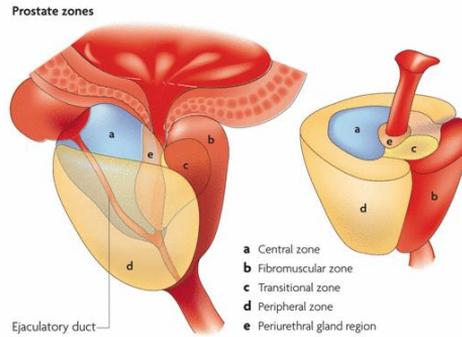


Figure 1.2: The zonal anatomy of the prostate. In addition to the three anatomical zones (peripheral zone, transition zone, and central zone) the prostate contains an area of fibromuscular stroma and a periurethral gland region (area around the urethra). Image obtained from De Marzo *et al.*⁴

1.2 Prostate cancer epidemiology

On a global level, prostate cancer is the most frequently diagnosed cancer in males, and one of the leading causes of death from cancer.^{5–7} Almost 75% of prostate cancer cases are diagnosed in developed countries.⁸ The main reasons for this are the higher average age of the general population in developed countries compared to developing countries, and secondly, the introduction of prostate specific antigen (PSA) blood tests in developed countries (Section 1.3).

About one man in six is affected by the disease during his lifetime,⁷ and about 3% will die of it.^{9–11} In the USA, the estimated number of newly diagnosed prostate cancers is slightly over 230,000 cases and almost 30,000 men will die from it yearly (Figure 1.3).^{7,12} In the Netherlands, these yearly numbers are approximately 11,000 new cases, and about 2,500 deaths.¹³ The main reason for this high incidence-to-mortality ratio is that most of the prostate cancers found are indolent, i.e. will not cause death. This is evidenced by both the high 10-year survival rate (77%), as well as the incidence of prostate cancer on autopsy in men who died of other causes.¹⁴

Prostate cancer has been known as a disease of elderly men. Autopsy studies have revealed that about 30% of men at age 50 have prostate cancer, at age 80 this increases to about 80%.^{10,11,15} However, only about 30% of the detected cancers are clinically significant.^{10,11} Although most prostate cancers diagnosed at an early stage have an indolent course, local tumor progression and aggressive metastatic disease may develop in the long term.¹⁶

1.3 Prostate cancer diagnosis in current clinical practice

Prostate cancer is generally detected through a combination of PSA blood serum concentrations, digital rectum examinations (DREs), and systematic transrectal ultrasound (TRUS) guided biopsies. PSA tests measure the concentration of PSA in the blood in

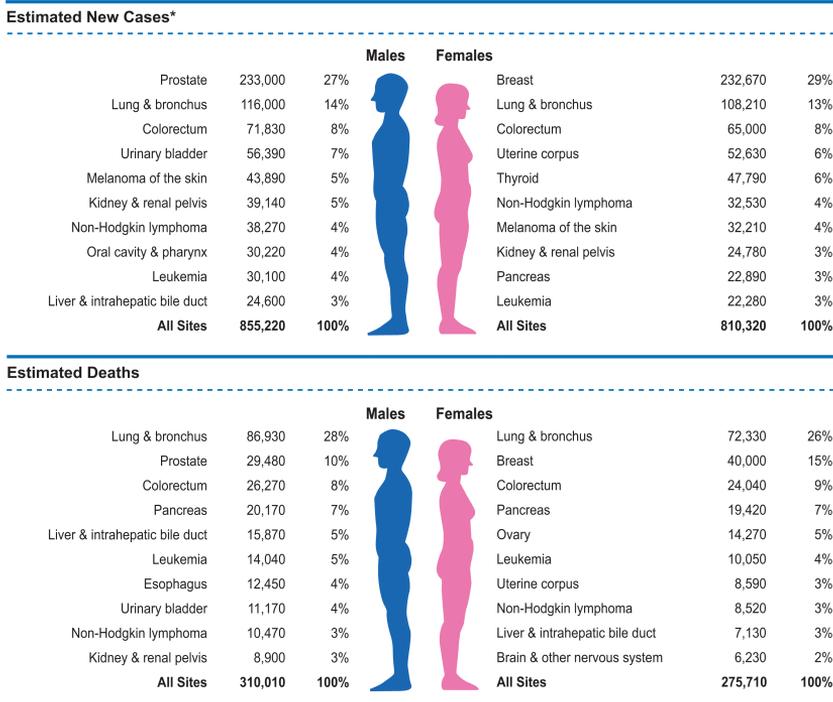


Figure 1.3: Cancer statistics in the United States in 2014. New cancer cases and deaths are estimated for the ten leading types of cancer, arranged by sex. Image obtained from Siegel *et al.*⁷

nanograms per milliliter (ng/mL). PSA is a biomarker that can be useful for the early detection of prostate cancer.¹⁷ It is a protease produced in the epithelial cells of the prostate and normally secreted into the glands. In individuals with a healthy prostate, the PSA level will be low as the PSA will be contained in the prostate gland. In individuals with prostate cancer or other prostate disorders (e.g. BPH or prostatitis) the PSA level can increase because of disruption of the glandular structure. The American Cancer Society guideline for the early detection of prostate cancer recommends that patients with a PSA level of ≥ 4.0 ng/mL should be referred for further examination.¹² To increase the sensitivity of the test, many other countries (including the Netherlands) lowered the threshold to 3.0 ng/mL, taking an increase of benign cases into account. The PSA blood test is also widely used in screening studies (discussed in Section 1.4), but remains a source of controversy due to its limited specificity.^{11,12,18}

In a DRE, the urologist will use a lubricated, gloved finger to inspect the surface of the prostate. Healthy prostate tissue is soft and smooth, whereas prostate cancer tends to feel as a firm, stony, and often asymmetrical lump. As only a small portion of the prostate gland can be felt, DRE usually tends to miss the more ventrally located cancers. Additionally, smaller tumors are difficult to detect by DRE. As such, DRE has a limited sensitivity and specificity for the detection of prostate cancer.^{19,20}

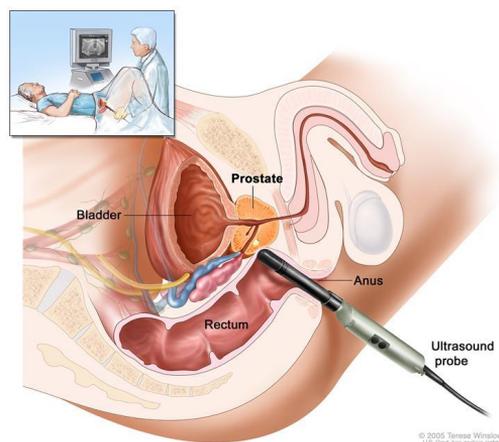


Figure 1.4: TRUS guided prostate biopsy. The patient is in dorsal or lateral decubitus position. The TRUS probe is inserted into the rectum to position the needle. Image obtained from Baumann *et al.*²⁹

After initial suspicion of prostate cancer has arisen due to either PSA or DRE, a TRUS guided biopsy is usually performed to make a definite diagnosis. Biopsy specimens are subsequently evaluated by a pathologist using the Gleason Scoring System. These topics will be discussed in Sections 1.3.1 and 1.3.2, respectively.

1.3.1 Ultrasound guided biopsy

Transperineal biopsies under finger guidance were the most common means of detecting prostate cancer until the introduction of transrectal/transperineal biopsies under transrectal ultrasound guidance. Transrectal ultrasound was already introduced in 1968 as a diagnostic device for prostate cancer.^{21,22} However, it was not until the early 1980s when the first TRUS guided biopsies were explored (Figure 1.4). At that time, hypoechoic nodules were seen as the main representation of prostate cancer, and therefore biopsies were merely targeted to these nodules.^{23,24} However, most of these nodules proved to be benign. With the introduction of the PSA test as indication for prostate biopsy, the need for ‘random’ sampling arose. In 1989, Hodge *et al.*²⁵ introduced the systematic sextant biopsy method. As originally described, six biopsies were obtained in the parasagittal plane halfway between the lateral border and midline bilaterally, from the base, mid-gland, and apex (Figure 1.5(a)). The prostate cancer detection rate increased, but still there was a high false-negative rate.^{24,26} As it became clear that most cancers originated in the peripheral zone, Stamey²⁷ suggested a ‘modified protocol’ in which the middle biopsies were moved more laterally to better sample the anterior horns of the peripheral zone (Figure 1.5(b)). Even the modified sextant biopsy scheme showed sampling errors, especially in enlarged glands, leading to various alternatives being explored.^{24,26} Extended biopsy schemes with eight, ten, or twelve cores were reported, which are currently still in use (Figures 1.5(c)–(e)). No differences were shown between the transrectal and transperineal approach in terms of cancer detection on initial 12-core prostate biopsy.²⁸

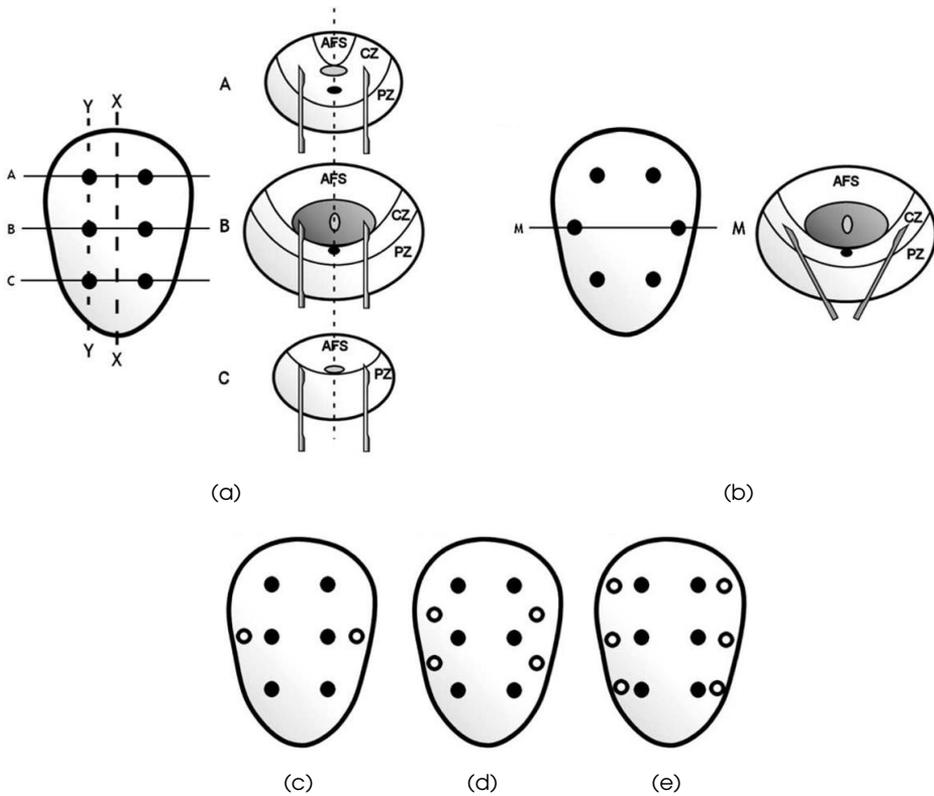


Figure 1.5: Schematic diagram of the various sampling patterns used. (a) The original sextant biopsy scheme as described by Hodge *et al.*²⁵ The coronal section shows six biopsies obtained in the parasagittal line (Y-Y), halfway between the lateral border and midline (X-X) on both right and left sides, from base, mid-gland, and apex. Images (A)-(C) demonstrate the needle trajectory in the axial plane at points A-C marked on the coronal view. (b) Coronal and axial view illustrating the modified sextant biopsy protocol. A larger amount of the peripheral is sampled by pointing the needle in an anterolateral direction. (c)–(e) Coronal representations showing extended 8-, 10-, and 12-core biopsy schemes, respectively. Image obtained from Raja *et al.*²⁴

Repeat and saturation biopsies

Even with the extended biopsy schemes, the initial biopsy may still be falsely negative.³⁰ Clinical suspicion can persist with e.g. increasing PSA levels. No matter what parameter is used to determine the need for a repeat biopsy, it is important to first address the adequacy of the initial biopsy. Number and direction of previous cores should be considered, as well as the prostate volume. Repeat biopsies should include areas where cancer may have been missed.^{24,26,28}

To minimise sampling error, more aggressive biopsy approaches have been applied. These so called 'saturation' biopsies involve ≥ 20 biopsy cores, evenly distributed throughout the gland via the transrectal or transperineal route. Using saturation biopsy, Stewart *et al.*³¹ detected cancer in 77 of 224 patients (34%) after previous negative biopsies.

New ultrasound techniques

Localization of malignant tissue on gray-scale ultrasound remains difficult and systematic TRUS guided biopsies are still routinely used in clinical practice. However, new ultrasound techniques are being explored that might help a targeted approach under ultrasound guidance. Color Doppler and power Doppler are looking for increased vascularity, which is a sign for prostate cancer. Targeted biopsy studies have been performed and reported a wide range of sensitivity.²³

A second technique is contrast-enhanced TRUS (CEUS), where a microbubble contrast agent is administered intravascular. Sano *et al.*³² reported that targeted biopsy using CEUS significantly enhanced cancer detection compared to systematic biopsy.

Lastly, elastography is a technique that measures tissue stiffness to distinguish hard (malignant) from soft (benign) tissue. Sensitivity and specificity have shown to increase when compared to systematic biopsy.³³

Post-prostate biopsy morbidity

Potential biopsy-related complications, including pain, infection, and bleeding, have implications on patient care. Rosario *et al.*³⁴ measured the effect adverse events within 35 days of 10-core TRUS guided biopsies in 1147 men. Pain was reported by 43.6% of men, fever by 17.5%, and 65.8% reported on haematuria. Anaesthesia can be used for pain control, which is especially necessary for transperineal biopsies. To minimize infection rates of transrectal biopsies, patients will commonly receive some antibiotics.^{24,28}

1.3.2 Gleason grading of prostate cancer

The Gleason Scoring System is named after Donald F. Gleason, who developed it with other colleagues at the Minneapolis Veterans Affairs Hospital during the 1960s.³⁵ This unique grading system for prostate carcinoma was based solely on the architectural pattern of the tumor. The system was updated in 2005 by International Society of Urological Pathology (ISUP) consensus conference.³⁶ Gleason grades range from 1 – 5, where 5 is considered the most aggressive pattern (shown in Figure 1.6). The descriptions of the different patterns are:

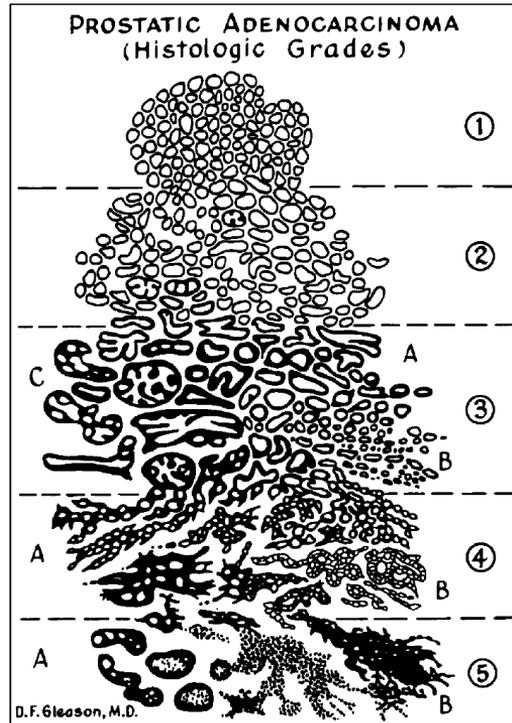


Figure 1.6: Schematic representation of the different Gleason grades assigned to histologic patterns of prostatic adenocarcinoma. Image obtained from Humphrey³⁷

1. Very well differentiated, small, closely packed, uniform, glands in essentially circumscribed masses.
2. Similar (to pattern 1) but with moderate variation in size and shape of glands and more atypia in the individual cells; cribriform pattern may be present, still essentially circumscribed, but more loosely arranged.
3. Similar to pattern 2 but marked irregularity in size and shape of glands, with tiny glands or individual cells invading stroma away from circumscribed masses, or solid cords and masses with easily identifiable glandular differentiation within most of them. May be papillary or cribriform, which vary in size and may be quite large, but the essential feature is the smooth and usually rounded edge around all the circumscribed masses of tumor.
4. Large clear cells growing in a diffuse pattern resembling hypernephroma; may show gland formation. Raggedly infiltrating, fused-glandular tumor; glands are not single and separate, but coalesce and branch.
5. Very poorly differentiated tumors; usually solid masses or diffuse growth with little or no differentiation into glands. Can resemble comedocarcinoma of the breast; almost absent gland pattern with few tiny glands or signet cells.

A Gleason score is assigned by the pathologist by summing two numbers; the first number indicates the grade of the most common tumor pattern in the specimen, the

second number indicates the second most common pattern. If only one pattern is present in the tissue sample, the corresponding grade is multiplied by two to give the score. There is a difference in determining the Gleason score from a biopsy sample and radical prostatectomy specimens. A biopsy sample represents only a small part of tumor. If there are more than two patterns present in the biopsy specimen, the second number should refer to the remaining pattern with the highest grade. In a prostatectomy sample, the pathologist bases the primary and secondary Gleason grades on their prevalence. When a third pattern contains at least 5% of the total tumor volume, a tertiary grade can be included in the Gleason score.

The attending physician will use the biopsy Gleason score and other clinical parameters (i.e. PSA level, number of positive biopsy cores) to make a treatment decision.

1.3.3 Treatment options

When diagnosed with prostate cancer, there are several treatments possible. The most common choices are: active surveillance, radical prostatectomy, radiotherapy, and focal therapy.

Active surveillance can be provided to men with a low grade, localized, well-differentiated prostate tumor. It involves conservative monitoring of the tumor by repeated PSA measurements, DREs, TRUS guided biopsies, or even MR imaging (see also Section 1.6). Patients will not be treated immediately, though the urologist can intervene when the cancer progresses. Several studies have shown that in men with untreated, low-risk prostate cancer the 10- to 20-year survival rates are similar to an age-matched group of men without prostate cancer,^{38–40} showing potential for active surveillance. Initial results on active surveillance show that mortality rates are low, with moderate rates of intervention over the first few years.^{41,42}

Radical prostatectomy and radiotherapy are ‘whole gland’ treatment options with intention to cure. Radical prostatectomy involves the complete surgical removal of the cancerous prostate. Radiotherapy can either be external beam radiotherapy or internal brachytherapy. In external beam radiation therapy, the patient receives radiation from an external source. Internal brachytherapy involves the implantation of radioactive seeds into the prostate. Cancer recurrence and survival rates are relatively similar. However, side-effects like urinary leakage and erectile dysfunction are reported and may play a role in the patients’ decision of treatment.^{43–46}

Recently, minimal invasive focal therapies have been under investigation. Several options are available: laser interstitial thermotherapy (LITT), cryo-ablation, and high-intensity focused ultrasound (HIFU). Although initial results are promising, especially for localized, low-grade prostate cancer, they are currently not yet widely available clinically.

1.4 Prostate cancer screening

The growth and aging of the population are causing an increase in the number of prostate cancer diagnoses and an increase in men who will require treatment for their malignancy.

Screening can help find cancer at an early stage when the disease is easily manageable. However, caution is required for potential overtreatment.

Possible methods used in prostate cancer screening are DRE and PSA blood testing, usually combined with subsequent TRUS guided biopsy. DRE or PSA testing is essentially used as a triage test for the more invasive TRUS guided biopsies. PSA testing requires a predetermined cut-off value, which limits the sensitivity of the screening program. The PSA cut-off level is a source of discussion.⁴⁷⁻⁴⁹ Lowering the cut-off value will increase the sensitivity, but reduce the specificity.⁵⁰

Screening trials in Europe and the USA include respectively the European Randomized Study of Screening for Prostate Cancer (ERSPC) and the Prostate, Lung, Colorectal, and Ovarian (PLCO) Cancer Screening Trial.⁵¹⁻⁵³ Results show that screening helps to diagnose prostate cancer at an earlier stage and was associated with an increase in incidence.⁵⁴ The ERSPC trial showed a mortality reduction of 20%,⁵² and when adjusted for nonattendance and contamination this reduction increased to approximately 30%.⁵⁵ However, official statistics tended to overreport prostate cancer as an underlying cause of death, which would overestimate the true effect in favor of screening.⁵⁶ Another side-effect is that screening would cause a large amount of over-diagnosis and over-treatment. To save one life, 1055 men had to be screened and 37 men had to be treated for prostate cancer.⁵³

So there is certainly potential for prostate cancer screening, but currently controversy regarding the effectiveness still exists.⁵⁴ An alternative technique with higher specificity for prostate cancer might make screening more feasible. Alternatives are being explored (e.g. prostate MRI, Section 1.6).

1.5 Drawbacks of current practice

A PSA test followed by systematic (on average 12 core) TRUS guided biopsy is the currently internationally accepted diagnostic procedure to detect prostate carcinoma and determine patient management.²⁸ However, this diagnostic procedure is subject to false-positive as well as false-negative results. First of all, the PSA blood test is often false-positively elevated due to the fact that elevated PSA levels are also measured at benign conditions such as prostatitis or BPH. Its specificity is therefore relatively low.^{50,57} Also, false-negative results can occur if men with prostate cancer do not have elevated PSA levels. Pelzer *et al.*⁵⁸ showed that more than one third of prostate cancer cases occurred in the lower PSA ranges (2.0-3.9 ng/mL).

Furthermore, the subsequent TRUS guided biopsies have a relatively poor detection rate due to sampling errors (some examples are shown in Figure 1.7). Reason for this is that localization of malignant tissues on ultrasound is difficult. Up to 30% of the prostate cancer lesions are isoechoic and undetectable by gray-scale ultrasound.^{23,59} The ultrasound guided approach is thus merely used to guide systematic biopsies in which specific regions throughout the prostate are sampled without knowing where tumors are located, rather than targeted biopsy of a palpable nodule or a lesion visible by

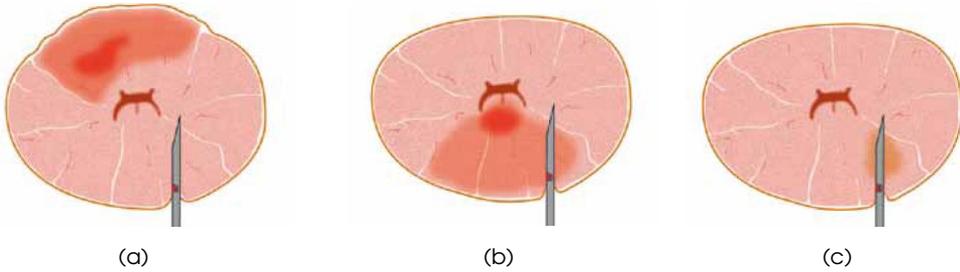


Figure 1.7: Cross sections of the prostate showing the limitations of TRUS guided biopsy. (a) The needle penetrates next to the tumor or does not reach it. (b) Wrong part of the tumor is biopsied causing underestimation of aggressiveness. (c) Insignificant (non-aggressive) tumor is biopsied.

imaging. Systematic TRUS guided biopsy misses nearly a quarter of detectable cancers on the first biopsy session and has a low sensitivity of around 40%.^{30,60,61} Several studies have demonstrated discrepancies between the Gleason score of the biopsy tissue and the subsequent radical prostatectomy specimen.^{62–65} Significant cancers are missed (Figure 1.7(a)) or underestimated (Figure 1.7(b)), and there is overtreatment due to overdiagnosis (Figure 1.7(c)).

Combining the results of PSA testing and TRUS guided biopsies, we can conclude that there is a need for a more accurate method for detecting prostate cancer and correctly determining the cancer aggressiveness.

1.6 MR imaging of the prostate

Magnetic resonance imaging (MRI) of the prostate made its emergence in the 1980s.⁶⁶ The zonal anatomy of the prostate could be visualized on T2-weighted imaging due to high spatial resolution and high tissue contrast. Current state-of-the-art prostate MRI is characterized by its multiparametric approach. Anatomical T2-weighted imaging is combined with functional imaging techniques such as dynamic contrast-enhanced (DCE), diffusion-weighted imaging (DWI), and magnetic resonance spectroscopic imaging (MRSI). Functional parameters provide additional information on biological properties of prostatic tissue. Modern prostate MRI is usually acquired on a 1.5 or 3 tesla (T) MRI scanner. A radiofrequency-emitting coil is placed next to the prostate using either a (surface) pelvic phased-array coil or an (internal) endo-rectal coil.⁶⁷

T2-weighted imaging is the best modality for anatomical assessment of the prostate and its surrounding structures. It has the highest resolution and the best soft tissue contrast. Usually three orthogonal views are acquired, i.e. transversal, sagittal, and coronal, with a high in-plane resolution and relatively thick slices (Figures 1.8(a)–(c)). The central zone, transition zone, and fibromuscular stroma are usually hard to differentiate radiologically and are grouped together as the central gland.⁶⁸ The central zone has usually a dark appearance with a chaotic structure, opposing the bright homogeneous appearance of the peripheral zone.

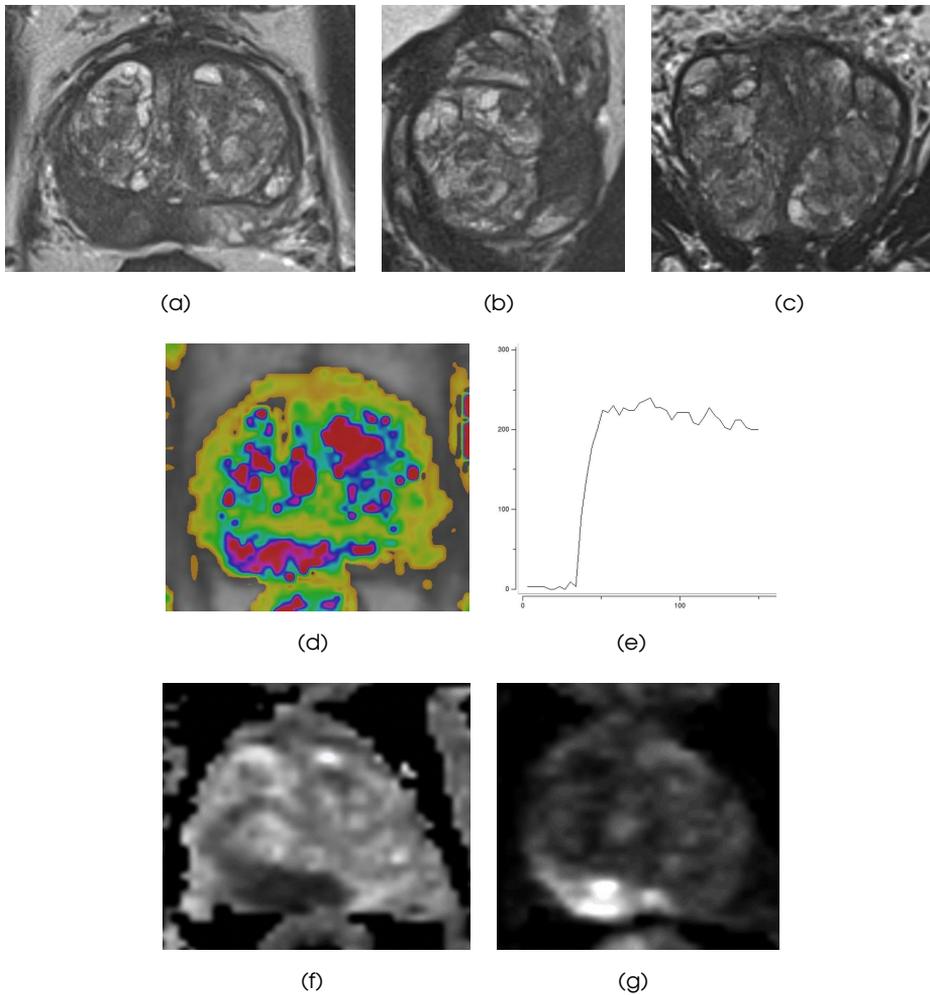


Figure 1.8: Example of a multiparametric MRI. (a) Transversal T2-weighted image. (b) Sagittal T2-weighted image. (c) Coronal T2-weighted image. (d) DCE image. (e) Curve of the DCE image. (f) ADC map. (g) DWI with $b = 1400$.

DCE imaging is based on the permeability of blood vessels and extravasation of contrast agent into the adjacent tissue.⁶⁹ A sequential set of T1-weighted images is acquired over time following the administration of an intravenous contrast agent. Leaky endothelial cells have an increased permeability causing fast contrast enhancement, which is a typical feature of prostate cancer. The enhancement pattern can be expressed in different curve types as illustrated in Figure 1.9. Figure 1.8(d) shows an example of a DCE image, the corresponding curve is depicted in Figure 1.8(e).

DWI quantifies the random Brownian motion properties of water molecules in tissue.⁷⁰ The degree of restriction to water molecules in biologic tissue is inversely correlated to the cellular density. Tumors often show restricted diffusion compared to benign tissue. The net displacement of molecules is called the apparent diffusion coefficient (ADC), which can be derived from a series of diffusion images using different parameters (i.e. *b*-values). An example of an ADC map and corresponding *b*1400 image is shown in Figures 1.8(f),(g) respectively.

MRSI allows to evaluate changes in metabolite concentrations within the prostate.⁷¹ The ratio of choline and creatinine relative to citrate is used as marker for prostate cancer.

1.6.1 Prostate cancer diagnosis on MRI

Currently, multiparametric (mp)-MRI is the most sensitive and specific technique for localizing prostate cancer.⁷² It has shown great potential in the localization and grading of prostate cancer.⁷³ A combination of anatomical T2-weighted MRI, dynamic contrast-enhanced MRI, and diffusion-weighted MRI improves the accuracy of prostate cancer detection over T2-weighted imaging alone.^{74–76} Additionally, recent research has investigated the correlation between DWI and tumor aggressiveness. The apparent diffusion coefficient (ADC) determined at DWI has proven to be inversely correlated to the Gleason grade in peripheral zone prostate cancer.^{77–80}

Although MRI for prostate cancer certainly has potential, interpretation of mp-MRI suffers from observer variability⁸¹ and requires a high level of experience.⁸² A major issue with broad adaptation was the professional disagreement on what parameters to use and how to interpret them.^{83,84} A group of prostate MR imaging experts have developed a set of clinical guidelines with the aim to standardize prostate MRI: the Prostate Imaging and Reporting Archiving Data System (PI-RADS).⁸⁵ The PI-RADS scoring system is summarized in Table 1.1. Bomers and Barentsz⁸⁶ provided a detailed explanation illustrated with examples for every single parameter in mp-MRI. The example in Figure 1.8 shows a lesion scored as PI-RADS 5 for all three parameters.

The ESUR guidelines recommend to perform mp-MRI consisting of at least T2-weighted imaging and two functional modalities (DCE and DWI), with MRSI being an optional parameter. Every modality is scored independently on a 5-point scale. Since no rules are specified for determining the final lesion score, several studies calculated a PI-RADS sum score.^{88–90} An update of the guidelines will prescribe that the ‘dominant’

Table 1.1: PI-RADS scoring system for multiparametric MR imaging of the prostate, as described by the ESUR guidelines.⁸⁵

Score	Criteria
<i>T2-weighted imaging for the peripheral zone (PZ)</i>	
1	Uniform high signal intensity (SI)
2	Linear, wedge shaped, or geographic areas of lower SI, usually not well demarcated
3	Intermediate appearances not in categories 1/2 or 4/5
4	Discrete, homogeneous low signal focus/mass confined to the prostate
5	Discrete, homogeneous low signal intensity focus with extra-capsular extension/invasive behavior or mass effect on the capsule (bulging), or broad (>1.5 cm) contact with the surface
<i>T2-weighted imaging for the transition zone (TZ)</i>	
1	Heterogeneous TZ adenoma with well-defined margins: 'organised chaos'
2	Areas of more homogeneous low SI, however well margined, originating from the TZ/BPH
3	Intermediate appearances not in categories 1/2 or 4/5
4	Areas of more homogeneous low SI, ill defined: 'erased charcoal sign'
5	Same as 4, but involving the anterior fibromuscular stroma or the anterior horn of the PZ, usually lenticular or water-drop shaped.
<i>Diffusion-weighted imaging (DWI)</i>	
1	No reduction in ADC compared with normal glandular tissue. No increase in SI on any high <i>b</i> -value image ($\geq b800$)
2	Diffuse, hyper SI on $\geq b800$ image with low ADC; no focal features, however, linear, triangular or geographical features are allowed
3	Intermediate appearances not in categories 1/2 or 4/5
4	Focal area(s) of reduced ADC but iso-intense SI on high <i>b</i> -value images ($\geq b800$)
5	Focal area/mass of hyper SI on the high <i>b</i> -value images ($\geq b800$) with reduced ADC
<i>Dynamic contrast enhanced (DCE)-MRI*</i>	
1	Type 1 enhancement curve
2	Type 2 enhancement curve
3	Type 3 enhancement curve
+1	For focal enhancing lesion with curve type 2–3
+1	For asymmetric lesion or lesion at an unusual place with curve type 2–3
<i>Magnetic resonance spectroscopic imaging (MRSI)</i>	
1	Citrate peak height exceeds choline peak height >2 times
2	Citrate peak height exceeds choline peak height times > 1, < 2 times
3	Choline peak height equals citrate peak height
4	Choline peak height exceeds citrate peak height > 1, < 2 times
5	Choline peak height exceeds citrate peak height >2 times

* Different curve types for DCE-MRI are illustrated in Figure 1.9

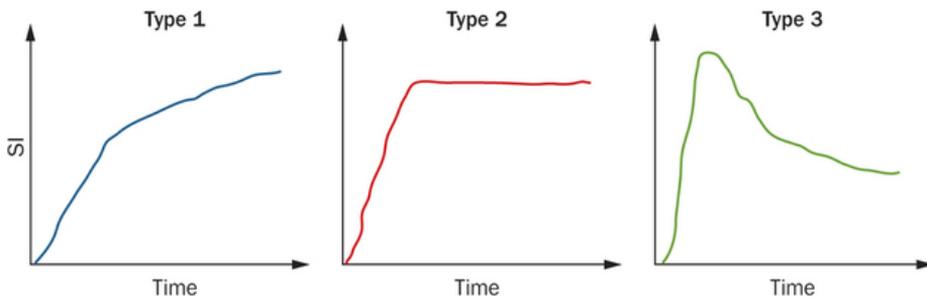


Figure 1.9: Curve types representing enhancement patterns on DCE-MRI. Type 1 represents progressive enhancement, type 2 represents rapid enhancement with plateauing, and type 3 represents rapid enhancement followed by a rapid wash out of the contrast material. Image obtained from Johnson *et al.*⁸⁷

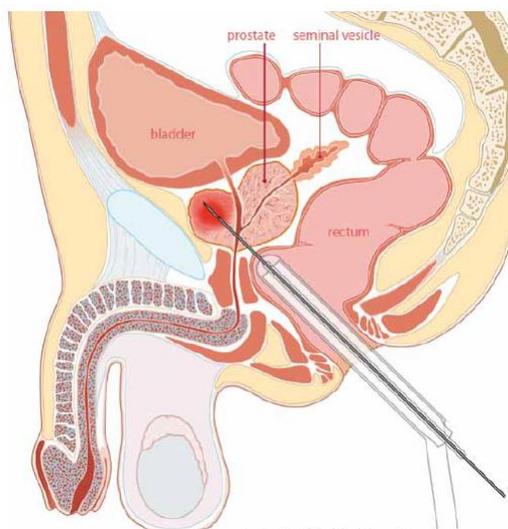


Figure 1.10: During the MRI-guided biopsy the worst part of the tumor can be specifically targeted. ⁸⁶

parameter should determine the final PI-RADS score, being DWI for peripheral zone and T2-weighted imaging for central gland. ⁸⁶

Several studies have evaluated the performance of the PI-RADS guidelines. These show that the PI-RADS score can help to localize possible prostate lesions and indicate the likelihood of cancer of suspicious lesions. ^{88,89,91}

1.6.2 MR guided biopsy

The first MR guided prostate biopsy was done in 1986. ⁹² Since then, MR imaging and biopsy techniques have improved significantly.

MR guided biopsy uses mp-MRI for accurate prostate cancer localization to direct the biopsy needle towards (the most aggressive part of) the prostate cancer, as depicted in Figure 1.10. T2-weighted imaging with additional functional sequences are used to define targets. Most commonly used techniques in clinical studies are DCE and DWI. ^{93–97} MR guided biopsies that are targeted to the lowest signal areas on the ADC map within the tumor determine the Gleason grade in exact concordance with prostatectomy in 88% of the cases, which is substantially higher than TRUS systematic biopsy (55%). ⁹⁸ MR guided biopsy has resulted in prostate cancer detection rates ranging from 38 – 59% using far less cores (median 4) compared to systematic TRUS biopsies (8 – 12 cores). ^{94,95,99–102}

The negative predictive value of mp-MRI for excluding significant prostate cancer has shown to be around 90%. ^{103,104} This means that mp-MRI can be used to help men at risk and decide whether they should proceed to prostate biopsy. Parts of the prostate that were negative at mp-MRI do not require biopsy, leading to a reduction of the total number of biopsies (up to 50% ¹⁰⁴). A study on cost-effectiveness showed that total costs of an MRI strategy are comparable to TRUS guided biopsy, while potential reduction of

overdiagnosis and overtreatment leads to an improvement in the quality of life.¹⁰⁵ MR guided biopsy can therefore be a more cost-effective solution than the systematic TRUS guided biopsy.

1.7 MR-TRUS fusion

Despite its versatile capabilities, MRI is not as widely available or as easy to apply to prostate imaging as is ultrasound (US). Issues of cost, access, scanner time, technical requirements and radiologists' acceptance and understanding of the procedure are continuing challenges.¹⁰⁶ By combining advantages of both MR and TRUS imaging, MR guided TRUS biopsy is a potentially more accessible and practical solution than in-bore MR guided biopsies. Pre-acquired MR images can be used to enhance TRUS imaging and improve needle guidance by registration of the two modalities.¹⁰⁷ Accurate MR-TRUS registration requires to take into account prostate deformation and motion inherent to TRUS probe insertion and prostate scanning. Available methods vary in accuracy, speed, and user-friendliness. Two strategies can be distinguished: cognitive fusion and computational fusion.

1.7.1 Cognitive fusion

Cognitive fusion is the first strategy using MR-TRUS registration. It fuses the two modalities by means of visual or cognitive fusion (sometimes referred to as mental fusion). It is the simplest MR guided biopsy technique and requires no additional equipment. With this technique, the physician performing the TRUS guided biopsy reviews the lesion on MRI and uses this knowledge to aim the biopsy needle at the appropriate prostate area for a targeted MR guided TRUS biopsy.^{108–110} The reported results of cognitive fusion biopsy are contradictory: a study by Puech *et al.*¹¹¹ did not show a significant difference between computer-assisted MR-TRUS fusion and cognitive fusion, whereas a study by Delongchamps *et al.*¹¹² showed that cognitive fusion biopsies do not perform better than systematic TRUS guided biopsies. The main disadvantage of this technique is that it requires experience and training and leads to inaccuracies, subjectivity, variability, and lack of reproducibility.¹⁰⁹ As the accuracy of cognitive fusion depends very much on the skills of the operating physician, it is likely that this technique is not as effective at locating lesions for biopsy as direct in-bore MR and computer-assisted MR guided TRUS biopsies.

1.7.2 Computational fusion

Computational (or computer-assisted) registration of MR and US images is the second MR-TRUS registration strategy. Compared to cognitive fusion, it is potentially a more accurate way of image fusion requiring less operator skills but more computation time. MR image information is very different from information obtained from US images. Therefore, MR-US registration methods are often surface-based, i.e. the capsule is aligned by registering a surface representation reconstructed typically from cross-sectional contours.

The main challenge is to compensate for shape differences between MR and US images due to prostate deformation and motion. Computer-assisted registration methods can be roughly subdivided into two categories: rigid and non-rigid registration methods.

Computer-assisted rigid registration is a relatively easy and fast computation-based registration method. Xu *et al.*¹¹³ describe a method for the real-time rigid registration of MR and TRUS images during freehand transrectal biopsy. A reconstructed 3D TRUS volume was manually registered with a 3D MRI volume. Rigid motion compensation is based on an image registration between the reference 3D US volume and the intra-operative 2D US images. However, the prostate gland is not a rigid structure. Prostate motion can arise from a number of causes, of which the most important one is probably the insertion of the TRUS probe. Significant gland motion can therefore occur between MR and TRUS imaging.¹¹⁴ The disadvantage of rigid registration is that it does not take any of these motions into account. To reduce potential errors due to prostate deformation on TRUS images, Ukimura *et al.*¹¹⁵ introduced a plastic outer-frame of the TRUS probe that was placed in the rectum during MR image acquisition.

Computer-assisted non-rigid registration, on the other hand, is able to compensate for deformations of the prostate. Singh *et al.*¹¹⁶ describe a manual method for the real-time non-rigid registration of MR and TRUS images. This method, however, requires significant user interaction. Automatic registration is more challenging and requires more computation time, but has the advantage of being less dependent on operator skills. Narayanan *et al.*¹¹⁷ propose a non-rigid registration that was achieved by an initial deformable registration of the prostate surface, segmented from both the MR and TRUS images, followed by a linear elastic warping of the gland volume using an adaptive focus deformable model with surface point displacements as boundary conditions. Mitra *et al.*¹¹⁸ present a method to non-rigidly register TRUS and MR images in corresponding 2D slices. The Bhattacharyya distance is used to establish point correspondences on manually segmented prostate contours. An extended non-linear thin-plate spline (TPS) algorithm was applied to the corresponding point sets. The performance of the proposed method was compared against traditional B-splines and TPS-based deformable registration methods and has a significantly better registration accuracy. A 3D prostate biopsy tracking system with deformation estimation was published by Baumann *et al.*²⁹ A volume-swept 3D US-based tracking system solves the patient motion problem with an a priori model of rectal probe kinematics. Prostate deformations are estimated with elastic registration. By incorporating the algorithm proposed by Martin *et al.*¹¹⁹, MR to 3D TRUS registration is performed for clinical applications. They build a mesh from the MR volume and shape and volume constraints are used to guide surface deformation.

There are many different methods, but in general deformable non-rigid registration is more accurate than rigid registration.^{112,120,121} However, many methods are based on relatively simple volume interpolation that are not always physically plausible.¹²² Image volumes can be stretched and moved causing the anatomy to look artificially altered.

Internal prostate gland motion and deformation can be better predicted by applying biomechanical modeling using finite element (FE) analysis.^{123–125} A biomechanical model of the prostate can be constructed by assigning boundary conditions and elastic properties to the tissue. The prostate deformation can be simulated and internal gland motion can then be predicted. Alterovitz *et al.*¹²³ use a biomechanical model based registration algorithm to non-rigidly register MR and MR spectroscopic images. Bharatha *et al.*¹²⁴ apply a 3D FE-based deformable registration algorithm to pre- and intraoperative MR studies. A biomechanical model of soft-tissue deformation was also used to predict the actual internal prostate deformation due to a TRUS probe for MR-TRUS registration.¹²⁵ This method is based on a side-firing TRUS probe and has been applied to transperineal MR guided TRUS biopsies.

1.7.3 Clinical MR-TRUS fusion systems

Multiple MR-TRUS fusion systems based on different computation registration algorithms have been developed. The existing systems with published clinical data are summarized in Table 1.2.¹⁰⁹ The general workflow is to acquire pre-biopsy diagnostic MR images used to identify lesions suspicious for prostate cancer. During the biopsy session, MRI and real-time TRUS images are superimposed and displayed either side-by-side or as blended fusion image.

One of the major differences between the different fusion systems is the registration method. Some clinically available devices are based on a rigid registration method, mostly using an electro-magnetic (EM-) tracker placed on the TRUS probe to track movements of the probe. Patient movement or prostate deformation are not taken into account. Other devices do correct for movement and deformation by tracking the organ itself instead of the TRUS probe. These incorporate a non-rigid registration algorithm. Another solution to reduce prostate deformation due to the TRUS probe is by transperineally biopsying the prostate after MR-TRUS fusion. Some systems have the additional option to archive the biopsy location.

Another major difference is the amount of manual operator input. Some methods require manual identification of paired landmarks or manual prostate segmentation. Others are more automated, with automatic segmentation and the ability to correct for motion compensation. Some systems require additional manual 'fine-tuning'. Less human input increases the reproducibility as there is less room for (manual) errors. Learning curves may also vary between the different systems.¹⁰⁹

The overall results of clinical studies show that targeted prostate biopsy using MR-TRUS fusion has a significantly higher tumor detection rate compared to conventional systematic TRUS guided biopsies (Table 1.3).^{111,112,126–129} These studies use different commercially available clinical fusion systems, and all of them show a higher detection rate with MR guided TRUS biopsy of especially clinically significant prostate cancer when compared to systematic TRUS guided biopsy. Diagnosis of insignificant disease is avoided. MR guided TRUS biopsy upgrades and detects higher Gleason grade cancer in

Table 1.2: Specification summary of MR-US fusion systems (adapted from Logan *et al.* 109).

Fusion system - Trade name (Manufacturer)	Principle investigator location	MRI			US			Biopsy	
		MRI	Parameters used to define target	Endorectal/ pelvic coil	US image acquisition	Method of image registration	Tracking mechanism		Biopsy route
UroNav (In Vivo Corp./Philips)	Bethesda, MD, USA	3T Philips	T2W, DCE, DWI, MRSI	Yes/Yes	Manual US 2D sweep. Freehand manipulation of US probe.	Rigid	EM tracking US	Trans- rectal	Minimum 2/ 12-core TRUS
Artemis (Eigen)	Los Angeles, CA, USA	3T Siemens	T2W, DCE, DWI	No/No	Manual rota- tion along a fixed axis (US probe on a tracking arm)	Elastic	Mechanical arm with encoded joints	Trans- rectal	Mean 2.2/ 12-core TRUS
Urostation (Koeelis)	Paris, France Oslo, Norway Grenoble, France Heidelberg, Germany	1.5T Siemens 1.5T Siemens 3T Philips 3T Siemens	T2W, DCE, DWI T2W, DWI T2W, DCE, DWI T2W, DCE DWI	Yes/Yes Yes/No No/No No/No	Automatic US probe rotation, three different volumes elastically registered Custom-made biplane TRUS probe mounted on a stepper	Elastic	Image-based registration	Trans- rectal	Minimum 2/ 10-12-core TRUS Minimum 2/ 12-core TRUS 2/ 12-core TRUS Median 4/ 12-core TRUS
BiopSee (Pi Medical /MedCom)	Paris, France Lille, France Chiba, Japan	1.5T Siemens	T2W, DCE DWI	Yes/Yes	Manual US sweep. Free- hand rotation of US probe.	Rigid	Stepper with two built-in encoders	Trans- perineal	Minimum 2/ 10-12-core TRUS Minimum 2/ 12-core TRUS 1-2/ 10-core TRUS
Virtual Navigator (Esaote)	Paris, France Lille, France Chiba, Japan	1.5T Philips	T2W, DCE DWI	No/Yes	Real-time biplanar TRUS	Rigid	EM tracking US and needle	Trans- rectal or trans- perineal	Minimum 2/ 10-12-core TRUS Minimum 2/ 12-core TRUS 1-2/ 10-core TRUS

24 – 32% of patients.^{111,112,128} However, this does not (yet) reach the performance of in-bore MR guided biopsy which has shown a 41% reduction of TRUS undergrading.⁹⁸ For correct Gleason grading with MR guided TRUS biopsy, an accurate spatial registration of MR and US images is required. Current MR-US fusion systems may require improvement to be able to (partly) replace in-bore MR guided biopsies. There certainly is potential for fusion biopsy but so far, there is no clear consensus on which methodology is optimal for screening, detection or surveillance, nor on the specific indications.

1.8 Outline of this thesis

Current clinical practice lacks sensitivity for prostate cancer detection. With the increasing number of PSA tests, or even screening in the future, an alternative technique for prostate cancer diagnosis is required. MRI has shown to be much better in prostate cancer detection, but is not ideal for biopsying the increasing number of patients. MR-TRUS fusion is an upcoming technique for prostate biopsies. Recent studies showed that MR-TRUS fusion biopsies are better than the systematic TRUS guided biopsies. However, not much is known about the requirements and whether it is as good as in-bore MR biopsies. It is not yet clear what role MR-TRUS fusion can potentially play in prostate cancer diagnosis. The aim of this thesis is to investigate whether MR guided TRUS fusion biopsy is viable in clinical practice. Both technical requirements and clinical usability are addressed.

In chapter 2, the viability of MR-TRUS fusion biopsies as alternative to systematic TRUS guided biopsies is discussed. It includes a short overview of advantages and disadvantages of MR-TRUS fusion biopsies.

Chapter 3 focuses on the required registration accuracy. Many prostate cancers have a high-grade focal hotspot. Targeting this highest Gleason grade component solely based on fusion requires an accurate registration algorithm. Small targets might be missed with MR guided TRUS biopsies. The goal of this study was to determine the required registration accuracy, and how this is related to tumor volume. An estimation of the technical registration accuracy is made by simulating biopsies on a tumor population.

In chapters 4 and 5 the design of a surface-based registration method with biomechanical regularization is presented. Surface-based registration methods have their limitations, especially with respect to registration accuracy. Biomechanical modeling can better control internal prostate deformation. The method developed extends a commonly used non-rigid surface-based registration method with biomechanical modeling. The registration accuracy of this enhanced method was compared to the regular registration method to see whether this indeed improves. Chapter 4 evaluates the accuracy for MR-MR registration. Subsequently, in chapter 5 the method is extended further and applied to MR-TRUS registration.

Chapter 6 is concerned about the cancer visibility on TRUS images. Prostate cancer visible on TRUS using prior knowledge of MRI can be targeted under TRUS guidance, benefitting especially fusion biopsies. The aim of this observer experiment was to de-

Table 1.3: Patient-based histological biopsy outcomes by fusion system (adapted from Logan *et al.*,¹⁰⁹).

Fusion system - Trade name (Manufacturer)	Principle investigator location	Patient inclusion criteria	MRI			Biopsy results		Additional/notable study conclusions
			Defining lesion suspicion for prostate cancer	# Patients with MRI-suspicious lesions	Prostate cancer detection in patients with MRI lesion (no. patients)	Prostate cancer TB;SB* P	P	
UroNav (In Vivo Corp./Philips)	Bethesda, MD, USA	Aug 2007-Aug 2012	Low, moderate, or high	Low - 123 (21%) (21%); Moderate - 370 (64%); High - 89 (15%) 151/171 (88%)	315/582 (54%)	253/315 patients (80%); 255/315 patients (81%) 101/486 cores (20.8%); 127/1741 cores (7.3%)	-	TB upgrades and detects higher Gleason score in 36% of patients compared with TRUS. High suspicion associated with high upgrade. TB is three times more likely to identify disease than SB with greater detection of intermediate- to high-risk disease. Biopsy correlates with MR suspicion.
Artemis (Eigen)	Los Angeles, CA, USA	Mar 2010-Sept 2011	Score 1-5 (normal to highly suspicious)	82/133 (62%)	84/151 (56%)	62/82 patients (76%); 44/133 patients (33%) 60/115 targets (52%); 6/42 patients (14%)	0.001	TB cancer detection significantly higher than SB. Cognitive TB not significantly different from SB. 10 patients negative MRI all negative SB. 97% MRI targets successful, 52 positive for cancer.
Urostation (Koelis)	Paris, France	Jan 2011-Mar 2012	Yes/No	80/90 (89%) patients. Lesions - High (55), Medium (6), Low (4)	71/82 (87%)	62/82 patients (76%); 44/133 patients (33%) 60/115 targets (52%); 6/42 patients (14%)	-	Urostation has good accuracy for targeting suspicious areas on MRI. TB detects significantly more cancer SB and of greater significance. Patients without suspicious MR-lesions were diagnosed with intermediate-risk disease.
BiopSee (Pi Medical /MedCom)	Grenoble, France Heidelberg, Germany	Nov 2011-Aug 2012 June 2010-Dec 2011	PI-RADS Highly suspicious, questionable or not suspicious	Highly suspicious: 104/347 (30%). Questionable: 149 (43%). Not suspicious 94 (27%)	11/20 (55%) Overall: 200/347 (58%). Highly suspicious: 82.6%. Questionable: 67%. Not suspicious: 14.8%	386/1281 cores (30%); 523/6326 cores (8.2%)	0.01	Rigid system TB were significantly higher than SB. Cognitive TB not significantly different from SB. Clinically significant cancer 52% SB, 67% TB patients (P = 0.001). Cognitive vs platform fusion not significantly different detection/grading. TB cores revealed more cancer than SB.
Virtual Navigator (Esaote)	Paris, France	Jan 2011-Mar 2012	Yes/No	78/131 (59%)	78/78 (100%)	64/78 patients (82%); 60/131 patients (46%) 66/95 patients (69%); 56/95 patients (56%)	-	Rigid system TB were significantly higher than SB. Cognitive TB not significantly different from SB. Clinically significant cancer 52% SB, 67% TB patients (P = 0.001). Cognitive vs platform fusion not significantly different detection/grading. TB cores revealed more cancer than SB.
HI RVS/Real-Time Virtual Sonography (Hitachi)	Chiba, Japan	Feb 2007-Aug 2009	1-5 (unlikely to highly likely) Yes/No	95/95 (100%) 85/85 (100%)	52/85 (61%)	62/192 cores (32%); 75/833 cores (9%)	< 0.01	Rigid system TB were significantly higher than SB. Cognitive TB not significantly different from SB. Clinically significant cancer 52% SB, 67% TB patients (P = 0.001). Cognitive vs platform fusion not significantly different detection/grading. TB cores revealed more cancer than SB.

* TB: targeted biopsy; SB: systematic biopsy

+ Combination of cognitive and Vnav fusion cores

termine the proportion of tumors that are visible when using prior knowledge of MRI appearance.

In chapter 7, the clinical feasibility of a MR-TRUS fusion biopsy system is tested. A simple EM-based rigid registration technique can be enhanced with local reference augmentation, thereby optimizing registration accuracy locally around the lesion. Local MR-TRUS fusion biopsy may be a viable method providing a definite diagnosis for a selection of patients. If not, MR guided biopsy will be recommended. Based on the initial results, an indication of the cancer detection rate and the representativeness is given.

This thesis is concluded with a summary of the main results and a general discussion in chapter 8. Clinical implications and future perspectives are provided as well.

2 – A viable alternative?

Wendy J. M. van de Ven, Jelle O. Barentsz

Original title: Prostate cancer: MRI/US-guided biopsy – a viable alternative to TRUS-guidance

Published in: Nature Reviews Urology

Abstract

MRI/ultrasonography (MRI/US)-fusion biopsy outperforms systematic ultrasonography-guided biopsy, detecting more high-grade prostate tumours while being less able to detect low-grade cancer, thus preventing overtreatment of indolent tumours. Any of several MRI-guided biopsy techniques has the potential, therefore, to replace systematic transrectal ultrasonography-guided prostate biopsies in the future.

Systematic transrectal ultrasonography (TRUS)-guided biopsy is the current clinical standard method for diagnosing prostate cancer. However, TRUS-guided biopsy can miss and undersample aggressive tumours and detect indolent cancers by chance. Multi-parametric (mp)-MRI has been shown to be highly accurate in detecting and localizing intermediately aggressive and highly aggressive cancers. Biopsy under direct MRI or MRI/ultrasonography (MRI/US) guidance is, therefore, rapidly emerging as an alternative to TRUS-guided biopsy. Siddiqui *et al.*¹²⁸ are one of the first groups to report a large prospective study comparing MRI/US-fusion-guided biopsy with systematic TRUS-guided biopsy. They show that targeted MRI/US-fusion-guided biopsy detects a higher number of aggressive cancers than TRUS-guided biopsy, and avoids detection of indolent cancers. These results are in line with other studies.^{111,112,129}

However, caution is required before embarking on immediate large-scale implementation of MRI-guided biopsy techniques for men with suspected prostate cancer. An experienced MRI radiologist is crucial for obtaining good biopsy samples, as optimal acquisition and standardized interpretation of mp-MR images is essential. Acquisition and interpretation of the mp-MR images requires skills that can only be obtained by good training and experience. Minimal requirements for prostate mp-MR image acquisition and standardization for reporting (PI-RADS) have recently been published,⁸⁵ which will help to improve the general reliability of the techniques.

Furthermore, any MRI-guided biopsy technique used clinically should be state-of-the-art. Several MRI-guidance techniques – including direct ‘in-bore’ MRI-guided, MRI/US-fusion-guided, and cognitive-fusion-guided biopsy – exist,¹¹⁰ but not all are equally accurate. Direct MRI-guided biopsy⁹⁵ is likely to be the most accurate technique as it is less prone to fusion and motion errors. Thus, direct image-guided biopsy is used in most oncologic applications and can easily locate a lesion detected on a previous MRI study, enabling very accurate targeting. With this technique, aggressive cancers as small as 2 mm in diameter can be targeted. Hambrock *et al.*⁹⁸ compared direct MRI-guided biopsy to TRUS-guided biopsy using prostatectomy as reference standard. Using direct MRI-guided biopsy resulted in a 41% reduction of TRUS undergrading of intermediately aggressive and highly aggressive tumours. This result is greater than the 32% reduction after using MRI/US-fusion-targeted biopsy reported by Siddiqui *et al.*¹²⁸ However, direct MRI-guided biopsy also has potential disadvantages: it is not yet widely available and can be relatively expensive compared with TRUS-guided biopsy. However, cost effectiveness has not been studied for this technique, so it remains unclear what the effects are on the total cost for health-care systems and the potential improvement in patients’ quality of life.

The second MRI-guided biopsy method is MRI/US-fusion-guided biopsy. This might seem an attractive alternative to direct MRI-guided biopsy, because of the limited availability of the latter technique. However, as it is indirect, it is, therefore, prone to a large variation in accuracy. Furthermore, collaboration of a skilled MRI radiologist and a urologist familiar with MRI – which is not available in all centres – is a prerequisite for carrying

out the biopsy procedure. Siddiqui *et al.*¹²⁸ have reported excellent results, as their group contains two highly skilled prostate MR-radiologists, who were directly involved in the biopsy procedure. Furthermore, they used an advanced technique compensating as much as possible for changes in prostate shape between MR and TRUS images. Additionally, their procedure included motion correction during scanning. Any misregistration will negatively affect the biopsy outcome. Some MRI/US-fusion techniques provide similar technologies, but others do not include these advanced solutions – their registration often does not compensate for difference in prostate shape and motion correction and the target registration accuracy is, therefore, expected to be less optimal. Thus, each different MRI/US-fusion technique needs to be validated before its widespread use.

To achieve good results with MRI/US-fusion-guided prostate biopsies, optimal registration accuracy is critical. Van de Ven *et al.*¹³⁰ have shown that a registration accuracy of 1.9 mm is required for correctly grading 95% of tumours with MRI/US-fusion biopsy. To our knowledge, only one study¹²⁵ has reported the actual target registration error of MRI/US-fusion. That particular technique resulted in a median target registration error of 2.4 mm. At this accuracy, it is likely that smaller (3–5 mm) lesions are missed. Siddiqui *et al.*¹²⁸ do not report on their target registration error. To compensate for this potential error, they sample 2–3 cores per lesion, which is more than usually required with direct MRI-guided biopsy. However, it remains unclear whether small, highly aggressive focal tumour ‘hot spots’ were accurately sampled using this approach. A further critical technological element is the ability to accurately register an MR image to an ultrasonograph image during biopsy in real-time.

Another drawback of MRI/US-fusion is that it relies on accurate prostate segmentation. This means that the prostate needs to be outlined – manually or semiautomatically – on both MR and US images. This segmentation is a time-consuming task and is operator dependent. Siddiqui *et al.*¹²⁸ do not report the time needed for prostate segmentation, nor provide details about the used method and its accuracy.

Furthermore, with MRI/US-fusion it is tempting and very easy for the urologist to take random biopsy samples at the same time and, therefore, find insignificant cancer, thereby removing one of the advantages of targeted biopsies.

The third MRI-guided prostate biopsy method is cognitive-fusion. With this technique the physician performing the TRUS-guided biopsy reviews the lesion on mp-MRI and uses this information to select the appropriate area for a targeted TRUS-guided biopsy. The reported results of cognitive-fusion biopsy are contradictory: a study by Puech *et al.*¹¹¹ did not show a significant difference between MRI/US-fusion and cognitive-fusion, whereas a study by Delongchamps *et al.*¹¹² showed that cognitive-fusion biopsies do not perform better than TRUS-guided biopsies. As the accuracy of the cognitive-fusion technique depends very much on the skill of the operator, it is likely that this technique is not as effective at locating lesions for biopsy as direct MRI and MRI/US-fusion biopsy.

Overall, we agree with the conclusion drawn by Siddiqui and colleagues,¹²⁸ who assert that MRI-guided biopsy will replace TRUS-guided biopsy. However, good quality

MR image acquisition and standardized (PI-RADS) interpretation, combined with accurate MRI-guided biopsy, is essential. Advanced targeted MRI/US-fusion guided biopsy techniques are already more accurate than systematic TRUS-biopsies. However, targeting lesions relies solely on the accuracy of the fusion method used, so one must keep in mind that small (3–5 mm) focal hot spots of aggressive cancer are prone to being missed even with optimal MRI/US-fusion techniques. Thus, small lesions or lesions that are difficult to reach with MRI/US-fusion biopsy should be biopsied under direct MRI-guidance. Larger lesions can be targeted using MRI/US-fusion alone. Future studies should be performed to determine the threshold tumour size and to compare the accuracy of both techniques.

3 – Required registration accuracy

Wendy J. M. van de Ven, Christina A. Hulsbergen-van de Kaa, Thomas Hambrock, Jelle O. Barentsz, Henkjan J. Huisman

Original title: Simulated required accuracy of image registration tools for targeting high-grade cancer components with prostate biopsies

Published in: European Radiology

Abstract

Objectives: To estimate the required spatial alignment accuracy for correctly grading 95% of peripheral zone (PZ) prostate cancers using a system for multiparametric magnetic resonance (MR) guided ultrasound (US) biopsies.

Methods: PZ prostate tumours were retrospectively annotated on multiparametric MR series using prostatectomy specimens as reference standard. Tumours were grouped based on homogeneous and heterogeneous apparent diffusion coefficient (ADC) values using an automated ADC texture analysis method. The proportion of heterogeneous tumours containing a distinct, high Gleason grade tumour focus yielding low ADC values was determined. Both overall tumour and high-grade focal volumes were calculated. All high-grade target volumes were then used in a simulated US biopsy system with adjustable accuracy to determine the hit-rate.

Results: An ADC determined high-grade tumour focus was found in 63% of the PZ prostate tumours. The focal volumes were significantly smaller than the total tumour volumes (median volume of 0.3 mL and 1.1 mL respectively). To correctly grade 95% of the aggressive tumour components the target registration error (TRE) should be smaller than 1.9 mm.

Conclusions: To enable finding the high Gleason grade component in 95% of PZ prostate tumours with MR guided US biopsies, a technical registration accuracy of 1.9 mm is required.

3.1 Introduction

Prostate cancer is the second most common diagnosed malignancy in men in the Western World, and one of the leading causes of death from cancer.¹³¹ The current routine clinical standard method for making a definite diagnosis of prostate cancer is transrectal ultrasound (TRUS) guided biopsy. As prostate cancer is rarely visible on grey-scale ultrasound, TRUS is merely used to guide systematic biopsies. This systematic approach misses nearly a quarter of detectable cancers on the first biopsy.³⁰ Furthermore it substantially underestimates the true Gleason score compared to radical prostatectomy specimens. In about 40% of Gleason scores ≥ 7 on prostatectomy, the biopsy revealed a lower Gleason score.^{62,64,98} So the number of correctly detected aggressive tumours is rather low with TRUS guided biopsy. For correct treatment decision and risk stratification, improved methods for correctly determining the Gleason score on biopsy are needed.

Magnetic resonance (MR) guided MR biopsy is a very promising technique for prostate biopsies. Firstly, multiparametric MR imaging (MRI) has proven to be an effective technique to localize prostate cancer.⁷³ A combination of anatomical T2-weighted MRI, dynamic contrast-enhanced MRI, and diffusion weighted MRI (DWI) improves the accuracy of prostate cancer detection over T2-weighted imaging alone.^{75,76} Secondly, it has been shown that MR guided MR biopsy significantly increases the tumour detection rate as compared to TRUS systematic biopsy.⁹⁴ Additionally, recent research has investigated the correlation between DWI and tumour aggressiveness. The apparent diffusion coefficient (ADC) determined at DWI has proven to be inversely correlated to the Gleason grade in peripheral zone (PZ) prostate cancer.⁷⁷⁻⁷⁹ MR guided MR biopsies are therefore targeted to the lowest signal areas on the ADC map within the tumour. It has moreover been shown that ADC guided biopsy determines the Gleason grade in exact concordance with prostatectomy in 88% of the cases, which is substantially higher than TRUS systematic biopsy (55%).⁹⁸ However, disadvantages of MR guided MR biopsies are that such a system is not widely available and is costly.

MR guided TRUS biopsy is potentially a more cost-effective alternative. The question remains however whether this can also result in a correct sampling of the most aggressive part of the tumour and thus accurately predict its true aggression. An important aspect of this method is the correct spatial alignment of the MR and TRUS images using fusion methods. For merely detecting the tumour, MR-TRUS fusion with reasonable accuracy may be sufficient. But accurate Gleason grading depends on accurate targeting of biopsies to the most aggressive tumour component. Many clinically significant tumours show different Gleason patterns within the same tumour.^{132,133} These so-called heterogeneous tumours thus require a more accurate registration method for a correct Gleason grading as the biopsy needs to be targeted to the smaller high-grade tumour volume component.

Fusion of MR and TRUS images is considered difficult and topic of current research in image registration. Recent works have investigated several MR to US registration methods, including rigid as well as nonrigid methods able to compensate for deformations. Reported mean surface error is 3.3 mm, increasing to up to 12.7 mm in apex and

base.¹¹⁶ However, this is based on the root mean square distance between TRUS-based and MRI-based segmentations of the prostate. Reported median target registration errors (TREs) are 5.1 (rigid) and 2.4 mm (nonrigid) in the mid plane, but increase at apex and base.¹²⁵ Clinical studies using rigid registration reported a significantly increased tumour detection rate upon targeted prostate biopsy with MR-US fusion compared to conventional TRUS guided biopsies.^{127,134} Accurate Gleason grading depends however on accurate targeting of biopsies in the most aggressive tumour component.

In this article, we investigate the required accuracy of the registration for a correct Gleason grading with MR guided US biopsies. The current required accuracy is based on the widely used cutoff value of 0.5 mL for clinically significant tumour volumes.^{121,125} We hypothesize that for a correct Gleason grading of heterogeneous tumours, a higher accuracy is required. This registration accuracy depends on the size of the most aggressive tumour component, which we define as the high-grade tumour focal spot. Aggressive tumour components can be distinguished on multiparametric MRI (especially ADC) but not on US. We therefore used the ADC map to automatically determine the volume of the focal spot within an annotated tumour region. We first investigate the proportion of tumours being heterogeneous on ADC. Secondly, we determine the volume distribution of the most aggressive component of the heterogeneous tumours. Using this volume distribution, we then estimate the required maximal technical registration error for taking a representative biopsy of the most aggressive component under MR to US guidance by using a simulation system.

3.2 Materials and methods

3.2.1 Patients

Between August 2006 and January 2009, 56 consecutive patients with PZ prostate cancer, scheduled for radical prostatectomy, were referred from the departments of urology at the Radboud University Nijmegen Medical Centre and Canisius Wilhelmina Hospital in Nijmegen, The Netherlands, for clinically indicated routine MRI of the prostate. In all patients, prostatectomy was performed within 6 weeks of MR imaging. The requirement to obtain institutional review board approval was waived.

Five of the 56 patients were excluded owing to severe motion artifacts ($n = 3$), widespread intraprostatic hemorrhage ($n = 1$), or severe ghosting artefacts on the MR images ($n = 1$). The remaining data set contains 51 patients with 62 PZ tumours.

3.2.2 MR imaging protocol

Multiparametric MR imaging was performed on a 3.0-T MR system (Trio Tim; Siemens, Erlangen, Germany) with the use of both an endorectal coil (Medrad, Pittsburgh, PA, USA) and a pelvic phased-array coil. The endorectal coil was filled with a 40 mL perfluorocarbon preparation (Fomblin; Solvay-Solexis, Milan, Italy). Peristalsis was suppressed with intramuscular administration of 20 mg butylscopolamine bromide (Buscopan; Boehringer-

Ingelheim, Ingelheim, Germany) and 1 mg of glucagon (Glucagen; Nordisk, Gentofte, Denmark).

The imaging protocol included anatomical T2-weighted turbo spin-echo MR imaging in transverse, coronal, and sagittal planes, covering prostate and seminal vesicles. Axial DWI was performed using a single-shot echo-planar imaging sequence with diffusion-module and fat-suppression pulses. Water diffusion was measured in three directions using b -values of 0, 50, 500, and 800 s/mm². The ADC maps were automatically calculated by the imager software using all four b -values and a mono-exponential decay fit.

3.2.3 Histopathology

After radical prostatectomy, prostate specimens were uniformly processed and entirely submitted for histological investigation. After histological staining, all specimens were evaluated by one expert urological pathologist with 19 years of experience. The entire tumour volume was outlined on each step section (Figure 3.1(a)). Each individual tumour was graded according to the 2005 International Society of Urological Pathology Modified Gleason Grading System³⁶ and staged according to the 2002 TNM classification. See Hambrock *et al.*⁷⁸ for a summary of the clinical and pathological tumour characteristics.

3.2.4 MR tumour annotation

Retrospectively, annotations of MR images (Figures 3.1(b)–(c)) were performed in consensus by one radiologist and one urologist. All annotations were performed using an in-house developed MR viewing and reporting system.¹³⁵ ADC maps were acquired in the same orientation and with similar thickness as the histopathology step sections. A previously described translation technique was used to match the tumour-containing regions on prostatectomy specimens to ADC maps.⁷⁸ Using histopathology as reference standard, a region of interest was placed on the ADC map over the whole tumour-containing region (Figure 3.1(c)).

3.2.5 Focal volume segmentation

We used an automated method to determine the presence and size of a tumour focal spot (cluster of low ADC values within annotated tumour region). To summarise, it was first evaluated if the tumour was heterogeneous on ADC and thus contained a dark ADC tumour focus. Second, the focal spot was automatically detected and its volume determined.

Low ADC values within the tumour annotation were considered aggressive components for the purpose of this study as aggressiveness showed an inverse relationship with ADC values and MR guided MR biopsies are targeted to these low signal areas on ADC. Therefore, we defined the darkest connected tumour region within the annotation on the ADC map as the aggressive tumour focus.

The segmentation of the high-grade focus was done by means of a 3D region growing within the tumour annotation, taking the voxel with the lowest ADC value within the

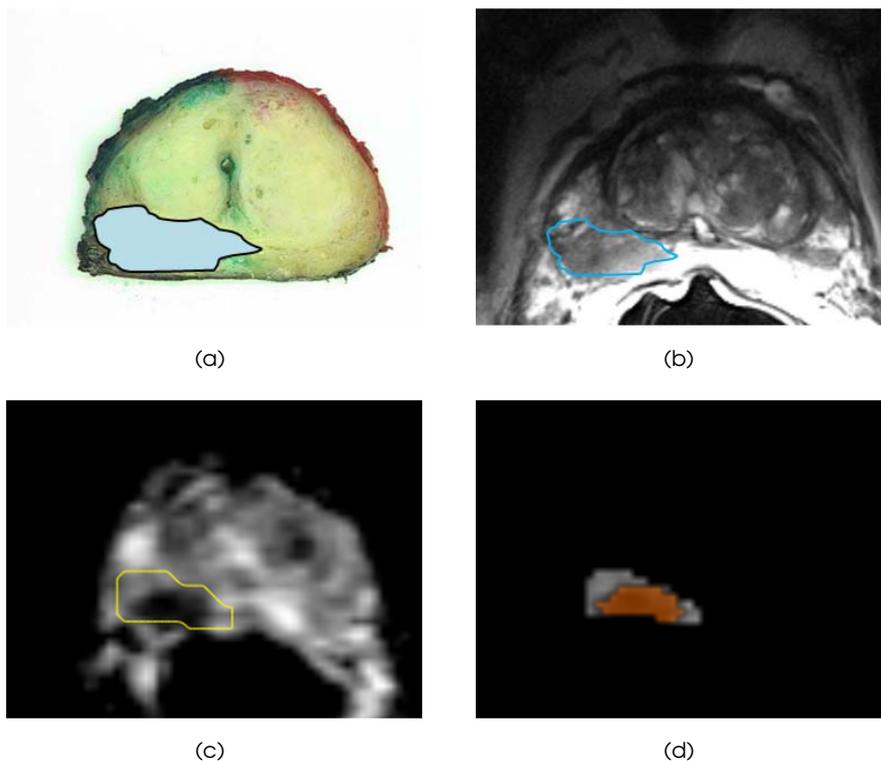


Figure 3.1: Patient with a peripheral zone tumour revealing Gleason 4 + 3 (+5) on final pathology. (a) Prostatectomy step section with the tumour delineated in light blue. (b) Anatomical T2-weighted MR image. A large tumour region corresponding to the step section is seen in the peripheral zone (blue delineation). (c) On the ADC map, water restriction is clearly visible for the same lesion. Regions of interest are annotated on the smoothed ADC map in correspondence with the prostatectomy step section (yellow delineation). (d) The segmentation of the focal finding based on ADC values (orange region). A seeded region growing was applied to detect a cluster of low ADC values within the tumour outline.

annotated tumour region as seed point (Figure 3.1(d)). The upper threshold of the region growing was set at $1.07 \times 10^{-3} \text{mm}^2/\text{s}$, which is based on Hambrock *et al.*⁷⁸ At this setting, most of the high-grade tumour components (primary Gleason grade 4 and any 5) and half of the intermediate-grade tumour components (secondary Gleason grade 4) can be differentiated from low-grade and normal PZ tissue. To reduce image noise, a 3D Gaussian smoothing filter ($\sigma = 0.50$ voxels) was applied to the ADC map before analysis.

The focal volume was calculated by counting the voxels segmented by the region growing. An aggressive tumour focus will be detected if the tumour contains a substantial amount of voxels both below and above the threshold of $1.07 \times 10^{-3} \text{mm}^2/\text{s}$. We recorded a focal spot if its volume was between 5% and 95% of the total tumour volume, a threshold which is also commonly used for assigning the secondary Gleason grade at pathology.^{36,136} When a focal spot was detected, the tumour was assigned to the heterogeneous group; if none, then two types of homogeneous tumours can be distinguished: a tumour with almost all ADC values above the threshold (homogeneous bright, focal spot $< 5\%$) and a tumour with most values below this threshold (homogeneous dark, focal spot $> 95\%$).

3.2.6 Registration accuracy and hit-rate

The required registration accuracy depends on the volume to be targeted. To determine the hit-rate as a function of accuracy we used a simulated image registration method. The simulation system computes the likelihood of a hit for a given TRE and target volume. The simulation was performed on the whole tumour population and the outcome allows determining the required TRE given a requested hit-rate. Simulations were done on the whole tumour volumes as well as the aggressive target volumes (cluster of low ADC values and homogeneous low signal intensity tumours on the ADC map).

The simulator is described in Hu *et al.*¹²⁵ The registration error is defined as the distance between the true centre of the target volume and the projected location as simulated by the registration method. The x -, y -, and z -components of that error are assumed to be independently normally distributed with standard deviation σ . The distance error will then follow a Maxwell-Boltzmann probability density function with a mean value of:

$$TRE = \sqrt{3}\sigma. \quad (3.1)$$

Thus, given a TRE, a probability (or hit-rate) can be computed for the projection to be within the volume to be targeted, where we assumed a spheroid shape with radius r . Figure 3.2 shows a graph of the TRE threshold as a function of hit-rate and volume.

3.2.7 Statistical analysis

The proportion of heterogeneous tumours was determined including the 95% confidence intervals. The Wilcoxon rank-sum test was performed to determine whether there is a

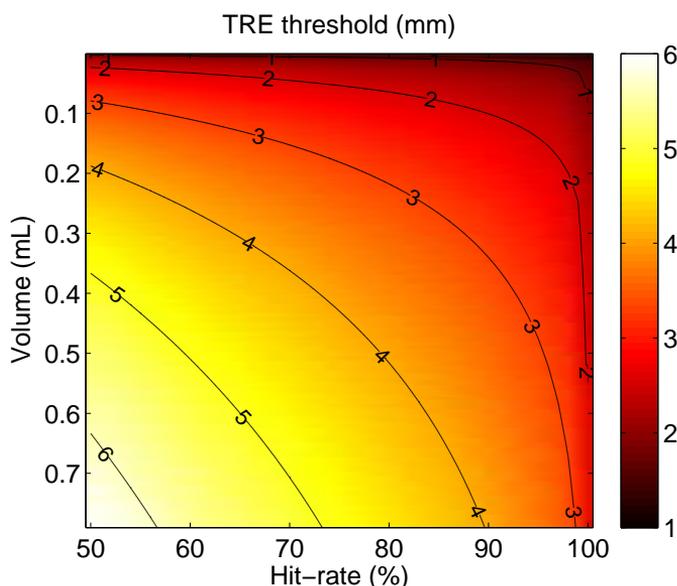


Figure 3.2: The TRE threshold as a function of the hit-rate and the tumour volume.

significant difference between the tumour and target volumes. This non-parametric test was used because a Shapiro-Wilk normality test proved that both tumour volumes and target volumes (including focal spots and homogeneous dark tumours) are not from a normally distributed population ($p < 0.001$). The Wilcoxon signed-rank test was used to determine whether there is a significant difference of both population median volumes with the 0.5 mL level of significant tumours. The required accuracy is based on the TRE threshold at which 95% of the targets are correctly graded.

Differences were considered to be significant when $p < 0.05$. Statistical analyses were performed with Matlab (The Mathworks, Inc., Nattick, MA, version 7.10.0).

3.3 Results

3.3.1 Proportion and volume of tumour foci

Of the 62 PZ tumours, 63% (39/62) were heterogeneous, 27% (17/62) had no focal spot at all, and 10% (6/62) had homogeneous low signal intensity on the ADC map (Table 3.1). The focal volumes in heterogeneous tumours are mostly below 0.5 mL, with a median of 0.3 mL (range 0.01 – 12.9 mL), and are significantly smaller than whole tumour volumes ($p = 0.006$).

A box-and-whisker plot for the two groups of tumour volumes is shown in Figure 3.3. The first group contains the whole tumour volumes. The second group contains the homogeneous dark tumours and the smaller focal volumes, together forming the aggressive target volumes. This latter group is important for a correct Gleason grading of aggressive tumour components. The distributions of the two groups differ significantly

Table 3.1: Sample size and proportion for each of the tumour groups. For each group, the minimum, median, and maximum tumour volumes are determined.

	All tumours	Homogeneous		Heterogeneous	
		Dark	Bright	Tumour	Focal spot
Sample size	62	6	17	39	39
Proportion (95% CI)	100%	10% (4 – 20%)	27% (18 – 40%)	63% (50 – 74%)	63% (50 – 74%)
Minimum volume	0.03 mL	0.05 mL	0.04 mL	0.03 mL	0.01 mL
Median volume	11.04 mL	0.63 mL	0.64 mL	1.48 mL	0.30 mL
Maximum volume	18.35 mL	2.69 mL	4.66 mL	18.35 mL	12.87 mL

($p = 0.008$). The tumour volume distribution is significantly different from a population with median 0.5 mL ($p < 0.001$); the target volumes are not significantly different from the 0.5 mL level ($p = 0.323$).

3.3.2 Required registration accuracy

For the estimation of the registration accuracy, we used the target volumes containing 39 tumour focal volumes and 6 homogeneous dark tumour volumes. The proportion of targets and tumours detected as a function of the TRE is shown in Figure 3.4. Overall, for detecting 95% of the high Gleason grade targets, an accuracy of 1.9 mm is required. Comparing this with the mere detection of tumour volumes, a registration with a TRE of 2.5 mm is sufficient.

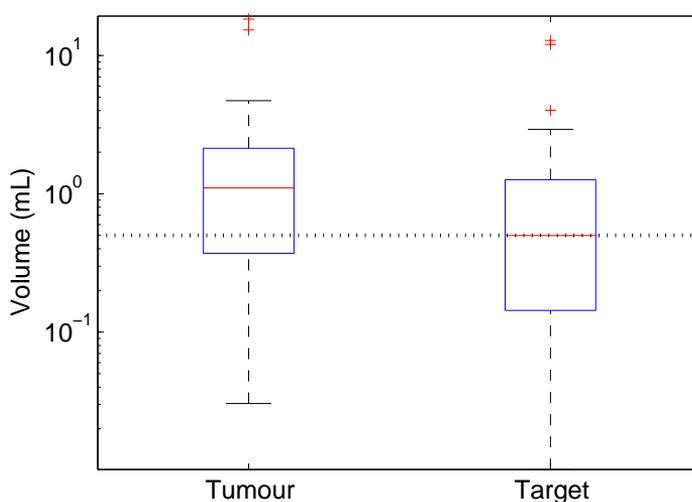


Figure 3.3: Box-and-whisker plot displaying the total tumour volumes (heterogeneous and homogeneous tumours) and the target volumes (focal spots and homogeneous dark tumours) on a logarithmic scale. The 0.5 mL cutoff value for clinically significant tumours is indicated by the dotted line.

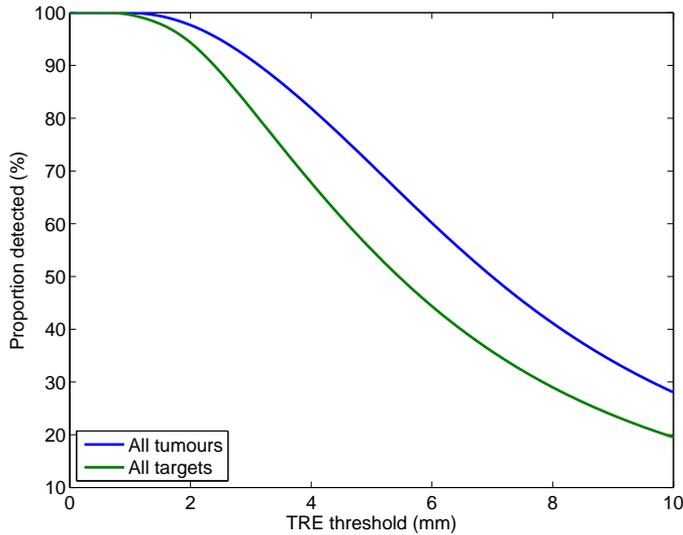


Figure 3.4: The proportion of tumours detected as function of TRE threshold. Two different groups of tumours are plotted: all tumour volumes and all target volumes.

3.4 Discussion

We have shown that 63% of the PZ tumours in our population were heterogeneous, containing a high-grade tumour focus. With 0.3 mL, the median focal volume was smaller than the cutoff value of 0.5 mL for a tumour considered being clinically significant. High-grade focal spots and homogeneous dark tumours were used for estimating the required registration accuracy for MR guided US biopsies. By simulation we determined that to correctly assess the aggressive component in 95% of the PZ tumours in our population, a technical registration accuracy of 1.9 mm is required.

More than half of the PZ tumours were heterogeneous with a high-grade tumour focus, which is in line with previous findings.^{132,133} Although the median target volume is not significantly different from the 0.5 mL level, still more than half of them are smaller than 0.5 mL. For a correct Gleason grading of especially these heterogeneous tumours, it is important to be able to sample the smaller high-grade tumour focus and not a random spot within the whole tumour volume. These focal spots therefore require a more accurate registration than a 0.5 mL tumour. Correctly determining the highest Gleason grade on biopsy is important for correct treatment decision and risk stratification.

The current described required accuracy is based on the cutoff value of 0.5 mL for a clinically significant tumour volume.^{121,125} Figure 3.2 shows that a TRE of 3.1 mm is required to detect 95% of these 0.5 mL tumours. Figure 3.4 shows that for detecting 95% of the PZ tumours in our data set, the required TRE is 2.5 mm. For detecting 95% of the high-grade targets, a registration accuracy of 1.9 mm is required. Especially the volume difference between heterogeneous tumours, which constitute more than half of

the tumours, and their focal volumes lead to a large difference in required accuracy. We therefore conclude that the 0.5 mL cutoff is insufficient to correctly grade prostate cancer.

The 95% level was chosen arbitrarily. It can be argued that a level of 90% or even lower is sufficient, thereby also decreasing the required accuracy. TRUS guided biopsies have a sensitivity of only 54% for high Gleason grades 4 and 5.⁹⁸ However, the same study has shown that a sensitivity of 95% for the high Gleason grades can be achieved with MR guided MR biopsies. MR guided TRUS biopsies have to at least approach this level to be a potential alternative for MR guided MR biopsies.

Several MR-TRUS registration methods have been published. Most of the described registration errors have a TRE that is most accurate in the mid plane of the prostate.^{116,125} The accuracy in that plane is sufficient to find most tumours, explaining the increased detection rates with MR-TRUS fusion.^{127,134} However, these systems (especially rigid registration systems) are not accurate enough to target high-grade focal spots either in the mid plane itself or especially in the apex and base of the prostate. This may result in biopsy specimens that undergrade the Gleason scores, as is also the case with regular systematic TRUS guided biopsies.^{62,64,98}

The patients in this study did not have MR guided TRUS biopsy, but for determining the required registration accuracy only the volume of the targets is important. The results of this study are based on the high-grade tumour volumes and only provide a theoretical measure of accuracy for the registration method itself. An accurate registration is important for US biopsy as there is no visual feedback like in MR. An initial large registration inaccuracy will never improve in clinical practice. Therefore, it is important that the registration is accurate enough to hit the high-grade tumour component. Correct placement of the biopsy gun and needle deflection are not taken into account. These will lead to another inaccuracy. So in real clinical practice there will be more limitations to MR guided TRUS biopsies. A clinical study investigating the Gleason grading with MR guided TRUS biopsy sessions will provide a better idea of the clinical implications. To our knowledge, no studies have investigated the Gleason grading with MR guided TRUS biopsies.

A first limitation of this study may be the bias of the data set in that it only contains patients who are already scheduled for a prostatectomy. The tumours investigated are thus relatively large and have a higher proportion of aggressive tumours. If data from a general population were taken, the mean tumour size would most likely decrease. For detecting these tumours and correctly grading them, the TRE threshold might thus be even lower than 1.9 mm.

The second limitation is that transition zone tumours were not included in this study. We assumed that low ADC values within the tumour correspond with the most aggressive tumour component. Transition zone tumours are known to have lower ADC values than PZ tumours;^{137,138} therefore, a different threshold is needed for their focal detection in this zone. Although it has been shown that the ADC values for transition and central zone cancerous tissue are significantly lower than normal prostatic tissue,^{139,140} no significant

correlation has been shown between ADC and the Gleason grade in transition zone tumours.^{80,138} In addition, the majority of prostate tumours arise in the peripheral zone.

We can conclude that for a correct Gleason grading under MR-US guidance, a technical registration accuracy of at least 1.9 mm is required throughout the prostate. With this registration accuracy 95% of the prostate cancers in our population will be correctly graded.

4 – MR-MR registration

Wendy J. M. van de Ven, Yipeng Hu, Jelle O. Barentsz, Nico Karssemeijer, Dean Barratt, Henkjan J. Huisman

Original title: Surface-based prostate registration with biomechanical regularization

Published in: Proceedings of the SPIE

Abstract

Adding MR-derived information to standard transrectal ultrasound (TRUS) images for guiding prostate biopsy is of substantial clinical interest. A tumor visible on MR images can be projected on ultrasound by using MR-US registration. A common approach is to use surface-based registration. We hypothesize that biomechanical modeling will better control deformation inside the prostate than a regular surface-based registration method. We developed a novel method by extending a surface-based registration with finite element (FE) simulation to better predict internal deformation of the prostate. For each of six patients, a tetrahedral mesh was constructed from the manual prostate segmentation. Next, the internal prostate deformation was simulated using the derived radial surface displacement as boundary condition. The deformation field within the gland was calculated using the predicted FE node displacements and thin-plate spline interpolation. We tested our method on MR guided MR biopsy imaging data, as landmarks can easily be identified on MR images. For evaluation of the registration accuracy we used 45 anatomical landmarks located in all regions of the prostate. Our results show that the median target registration error of a surface-based registration with biomechanical regularization is 1.88 mm, which is significantly different from 2.61 mm without biomechanical regularization. We can conclude that biomechanical FE modeling has the potential to improve the accuracy of multimodal prostate registration when comparing it to regular surface-based registration.

4.1 Introduction

Prostate cancer is the second most common diagnosed malignancy in men in the Western World, and one of the leading causes of death from cancer.¹³¹ The current routine clinical standard method for making a definite diagnosis of prostate cancer is transrectal ultrasound (TRUS) guided biopsy. Localization of malignant tissues on ultrasound is difficult as most lesions are not visible. Systematic TRUS guided biopsy therefore substantially underestimates the true Gleason score compared to radical prostatectomy specimens.^{62,64,98} Magnetic resonance imaging (MRI) has shown great potential in the localization and grading of prostate cancer^{75,76} and MR guided MR biopsy significantly increases the tumor detection rate when comparing it to TRUS systematic biopsy.^{94,95} However, disadvantages of MR guided MR biopsies are that such a system is not widely available and is costly.

MR guided TRUS biopsy is a potentially more cost-effective solution. Pre-acquired MR images can be used to enhance TRUS imaging and improve needle guidance by registration of the two modalities.²⁹ Clinical studies have shown that targeted prostate biopsy using MR-US fusion has a significantly higher tumor detection rate compared to conventional TRUS guided biopsies.^{127,134} However, correct Gleason grading with MR guided TRUS biopsy requires accurate MR-TRUS registration. We have recently shown that a registration accuracy of 1.9 mm is required for finding the high Gleason grade component in 95% of the tumors with MR guided TRUS biopsies.¹³⁰

MR image information is very different from information obtained with US images. Therefore, MR-US registration methods often use a surface-based registration, i.e. the capsule is aligned by registering a surface representation reconstructed typically from cross-sectional contours. Deformable surface-based registration using simple volume interpolation shows improved accuracy compared to rigid registration, but better accuracy is still required. An advanced biomechanical model of soft-tissue deformation can be used to better predict the actual internal prostate deformation.¹²² In this paper we evaluate a non-rigid surface-based registration method combined with biomechanical modeling for MR guided TRUS biopsies. Many anatomical landmarks in the prostate are visible on MR but not on US. Therefore we developed and tested our novel method on a surface-based MR to MR registration using MR guided MR biopsy data. The MR biopsy needle guide had an orientation and dimension comparable to a TRUS probe, therefore causing a similar deformation of the prostate. Besides, MR-MR registration can be useful for MR guided interventions.¹²⁰ The registration accuracy was determined by calculating the target registration error (TRE) using internal anatomical prostate landmarks in the MR guided MR biopsy data.

4.2 Methods

An overview indicating the different steps of the method we developed is shown in Figure 4.1. The additional steps taken for our surface-based registration method with

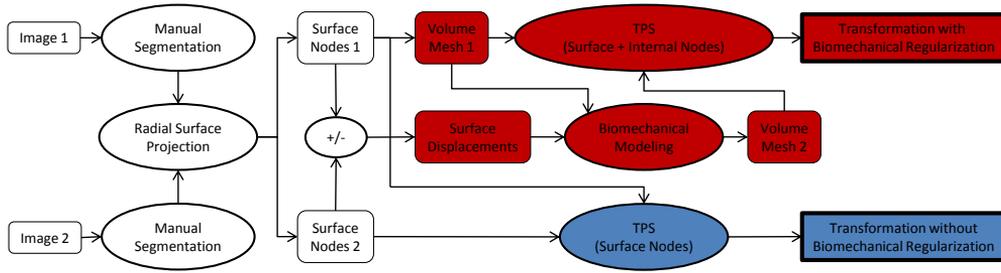


Figure 4.1: Flowchart showing the steps of our method. The red boxes indicate the additional steps taken in our method with biomechanical regularization, blue boxes indicate the steps for the regular non-rigid surface-based registration method.

biomechanical regularization are indicated in red. We compared our method with a regular surface based method (blue boxes).

4.2.1 Patient data

MR guided MR biopsy imaging data was collected from six consecutive patients who were scheduled for an MR guided prostate biopsy. MR images were acquired at the Radboud University Nijmegen Medical Centre on a 3-T MR system (MAGNETOM Skyra; Siemens, Erlangen, Germany). The dataset included T2-weighted images (slice thickness of 3 mm, in-plane resolution 0.8×0.8 mm) before and after insertion of a needle guide causing deformation of the prostate. The prostate was manually outlined in both images. The prostates had volumes in the range of 31 – 125 cc (Table 4.1).

4.2.2 Biomechanical modeling

A finite element (FE) model comprising 186 – 603 tetrahedral elements (Table 4.1) was constructed of the prostate from the outline before deformation (Figure 4.2). To deform the biomechanical model the surface nodes were displaced to match the deformed surface. The prostate surface node displacements were derived by radial projection from the prostate center of gravity (Figure 4.3).¹²¹ These surface node displacements were then used as a boundary condition in the FE simulation to predict the displacement of the internal mesh nodes. The initial and final positions of all nodes form a corresponding

Table 4.1: Patient data.

Patient	Prostate volume (cc)	No. of elements	No. of nodes	No. of surface points	No. of landmarks
1	42	186	61	48	7
2	33	251	74	52	8
3	43	457	126	86	7
4	61	603	150	92	8
5	31	365	101	68	7
6	125	563	138	83	8

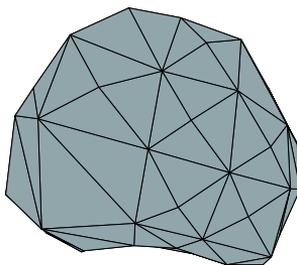


Figure 4.2: An example of a tetrahedral mesh obtained from the prostate contour before deformation caused by the needle guide.

node coordinate set. In the FE simulation, the prostatic tissue was assumed to behave as an isotropic, elastic material whose non-linear relationship between applied stress and strain is described by a neo-Hookean model with a shear and bulk modulus of respectively 7.5 kPa and 35 kPa.¹⁴¹ The simulations of prostate deformation were performed using a non-linear FE solver, which is implemented using a graphics processing unit (GPU) to enable parallel computations.¹⁴²

4.2.3 Surface-based registration

The non-rigid surface-based registration is based on a thin-plate spline (TPS) deformation algorithm, which aligns corresponding points. The three-dimensional (3D) TPS deformation field is used for non-rigid registration between the two images before and after deformation of the prostate. The two methods were compared, both of them rely on the TPS deformation algorithm. The first is the regular surface-based registration method, which uses only the corresponding prostate surface points for computation of the TPS

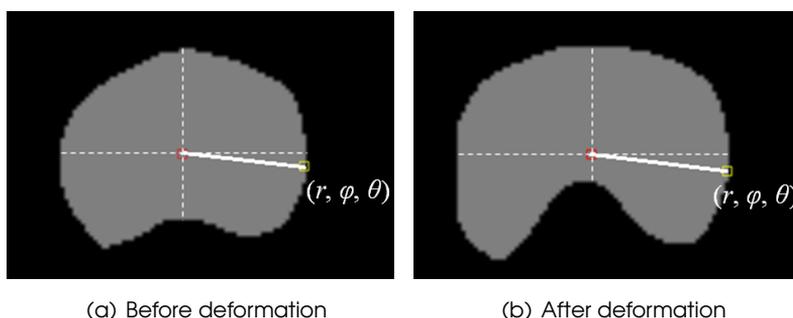


Figure 4.3: Equal angle parameterization to find corresponding surface points on manual prostate segmentations of images (a) before and (b) after deformation. The spherical coordinates of the surface point (yellow) were calculated with respect to the center of gravity (red) on the segmentation before deformation. The corresponding surface point on the image after deformation has the same angular coordinates (ϕ and θ) but a different radial distance (r).

deformation field. The second method uses both surface and internal node coordinates for computing the TPS and thus receives input from the biomechanical model.

4.2.4 Registration accuracy

A total of 45 patient specific anatomical landmarks (calcifications, cysts, etc.) in all regions of the prostate were manually annotated in both T2-weighted images to determine the TRE. These landmarks were equally divided over the six patients (Table 4.1). Nine of the landmarks were located in either apex or base (within first or last two slices of prostate visible in MR image). The TRE was defined as the Euclidean distance between registered (obtained from the deformation field) and real landmark positions (obtained from the deformed T2-weighted image) in 3D. We compared our method with biomechanical regularization to a regular surface-based registration method. A significant difference in TRE was tested with the non-parametric Wilcoxon rank-sum test.

4.3 Results

Figure 4.4 shows an example case with the real position of the anatomical landmarks before and after deformation of the prostate. The registered position of the landmarks after applying both methods is indicated as well. This case and others show that the TRE is smaller when biomechanical regularization was applied.

For each patient, the TREs of the landmarks determined by the surface-based registration with and without biomechanical regularization are shown in Figure 4.5. The overall median TRE of the surface-based registration with biomechanical regularization was 1.88 mm (range 0.59 – 6.83 mm), at the apex and base of the prostate the median TRE is 2.08 mm (range 1.52 – 4.23 mm). The overall median TRE without biomechanical regularization was 2.61 mm (range 0.69 – 8.18 mm) and was significantly different ($p = 0.003$). At apex and base the median TRE without biomechanical regularization was 2.46 mm and was not significantly different ($p = 0.190$).

4.4 Conclusion

In this paper we have shown that biomechanical regularization significantly improves a surface-based prostate registration method. Our method extends a non-rigid surface-based registration method with a biomechanical FE model which is able to better predict the internal deformation of the prostate. The median TRE of our method was 1.88 mm, which was significantly better than a median TRE of 2.61 mm obtained without using biomechanical regularization. These results are comparable to previous findings on non-rigid surface-based registration¹²¹ and biomechanical modeling based non-rigid registration.¹²²

In this study we used MR-MR registration for the evaluation of the accuracy. However, as our method is only based on prostate contour information it can also be applied for MR-US registration.

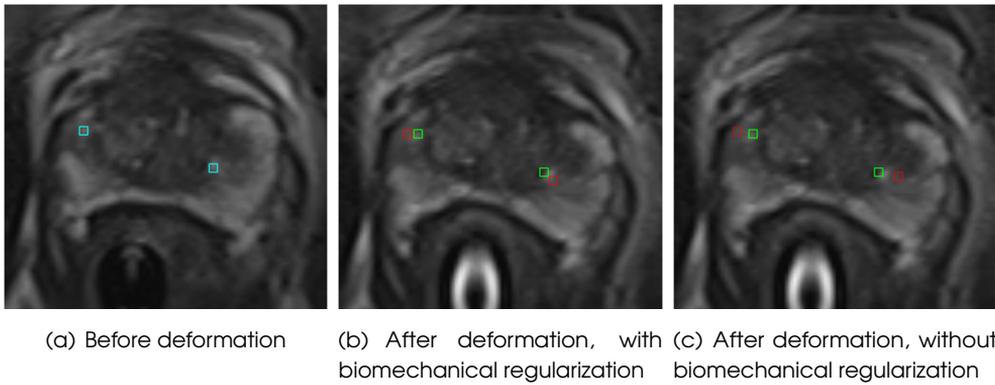


Figure 4.4: T2-weighted images of the prostate. (a) The left image shows the prostate before deformation with internal anatomical prostate landmarks in blue. (b)–(c) The middle and right images show the prostate after deformation with the real positions of the corresponding landmarks indicated in green and the registered landmarks in red after non-rigid surface-based registration (b) with and (c) without biomechanical regularization.

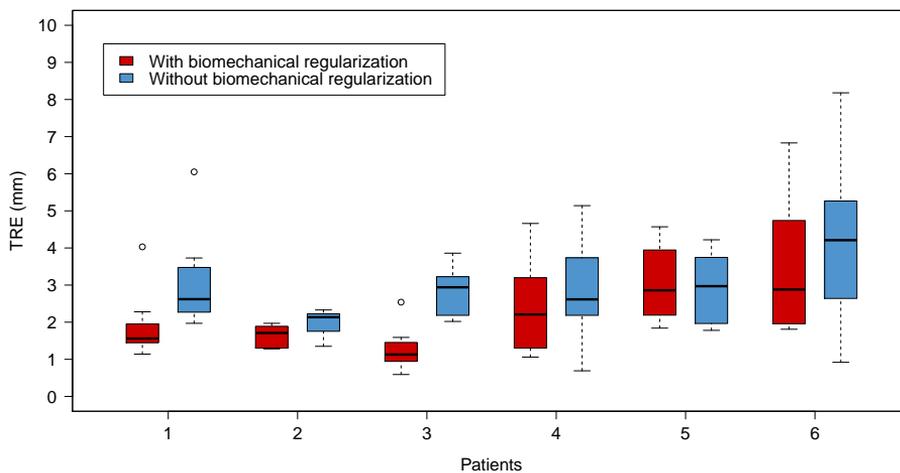


Figure 4.5: Boxplot comparing the TREs on a per patient basis of the non-rigid surface-based registration with biomechanical regularization (red) and without biomechanical regularization (blue).

5 – MR-TRUS registration

Wendy J. M. van de Ven, Yipeng Hu, Jelle O. Barentsz, Nico Karssemeijer, Dean Barratt, Henkjan J. Huisman

Original title: Biomechanical modeling constrained surface-based image registration for prostate MR guided TRUS biopsy

Published in: Medical Physics

Abstract

Purpose: Adding magnetic resonance (MR)-derived information to standard transrectal ultrasound (TRUS) images for guiding prostate biopsy is of substantial clinical interest. A tumor visible on MR images can be projected on ultrasound (US) by using MR-US registration. A common approach is to use surface-based registration. The authors hypothesize that biomechanical modeling will better control deformation inside the prostate than a regular non-rigid surface-based registration method. The authors developed a novel method by extending a non-rigid surface-based registration algorithm with biomechanical finite element (FE) modeling to better predict internal deformations of the prostate.

Methods: Data were collected from ten patients and the MR and TRUS images were rigidly registered to anatomically align prostate orientations. The prostate was manually segmented in both images and corresponding surface meshes were generated. Next, a tetrahedral volume mesh was generated from the MR image. Prostate deformations due to the TRUS probe were simulated using the surface displacements as the boundary condition. A three-dimensional thin-plate spline deformation field was calculated by registering the mesh vertices. The target registration errors (TREs) of 35 reference landmarks determined by surface and volume mesh registrations were compared.

Results: The median TRE of a surface-based registration with biomechanical regularization was 2.76 (0.81 – 7.96) mm. This was significantly different than the median TRE of 3.47 (1.05 – 7.80) mm for regular surface-based registration without biomechanical regularization.

Conclusions: Biomechanical FE modeling has the potential to improve the accuracy of multimodal prostate registration when comparing it to a regular non-rigid surface-based registration algorithm and can help to improve the effectiveness of MR guided TRUS biopsy procedures.

5.1 Introduction

Prostate cancer is a major international health problem. It is the most common diagnosed noncutaneous malignancy in men in the Western World and one of the leading causes of death from cancer.^{143,144} With growing prostate cancer awareness and increasing use of serum prostate-specific antigen (PSA) tests, the incidence of localized prostate cancer has grown tremendously. This test is very sensitive but nonspecific to prostate cancer and it has been shown that PSA-based screening followed by biopsy reduced mortality by 20%, but was associated with a high risk of overdiagnosis.⁵²

Transrectal ultrasound (TRUS) guided biopsy is currently the routine clinical standard method for making a definite diagnosis of prostate cancer and determining the treatment. Localization of malignant tissues on ultrasound (US) is difficult as up to 30% of prostate cancer lesions are isoechoic and not visible on gray scale US.^{23,59} This approach is therefore merely used to guide systematic biopsies in which specific regions throughout the prostate are sampled without knowing where tumors are located. This systematic TRUS guided approach may therefore lead to various sampling errors, e.g. missing significant cancer,³⁰ detecting insignificant cancer by chance,¹⁴⁵ or underestimating the cancer aggressiveness by sampling the less-aggressive tumor part.^{62,64,98} Underestimation of Gleason score may lead to incorrect patient risk stratification and suboptimal treatment choices. Therefore, a more accurate method for detecting prostate cancer and correctly determining the Gleason score on biopsy is needed.

Magnetic resonance imaging (MRI) has shown great potential in the localization and grading of prostate cancer.⁷³ A combination of anatomical T2-weighted MRI, dynamic contrast-enhanced MRI, and diffusion-weighted MRI improves the accuracy of prostate cancer detection over T2-weighted imaging alone.^{75,76} Arumainayagam *et al.*¹⁰³ showed that the negative predictive value of multiparametric (mp)-MRI for excluding significant prostate cancer was 89%. This means that mp-MRI can be used to help men at risk and decide if they should proceed to prostate biopsy. Parts of the prostate that were negative at mp-MRI do not require biopsy, leading to a reduction of the total number of biopsies.

Two targeted MR guided prostate biopsy approaches are under investigation, both using prebiopsy detection MRI to define potential targets.¹⁰⁶ The first is direct in-bore MR guided MR biopsy. As this technique is performed in-bore, it is less prone to fusion errors and therefore likely to be the most accurate MR guided technique. It has been shown that this direct in-bore MR guided MR biopsy significantly increases the tumor detection rate when comparing it to systematic TRUS guided biopsy.^{94,95} However, despite its versatile capabilities, MRI is not as widely available or as easy to apply to prostate imaging as is US. Issues of cost, access, scanner time, technical requirements, and radiologists' acceptance and understanding of the procedure are continuing challenges.¹⁰⁶

The second MR guided approach is MR guided TRUS biopsy, which is a potentially more accessible and practical solution. Preacquired MR images can be used to enhance TRUS imaging and improve needle guidance by registration of the two modalities.¹⁰⁷ Available methods vary in accuracy, speed, and user-friendliness. Registration can either

be performed mentally or computationally. The accuracy of mental fusion depends very much on the skills of the operating physician and shows some contradictory results.^{111,112} Computational registration of MR and TRUS images is potentially a more accurate way of image fusion requiring less operator skills but more computation time. MR image information is very different from information obtained with US images. To our knowledge, current published MR-US registration methods are therefore often surface-based, i.e. the capsule is aligned by registering a surface representation reconstructed typically from cross-sectional contours. Computer-assisted registration methods can be roughly subdivided into two categories: rigid and non-rigid registration methods. Different registration methods exist,^{29,113,115–118} but in general, deformable non-rigid registration is more accurate than rigid registration.^{112,120,121} However, many methods are based on relatively simple volume interpolation, which are not always physically plausible.¹²²

Internal prostate gland motion and deformation can be better predicted by applying biomechanical modeling using finite element (FE) analysis.^{123–125} A biomechanical model of the prostate can be constructed by assigning boundary conditions and elastic properties to the tissue. The prostate deformation can be simulated and internal gland motion can then be predicted.

The clinical value of MR guided TRUS biopsies is being investigated in several studies using different commercially available systems based on different registration methods.^{108,109} Overall, the results show that targeted prostate biopsy using MR-US fusion has a significantly higher tumor detection rate compared to conventional TRUS guided biopsies, especially for the clinically significant tumors.^{111,112,126–129} However, for correct Gleason grading with MR guided TRUS biopsy, an accurate spatial registration of MR and US images is required.¹³⁰ Current MR-US fusion systems do not reach this accuracy and therefore require improvement to be able to (partly) replace in-bore MR guided biopsies.

In this paper, we evaluate a non-rigid surface-based registration method combined with biomechanical modeling for transrectal MR guided TRUS biopsies. Regular non-rigid surface-based registration methods often use simple volume interpolation. We hypothesize that a biomechanical model of soft-tissue deformation can better predict the actual internal prostate deformation, resulting in a more accurate registration method. We therefore extend a non-rigid surface-based registration method¹²¹ with the biomechanical FE model described by Hu *et al.*¹²⁵ The deformation field was calculated by applying a thin-plate spline (TPS) algorithm to the FE mesh nodes (both internal and surface nodes). The registration accuracy was determined by calculating the target registration error (TRE) using internal anatomical prostate landmarks visible in both MR and US images.

This method was also used in our previous work,¹⁴⁶ where we applied the biomechanical modeling constrained registration algorithm to MR-MR registration. The method is now adapted so that it can be applied to MR-TRUS registration. Additionally, an initial rigid alignment is required for MR-TRUS registration. Also, we improved simulation

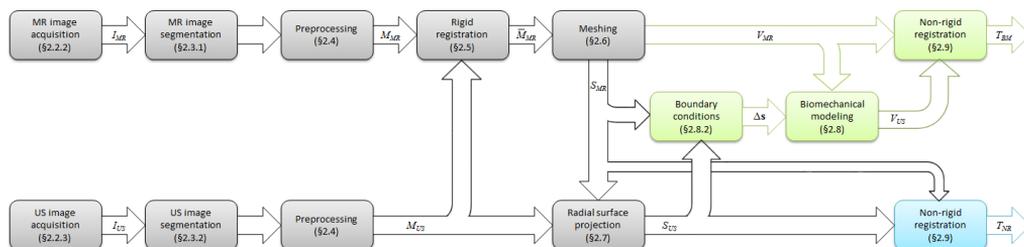


Figure 5.1: Flowchart showing the steps of our method. The green boxes indicate the additional steps taken in our method with biomechanical regularization; blue boxes indicate the steps for the regular non-rigid surface-based registration method. The gray boxes are common between both methods.

convergence by better conditioning of the mesh model. And, we automated the parameter settings for meshing and simulation. Compared to our previous work, the registration process is now fully automated and requires only manual intervention for the prostate segmentation.

5.2 Materials and methods

5.2.1 Overview

A schematic overview indicating the different steps of the method we developed is shown in Figure 5.1. The steps involved are summarized as follows:

- Acquire MR and TRUS images (Section 5.2.2).
- Segment the prostate gland in both MR and TRUS images (Section 5.2.3).
- Regularize the shape of the prostate gland by applying a smoothing filter (Section 5.2.4).
- Align the masked prostate images by rigid registration (Section 5.2.5).
- From the rigidly registered MR prostate mask, construct a three-dimensional (3D) tetrahedral volume mesh of the prostate gland (Section 5.2.6).
- Determine the surface displacements by applying radial surface projection to the prostate masks (Section 5.2.7).
- The deformation of the prostate due to the TRUS probe is simulated by a biomechanical model. The MR volume mesh will serve as input and the surface displacements are the boundary conditions. The final mesh will correspond with the prostate on the TRUS image (Section 5.2.8).
- A TPS based non-rigid registration algorithm is applied to construct the deformation field (Section 5.2.9).

The green boxes in the schematic overview indicate the additional steps taken for our surface-based registration method with biomechanical regularization. We compared our method with a regular surface-based method (blue boxes). The software system was implemented in MeVisLab¹⁴⁷ and automates the entire process of rigid registration, biomechanical modeling, and non-rigid TPS-based registration. Additionally, we used

Matlab, TetGen,¹⁴⁸ and NiftySim¹⁴² for meshing and modeling (Section 5.2.8). Preprocessing and evaluation are done in MeVisLab.

5.2.2 Data collection

Patient selection

Data in this study were collected from the ongoing Prostate Cancer Molecular Medicine (PCMM) project. The PCMM project is a large multicenter study focusing on prostate cancer. It addresses two major clinical needs: the need to reduce overdiagnosis and overtreatment of prostate cancer and the need for better therapy monitoring techniques for advanced disease. The PCMM study procedure involves the collection of biomaterials and an extensive imaging protocol including mp-MRI (T2-weighted, dynamic contrast-enhanced, and diffusion-weighted MRI) and US (gray scale, Doppler, and contrast-enhanced imaging) examination. The study was approved by the medical ethical committee, and all patients gave their written informed consent.

The Radboud University Medical Center in Nijmegen, the Netherlands, is one of the centers recruiting patients for the PCMM project. Data from ten patients diagnosed with prostate cancer at our center were collected to validate our registration method.

MR image acquisition

A MR imaging detection or staging protocol was used to acquire mp-MR images of all patients. A 3-T MR system (MAGNETOM Trio/Skyra; Siemens, Erlangen, Germany) with either a pelvic phased-array coil ($n = 6$) or an endorectal coil ($n = 4$) was used. For this study, we are only interested in the 3D T2-weighted transversal images. These had an in-plane resolution of 0.402 – 0.625 mm and a slice thickness of 3.0 – 3.6 mm.

TRUS image acquisition

TRUS images were acquired on a Toshiba Aplio XG machine (Toshiba Medical Systems, Japan) using a 4D end-firing transrectal transducer (Toshiba PVT-681MV; Toshiba Medical Systems, Japan). A 3D gray scale TRUS image of the prostate was made by automatically sweeping through the prostate with a scanning angle of 90° at a rate of 0.1 volumes/s. The image data were exported from the US machine and converted from a spherical to a Cartesian representation with an isotropic voxel size of 0.2 mm.

5.2.3 Segmentation

MR images

For the purposes of this study, the diagnostic T2-weighted transversal MR image of patient i (I_{MR}^i , where $i = 1 \dots 10$) was segmented by manually defining the contour of the prostate in every slice. The segmentations were made by a researcher (W.J.M.v.d.V.), who has three years of experience in prostate image analysis.

TRUS images

Due to the high resolution of the Cartesian TRUS images (I_{US}^i), these were downsampled to an isotropic resolution of 0.8 mm for segmentation purposes only (i.e. limiting the

amount of slices requiring segmentation). Prostate segmentations were manually made by the same prostate researcher (W.J.M.v.d.V.) who performed the MR image segmentations. To improve the segmentation of the prostate in I_{US}^i , three orthogonal projections were used. In each of the three views, the prostate contour was outlined in every 5-6 slices and interpolated in the intermediate slices using prior anatomical knowledge of the smoothness of the prostate gland (i.e. no bumps and pits). To create one image mask of the prostate contour, the orthogonal segmentations were interpolated by computing a 3D implicit function that reconstructs a surface as described by Heckel *et al.*¹⁴⁹ This 3D segmentation algorithm reduces segmentation times compared to slicewise manual segmentation.

5.2.4 Preprocessing

The MR image masks are resampled to an isotropic voxel size of 0.8 mm, matching the TRUS image masks. This is required to create a smoother volume mesh without a steplike surface. To reduce image noise and further regularize the surface shape, we applied a smoothing filter on masked MR and TRUS images. An isotropic Gaussian smoothing filter ($\sigma = 5$ voxels = 4 mm) using an approximate recursive infinite impulse response filter to speed up the computation was used.¹⁵⁰ Finally, a threshold was applied to create a binary image.

5.2.5 Rigid registration

The MR and TRUS images have a different world coordinate system. A rigid registration step aligns the binary prostate masks of both images. The smoothed TRUS image mask (M_{US}^i) is considered the fixed image and the smoothed MR image mask (M_{MR}^i) is the moving image. The objective is to find the rigid transformation (T_R) that optimizes the alignment.

The first step requires an initialization process to align the prostate center of gravity (CoG) of M_{MR}^i with the prostate center of gravity of M_{US}^i . This step substantially speeds up the rigid alignment as the prostates are usually far apart in space. Left-right orientation is matched before initialization. Next, the rigid registration algorithm optimizes translation and rotation in 3D without changing shape or scale. Image similarity was measured using sum of squared differences between the two prostate masks.¹⁵¹

5.2.6 Meshing

The rigidly registered MR image $\bar{I}_{MR}^i = T_R(I_{MR}^i)$ is now roughly aligned to the corresponding TRUS image I_{US}^i , i.e. positional and rotational differences are corrected. For a more accurate registration, the \bar{I}_{MR}^i needs to be deformed so that the segmented prostate shape (\bar{M}_{MR}^i) will fit on the prostate mask in M_{US}^i . A biomechanical model of the MR prostate will simulate the deformation due to the TRUS probe by taking surface displacements into account.

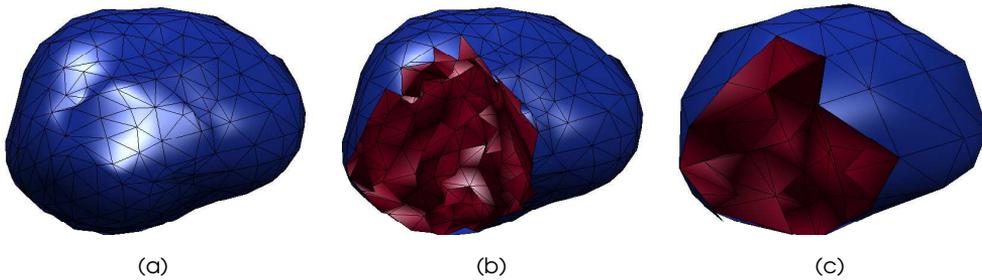


Figure 5.2: An example showing a tetrahedral volume mesh of the prostate contour obtained from the masked MR image: (a) shows the outer prostate surface; (b) shows some of the inner elements by taking out a quarter of the mesh; and (c) shows a coarser mesh of the same prostate containing less elements of a larger volume.

Prior to the actual simulation, a volume mesh of the MR prostate needs to be constructed. The rigidly registered MR image mask ($\bar{M}_{MR}^i = T_R(M_{MR}^i)$) is used to generate a volume mesh of the prostate (V_{MR}^i) consisting of Delaunay tetrahedra. To obtain the best quality of the tetrahedral volume mesh, we applied the refinement algorithm of Shewchuk¹⁵² as implemented by the TetGen mesh generator, which is a tool for generating tetrahedral meshes from 3D domains.¹⁴⁸ The quality of a tetrahedral mesh can be measured by the radius-edge ratio,¹⁵³ which we restricted to a maximum of 1.0. An example of a volume mesh is shown in Figure 5.2.

The number of elements and nodes in a mesh will first of all depend on the prostate volume. Second, the volume mesh can be further characterized by size requirements for the tetrahedra in the mesh and for the triangles describing the boundary surface mesh. We investigated the effect of the number of nodes on the registration accuracy by generating different volume meshes for each prostate.

5.2.7 Radial surface projection

To correct for the shape differences of the prostate between \bar{I}_{MR}^i and I_{US}^i , we need to determine the surface displacements. These surface displacements can be derived by subtracting surface node coordinates. Hence, we need to construct meshes with anatomically corresponding surface vertices of the rigidly aligned prostate masks \bar{M}_{MR}^i and M_{US}^i .

To achieve corresponding prostate surface meshes of \bar{M}_{MR}^i and M_{US}^i , we applied an algorithm we call radial surface projection. This method is based on the equal angle parameterization described by Karnik *et al.*¹²¹ Radial surface projection refers to the generated MR volume mesh (V_{MR}^i) which contains a number of surface nodes, i.e. mesh nodes located on the prostate surface (S_{MR}^i). The spherical coordinates of these surface mesh nodes can be determined. Hereby, we defined the prostate center of gravity of \bar{M}_{MR}^i as origin of the spherical coordinate system. Every n^{th} surface node of patient i will now be described by three numbers: the radial distance to the origin (r_{MR}^{in}), its polar angle (θ^{in}), and the azimuth angle (ϕ^{in}) (Figure 5.3).

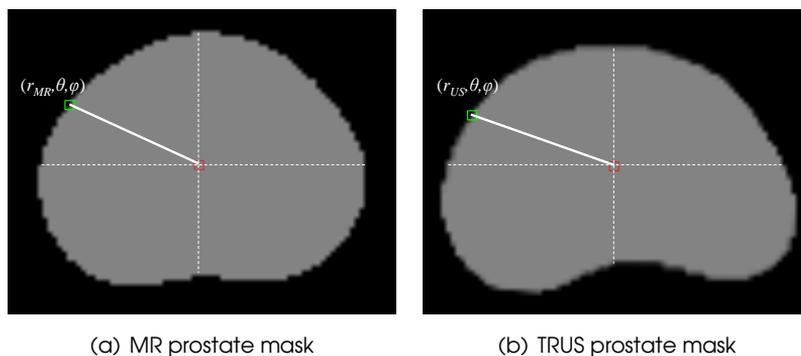


Figure 5.3: Radial surface projection to find corresponding surface points on manual prostate segmentations of MR images and TRUS images. The spherical coordinates of the surface point (green) were calculated with respect to the center of gravity (red) on the segmented MR image (a). The corresponding surface point on the TRUS image (b) has the same angular coordinates (ϕ and θ) but a different radial distance (r_{MR} and r_{US}).

To create a corresponding surface mesh of the prostate from the masked TRUS image (S_{US}^i), the two angular coordinates (θ^{in} and ϕ^{in}) are important. The prostate center of gravity of M_{US}^i is determined and is defined as the origin of the spherical coordinate system. Rays were shot from the origin at the same angular coordinates as derived from the MR surface nodes. For each ray, the point of intersection with the TRUS prostate surface is determined. At this point, a surface node is placed with coordinates $(r_{US}^{in}, \theta^{in}, \phi^{in})$. All surface nodes together will form the TRUS surface mesh (S_{US}^i), which will correspond to the MR surface mesh (S_{MR}^i).

5.2.8 Biomechanical modeling

A biomechanical model of the prostate can predict the deformation due to the insertion of a TRUS probe.¹²⁵ For an accurate registration that can be used during intraoperative TRUS guided procedures, the MR images need to be deformed to fit on the TRUS images. The MR volume mesh of the prostate (V_{MR}^i) will be used as input. For the biomechanical FE simulations of prostate deformation, material properties of the prostate and boundary conditions need to be specified. The simulations were performed using a nonlinear FE solver (NiftySim), which is implemented using a graphics processing unit (GPU) for significant solution speed gains.^{142,154} The simulations were executed on a desktop PC with a 2.26 GHz Intel® Xeon® dual CPU processor and 24 GB of RAM installed with a NVIDIA® GeForce™ 570 GTX. Depending on the number of elements, a simulation took around 5 – 60 s.

Material properties

In the FE simulation, the prostatic tissue was assumed to behave as a homogeneous, isotropic, nonlinear elastic material. Such materials are fully characterized by two out of four elastic moduli: bulk modulus, shear modulus, Young's modulus, and Poisson's

ratio.¹⁵⁴ In our case, we use the shear and bulk moduli to describe the nonlinear relationship between applied stress and strain of the neo-Hookean model of the prostate. These were set at, respectively, 7.5 and 35 kPa (corresponding to a Poisson ratio of 0.40).¹⁴¹

Boundary conditions

Boundary conditions are required to deform the biomechanical model of the prostate. As the surface displacements can be determined from the prostate contours in both modalities, these will be used as boundary condition. The MR surface nodes were displaced to match the deformed TRUS surface of the prostate. The surface node displacements were derived from the corresponding surface meshes (S_{MR}^i and S_{US}^i) generated by the radial surface projection algorithm described in Section 5.2.7. The spherical coordinates of the surface nodes are converted to a Cartesian coordinate system. The n^{th} surface node of patient i now has the coordinates $\mathbf{s}_{MR}^{in} = (s_{MR,x}^{in}, s_{MR,y}^{in}, s_{MR,z}^{in})$ and $\mathbf{s}_{US}^{in} = (s_{US,x}^{in}, s_{US,y}^{in}, s_{US,z}^{in})$ for S_{MR}^i and S_{US}^i , respectively. Surface displacements are calculated by

$$\Delta \mathbf{s}^{in} = \mathbf{s}_{US}^{in} - \mathbf{s}_{MR}^{in}. \quad (5.1)$$

These surface node displacements were then used as a boundary condition in the FE simulation, thereby restricting the movement of the nodes. The simulation predicts the displacement of the internal mesh nodes of V_{MR}^i and gives the locations of corresponding internal nodes of V_{US}^i .

5.2.9 Non-rigid surface-based registration

The non-rigid surface-based registration is based on a TPS deformation algorithm, which aligns corresponding point sets. The 3D TPS deformation field is used for non-rigid registration between the MR and TRUS images of the prostate. A corresponding point set is formed by all volume mesh nodes, i.e. surface nodes and internal nodes, of the MR volume mesh (V_{MR}^i) and the corresponding TRUS volume mesh (V_{US}^i). Correspondence of surface nodes is created by radial surface projection and correspondence of internal nodes is achieved by the biomechanical model. The resulting transformation (T_{BM}) can be applied to \bar{I}_{MR}^i to achieve biomechanical modeling constrained non-rigid surface-based registration to I_{US}^i .

Our method was compared to a regular non-rigid surface-based method, which also relies on the TPS deformation algorithm. In this case, only the corresponding prostate surface mesh nodes (S_{MR}^i and S_{US}^i) were used for computing the TPS deformation field, resulting in the non-rigid transformation T_{NR} . This method does not require the simulation step and therefore does not receive input from the biomechanical model.

5.2.10 Evaluation

Reference landmarks

Patient-specific anatomical landmarks were used as reference landmarks for the estimation of the registration accuracy. These landmarks were identified manually by the

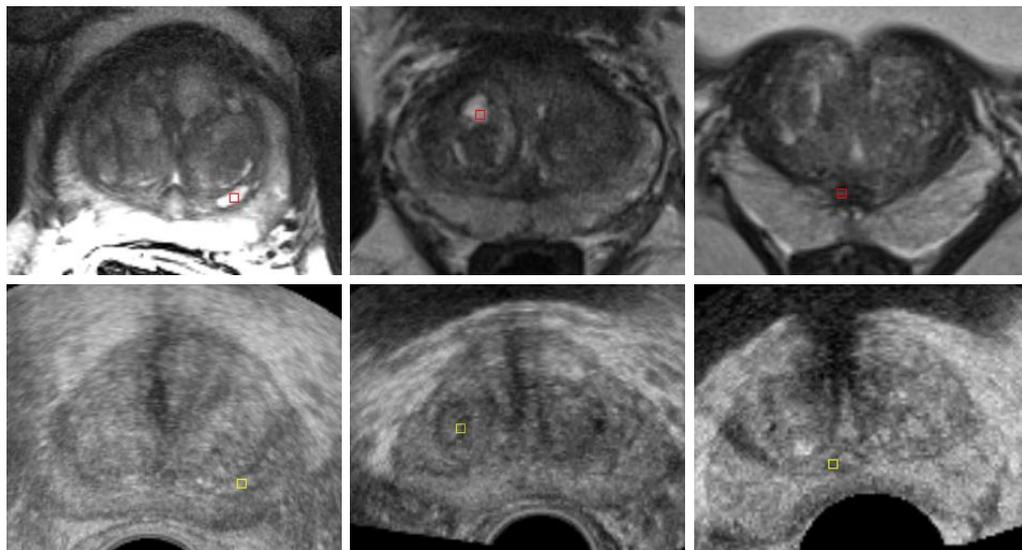


Figure 5.4: Some examples of anatomical reference landmark points. The three columns show reference landmarks in the corresponding MR images (top row) and TRUS images (bottom row) of three different patients.

prostate researcher (W.J.M.v.d.V.) who also performed the segmentations. All landmarks were checked by an interventional-radiologist (J.J.F.) with expertise in imaging techniques in prostate cancer. Reference landmarks are anatomical structures visible in both MR and TRUS images (examples in Figure 5.4). These are, for example, the urethra and the ducts of the seminal vesicles, but also calcifications and cysts. Calcifications are hyperechoic on the TRUS images and have a low intensity on the T2-weighted MR images; cysts are hypoechoic on the US images and appear as high intensity features in the MR images. The j^{th} sets of 3D coordinates of the landmark points in patient i were recorded in both \bar{I}_{MR}^i and I_{US}^i as $\bar{\mathbf{p}}_{MR}^{ij} = (\bar{p}_{MR,x}^{ij}, \bar{p}_{MR,y}^{ij}, \bar{p}_{MR,z}^{ij})$ and $\mathbf{p}_{US}^{ij} = (p_{US,x}^{ij}, p_{US,y}^{ij}, p_{US,z}^{ij})$, respectively.

A total of 35 reference landmarks in all regions of the prostate were annotated in both MR and TRUS images to determine the TRE. These landmarks were divided over the ten patients (Table 5.2). The mean distance (\pm standard deviation) of the landmarks to the prostate center of gravity is 12.02 ± 3.86 mm with a range of 3.80 – 19.93 mm.

Registration accuracy

The registration accuracy of the registration methods was evaluated by determining the TRE. The TRE was defined as the 3D Euclidean distance between registered (obtained from the deformed MR image \bar{I}_{MR}^i) and real positions (obtained from the TRUS image I_{US}^i) of corresponding pairs of reference landmarks. The initial TRE_R^{ij} for a given landmark j of patient i can be calculated after rigid alignment of I_{MR}^i and I_{US}^i . The regular non-rigid surface-based registration will provide TRE_{NR}^{ij} , and our biomechanical modeling constrained non-rigid surface-based registration TRE_{BM}^{ij} .

The TRE_m^{ij} for method m being either R for rigid, NR for non-rigid, or BM for biomechanical modeling constrained registration is

$$TRE_m^{ij} = \|\mathbf{d}_m^{ij}\| = \sqrt{(d_{m,x}^{ij})^2 + (d_{m,y}^{ij})^2 + (d_{m,z}^{ij})^2}, \quad (5.2)$$

where

$$\mathbf{d}_R^{ij} = (\mathbf{p}_{US}^{ij} - \bar{\mathbf{p}}_{MR}^{ij}), \quad (5.3)$$

$$\mathbf{d}_{NR}^{ij} = (\mathbf{p}_{US}^{ij} - T_{NR}(\bar{\mathbf{p}}_{MR}^{ij})), \text{ and} \quad (5.4)$$

$$\mathbf{d}_{BM}^{ij} = (\mathbf{p}_{US}^{ij} - T_{BM}(\bar{\mathbf{p}}_{MR}^{ij})). \quad (5.5)$$

Statistical analysis

Statistical analyses were performed using RStudio¹⁵⁵, the R package ‘nlme’ was used for linear mixed effects modeling.¹⁵⁶ Linear mixed effects statistical method can model both fixed and random effects and handle repeated measurements. These effects can be statistically evaluated using one test instead of less powerful multiple tests. We used a linear mixed effect model to evaluate the effect of the number of elements, nodes, and surface points on the TRE. Significant differences between the different registration methods were also determined by a linear mixed effect model. For the model, we considered the number of elements, nodes, and surface points as fixed effects. The landmarks were considered random effects. The TREs were evaluated against all these effects in one linear mixed effect model, giving p -values for each of the effects.

5.3 Results

Figure 5.5 shows some example cases with the reference position of the anatomical landmarks on MR and TRUS images of the prostate. The registered position of the landmarks after applying both registration methods is indicated in the TRUS image as well. These cases and others show that the TRE is smaller when biomechanical regularization was applied.

We evaluated the effect of the number of elements, nodes, and surface points on the registration accuracy for both the regular surface-based registration method and our biomechanical constrained registration method. In total, we performed 360 simulations for all ten patients. Some simulations diverged due to inadequate mesh quality (1706/3600). Also, the more complex meshes with more elements can lead to divergence. This can be solved by reducing the time step, which we did not do in this study. We were able to calculate a TRE on reference landmarks 8354 times. For these converging simulations, the number of elements varied between 33 and 3632, the number of nodes between 19 and 681, and the number of surface points between 18 and 218. On a landmark basis, we determined whether the number of elements, nodes, or surface points had an effect on

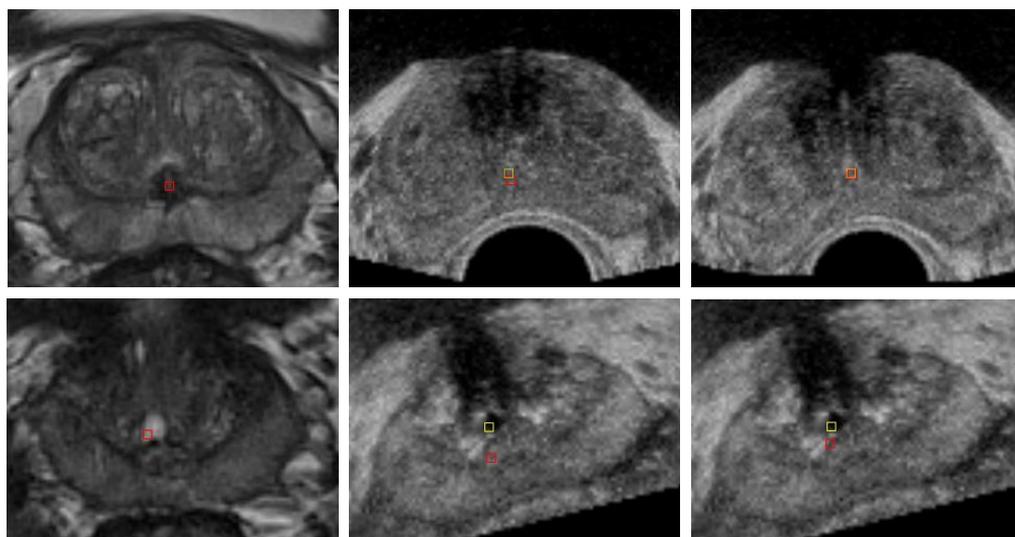


Figure 5.5: Examples from two different patients showing the real and registered positions of reference landmarks. Each of the two rows contains corresponding MR and TRUS images of the prostate of one patient. The left column shows the prostate MR image with an internal anatomical prostate landmark in red. The middle and right images show the corresponding prostate TRUS images of that patient where the yellow squares indicate the real positions of the reference landmarks and the red squares indicate the registered positions. The middle column shows the results of the regular non-rigid surface-based registration method and the right column of the biomechanical constrained registration method. Both cases show that the biomechanical model decreased the distance between the yellow and red squares (the TRE) and thus improved the registration accuracy. The example in the top row has a more accurate registration accuracy than the example in the bottom row for both registration methods.

the TRE and whether the biomechanical model improved the accuracy of the non-rigid registration method. A linear mixed effects model showed no significant difference for either of the mesh variables ($p > 0.35$), but did show that the biomechanical constrained registration method was significantly better than the regular non-rigid surface-based registration method ($p < 0.001$).

The results with the mesh characteristics in Table 5.1 were used for more in-depth analysis. For each patient, the TREs of the landmarks determined by the initial rigid and the non-rigid surface-based registration with and without biomechanical regularization are shown in Table 5.2. The overall median TRE of the initial rigid registration method was 3.64 mm (range 0.72 – 8.95 mm). The median TRE of the non-rigid surface-based registration without biomechanical regularization was 3.47 mm (range 1.05-7.80 mm). The overall median TRE of the non-rigid surface-based registration method extended with biomechanical regularization was 2.76 mm (range 0.81-7.96 mm). The Bland-Altman plot in Figure 5.6 shows the differences versus the averages of the non-rigid method with and without biomechanical modeling on a pairwise basis. The mean difference is -0.31 , indicating that on average, the TRE of the biomechanical modeling is smaller than the

Table 5.1: Characteristics of the prostate volume meshes obtained with an element volume bound of 0.15 ml and a coarse surface mesh representation. For each patient, the prostate volumes (determined by calculating voxels in segmented MR and TRUS images) are shown. Also, the number of elements, nodes, and surface points are indicated for the tetrahedral meshes of the prostate. The last column indicates the minimum and maximum displacements of the surface points. MR images of patients 2, 3, 4, and 8 were taken with an endorectal coil.

Patient	Prostate volume (cm ³)		No. of elements	No. of nodes	No. of surface points	Range of surface displacements (mm)
	MR	TRUS				
1	55	54	226	71	54	1.0 – 10.1
2	22	26	47	23	22	0.5 – 5.0
3	41	48	130	46	38	1.3 – 6.4
4	28	22	67	30	28	1.4 – 8.4
5	52	48	165	57	47	2.1 – 10.5
6	36	34	137	50	42	2.1 – 7.2
7	32	40	117	42	34	3.2 – 13.9
8	36	36	159	55	46	1.1 – 4.5
9	48	53	222	64	44	1.4 – 7.4
10	54	54	259	72	50	2.9 – 8.4

Table 5.2: Median TREs computed for registrations using the initial rigid registration method (R), the regular non-rigid surface-based registration method (NR), and the biomechanical modeling constrained surface-based registration method (BM).

Patient	No. of landmarks	Initial TRE _R (mm)	Final TRE _{NR} (mm)	Final TRE _{BM} (mm)
1	5	2.87	2.15	2.37
2	2	3.80	3.27	3.35
3	4	2.75	3.26	3.18
4	3	4.78	2.99	3.39
5	2	5.72	5.03	4.52
6	5	4.31	2.43	2.13
7	5	3.09	4.92	2.75
8	2	4.16	3.90	3.87
9	3	2.75	2.73	2.76
10	4	4.61	5.24	3.79
All (range)	35	3.64 (0.72 – 8.95)	3.47 (1.05 – 7.80)	2.76 (0.81 – 7.96)
Mean ± std		4.06 ± 2.20	3.93 ± 2.08	3.62 ± 2.13

regular non-rigid method. Also, the correlation of the TRE with the distance to the center of gravity is shown (Figure 5.7).

5.4 Discussion

Our biomechanical modeling constrained registration method has a median registration accuracy of 2.76 mm. The results are comparable with the results reported by Hu *et al.*¹²⁵ In their study, the median TRE is 2.40 mm after a deformable ‘model-to-image’ registration of MR and 3D TRUS images of the prostate. The biomechanical model significantly improved the regular non-rigid surface-based registration method and was also significantly better than the initial rigid registration, especially in strongly deformed shapes.

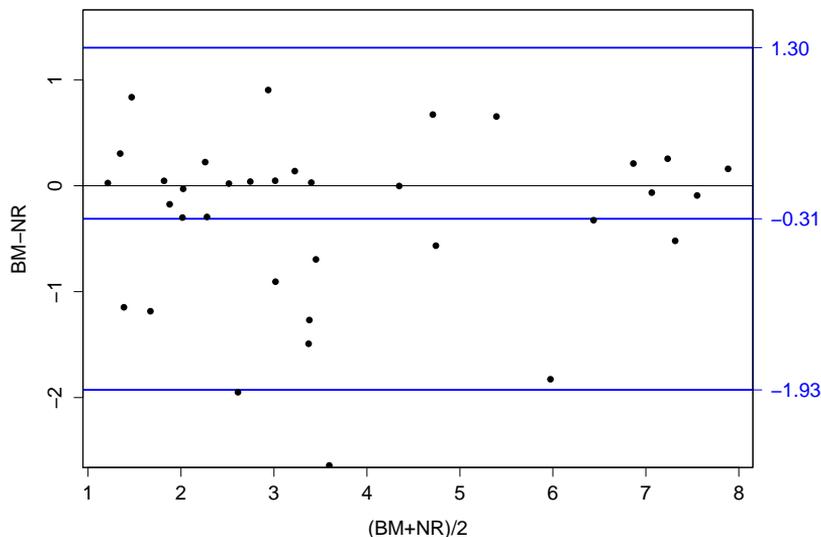


Figure 5.6: A Bland-Altman plot showing the differences versus the averages of the non-rigid method with (BM) and without (NR) biomechanical modeling on a pairwise basis. The points correspond to the 35 landmarks. The middle blue line indicates the mean difference and the top and bottom lines the 95% limits of agreement.

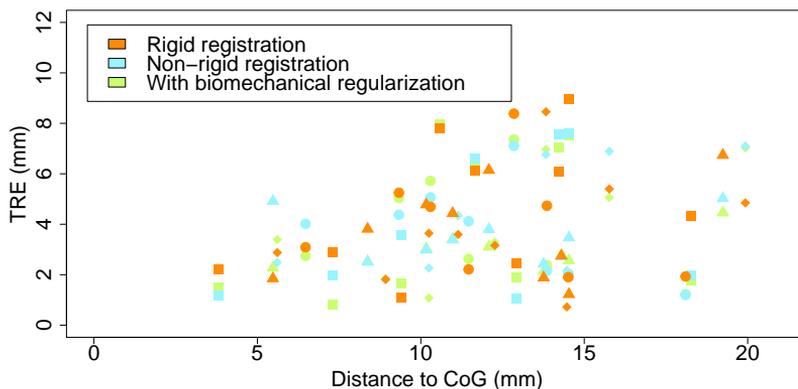


Figure 5.7: Scatterplot showing the TRE versus the distance to the prostate CoG of the initial rigid (orange) and the non-rigid surface-based registration with biomechanical regularization (green) and without biomechanical regularization (blue). Points corresponding to the same landmark can be found on one vertical line and are distinguished by the use of different symbols.

Our method is based on prostate contour information and can thus be applied to MR images with or without endorectal coil.

We compared our biomechanical modeling constrained method with the non-rigid surface-based registration algorithm published by Karnik *et al.*¹²¹ They do not use a biomechanical model to account for prostate deformations. Karnik *et al.*¹²¹ applied the non-rigid surface-based method to US-US registration and compared it to rigid surface-based registration as well as rigid and non-rigid image-based registration. Images were obtained at the beginning and end of the biopsy procedure. The mean TRE they found for the non-rigid surface-based registration was 2.09 mm. This is slightly better than our method, but this can be explained by the fact that images are from the same modality (both US) and taken only minutes after each other.

Our registration method extends the regular non-rigid surface-based method of Karnik *et al.*¹²¹ with the biomechanical model published by Hu *et al.*¹²⁵ Our method differs from that of Hu *et al.*¹²⁵ in that the biomechanical model is now applied to the more common transrectal MR guided TRUS biopsies instead of transperineal biopsies. Hu *et al.*¹²⁵ performed 500 simulations per patient to create a statistical motion model which is used for a model-to-image registration. We create a prostate-shape specific biomechanical model of the prostate for each patient and the results of the modeling step are used in the final TPS based non-rigid registration step. Our intention is to do only one simulation per patient and include specific knowledge of surface displacements. Our purpose was to show that a regular non-rigid method can be easily adapted by adding a biomechanical FE model which significantly improves the registration accuracy.

The distribution of reference landmarks with respect to the prostate center of gravity varies between 3.80 and 19.93 mm. The larger TREs correspond to landmarks that are further away from the center of gravity, probably caused by the prealignment of the centers (Figure 5.7). In case the prealignment is not optimal, this will cause a larger error further away from the center. In Table 5.2 it can be seen that for patient 3, the initial rigid registration performs better than any of the two non-rigid methods. This might be explained by the small deformation of the prostate in this patient. Also, for patients 7 and 10, the median TRE of the rigid registration is better than that of the regular non-rigid registration. This is mainly caused by the landmarks in the center of the prostate where the rigid method outperforms the regular non-rigid method. For the landmarks that are closer to the surface, the non-rigid method is better. However, for these two patients, the biomechanical regularization does improve the non-rigid registration and gives smaller median TREs than the rigid registration method.

The divergence of simulations may be solved by reducing the time step slightly or changing the meshing parameters. Varying the number of elements, nodes, and surface points did not have a significant effect on the registration accuracy of either the regular non-rigid registration or the biomechanical modeling constrained registration method. This means that the mesh characteristics do not matter and the results are parameter independent. Regardless the number of elements/nodes/surface points, the

biomechanical modeling did significantly improve the registration accuracy of the regular non-rigid surface-based registration method.

We have recently shown that for correctly Gleason grading 95% of the tumors, a registration accuracy of 1.9 mm is required.¹³⁰ By taking more than one biopsy from the same target, the probability of hitting the tumor can be increased. For our method with an accuracy of 2.76 mm, two or three biopsies would be sufficient for having a reasonable chance of hitting the tumor. This hit-rate depends on the volume of the target. When assuming the hotspot volume distribution published in Van de Ven *et al.*,¹³⁰ the hit-rate will be 85.2%, 97.8%, and 99.7% for 1, 2, and 3 biopsies, respectively. The regular non-rigid registration method has a lower hit-rate, being 75.1%, 93.8%, and 98.5% for 1, 2, and 3 biopsies, respectively. The increased accuracy thus allows for less biopsies to achieve 95% correct grading.

Clinical implementation of MR guided TRUS biopsy does, however, not only require accurate segmentation and registration. As is the case for any MR guided biopsy technique, good quality MR image and image interpretation are essential for carrying out the biopsy procedure in clinic.¹⁵⁷ Minimal requirements for multiparametric prostate MR image acquisition and standardization for reporting (PI-RADS) have recently been published,⁸⁵ which will help to improve the general reliability of the techniques.

A limitation of a surface-based registration method is that it depends on prostate segmentation, which is time consuming and operator-dependent. Inaccurate segmentation of either of the two images would negatively affect the registration accuracy. It was found that the interobserver variability of MR prostate segmentation had a median Dice similarity coefficient (DSC) of 0.87.¹⁵⁸ Automatic segmentation would speed up the process of segmentation and also limit the interobserver variability. But, automatic prostate segmentation is challenging for both MR and TRUS images¹⁵⁹. The PROMISE12 challenge (<http://promise12.grand-challenge.org/>) compares some recently published methods in prostate MR segmentation.¹⁶⁰ Participating algorithms showed a wide variety in methods and implementation, and average performance was good. However, automatic segmentation of the prostate is also not optimal yet and challenges in segmentation still remain. PROMISE12 showed that a combination of algorithms yielded better results, so individual segmentation algorithms can still be improved.

Another limitation is that the radial surface projection assumes a similar prostate orientation between MR and TRUS images. A rigid registration step is crucial for this aspect. Our rigid registration strategy incorporated both translational and rotational corrections. It automatically aligns the centers of mass and then optimizes translation and rotation in 3D using the sum of squared differences. By aligning the centers and optimizing translation and rotation, we tried to optimize the rigid registration as well as possible, but small misalignments might still be there. Any misalignment will affect the further steps taken in our registration method. Including landmark information may be a possible way to improve the initial rigid registration and is something to explore in future work.

The registration accuracy is estimated by determining the TRE of corresponding reference landmarks in both MR and TRUS images. The correct placement of these landmarks is therefore crucial. A variability in locating landmarks will exist leading to a certain localization error. To minimize this effect, the positions of all reference landmarks were checked by a radiologist. However, a localization error might remain influencing the registration accuracy.

Biomechanical models can potentially improve the registration accuracy if accurate mechanical properties and boundary conditions can be obtained, as stated by Chi *et al.*¹⁶¹ Obtaining tissue properties is difficult and limited due to technical difficulty in the calibration of material parameters and the availability of (*in-vivo*) human tissue for testing. On top of that, the mechanical properties of one organ can be quite different among patients. It also is known that the different zones of the prostate (peripheral and transition zones) have a different stiffness and that tumors are usually stiffer than normal prostatic tissue.¹⁶² We assumed similar uniform elastic properties for the whole prostatic organ for each patient. The registration accuracy can considerably be affected by the material uncertainty (around 30%¹⁶¹). Our registration method might be improved by enhancing the biomechanical model of the prostate and/or expanding the model with more organs. The model can be made more patient-specific by determining elastic properties on an individual patient basis, e.g. by means of elastography.

A current development in research focuses on the registration of prostate MR images with histology step sections from prostatectomy specimens.^{163,164} We have already shown before that the biomechanical constrained surface-based registration method can be applied to MR-MR image registration.¹⁴⁶ As our method is only based on prostate contour information, it may be adapted and applied to MR-histology registration as well.

5.5 Conclusions

In this paper, we have shown that biomechanical regularization significantly improves a surface-based prostate registration method. Our method extends a non-rigid surface-based registration method with a biomechanical FE model which is able to better predict the internal deformation of the prostate. The median TRE of our method was 2.76 mm, which was significantly better than a median TRE of 3.47 mm obtained without using biomechanical regularization. These results are comparable to the previous findings on non-rigid surface-based registration¹²¹ and biomechanical modeling based non-rigid registration.¹²²

6 – Cancer visibility on TRUS

Wendy J. M. van de Ven, J. P. Michiel Sedelaar, Marloes M. G. van der Leest, Christina A. Hulsbergen-van de Kaa, Jelle O. Barentsz, Jurgen J. Fütterer, Henkjan J. Huisman

Original title: Visibility of prostate cancer on transrectal ultrasound during fusion with multiparametric magnetic resonance imaging for prostate biopsy

Published in: Clinical Imaging

Abstract

Objectives: To determine TRUS visibility of MR lesions.

Methods: Data from 34 patients with 56 MR lesions and prostatectomy was used. Five observers localized and determined TRUS visibility during retrospective fusion. Visibility was correlated to PIRADS and Gleason scores.

Results: TRUS visibility occurred in 43% of all MR lesions and 62% of PIRADS 5 lesions. Visible lesions had a significantly lower localization variability. On prostatectomy, 58% of the TRUS visible lesions had a Gleason 4 or 5 component.

Conclusions: Almost half of the MR lesions were visible on TRUS. TRUS visible lesions were more aggressive than TRUS invisible lesions.

6.1 Introduction

Currently, the most commonly used method to diagnose prostate cancer is transrectal ultrasound (TRUS) guided biopsy. Localization of malignant tissue on TRUS is, however, difficult because most lesions are not visible.²³ TRUS guided biopsy is therefore at random and can miss or undersample aggressive tumours and detect indolent cancers by chance.^{60,61}

Multiparametric (mp)-MR imaging has shown to be highly accurate in detecting and localizing intermediate and highly aggressive cancers.^{73,75,76} Recently, a standardized Prostate Imaging-Reporting and Data System (PIRADS) to detect intermediate and high-grade cancers on mp-MR imaging was introduced,⁸⁵ which showed to improve diagnostic accuracy.^{88,89}

Targeted MR image guided biopsy techniques are a very promising alternative to systematic TRUS guided biopsy. In this respect, many different techniques are rapidly emerging, including direct in-bore MR, computer-assisted MR-TRUS fusion, and cognitive MR-TRUS fusion guidance. All of these techniques use prebiopsy MR imaging to define potential lesions for targeted biopsy. However, not all of them are equally accurate.¹¹⁰

The first technique is in-bore MR targeted biopsy, which has been shown to significantly increase the tumour detection rate compared to systematic TRUS guided biopsy especially for the clinically significant tumours⁹⁴ and reduces TRUS undergrading of aggressive tumours.⁹⁸ The second and potentially more accessible and practical solution is computer-assisted MR guided TRUS fusion biopsy.¹⁰⁸ Clinical studies show that targeted prostate biopsy using MR-TRUS fusion has an increased tumour detection rate especially for clinically significant tumours.^{111,112,126–129,165–167} The third technique is cognitive targeting. Reported results are contradictory.^{111,112} As the accuracy of cognitive fusion strongly depends on the skills of the operating physician, it is likely that this technique is only effective in the hands of a TRUS and MR expert.

We noted that some MR detected lesions are retrospectively visible on TRUS. These lesions may, therefore, be more accurately targeted on both computer-assisted and cognitive MR-TRUS fusion biopsies. These TRUS visible lesions may even be successfully targeted solely on TRUS, thereby providing more representative biopsy cores. A recent study by Ukimura *et al.*¹⁶⁸ showed that TRUS visibility may indeed facilitate targeted biopsies. However, they did not look at the visibility of lesions on TRUS with prior knowledge of MR appearance and PIRADS score. They also did not investigate correlation with Gleason scores. Knowledge on correlation of TRUS visibility with PIRADS and Gleason scores will help to predict whether the lesion requires a biopsy and to predict if a lesion will be visible on TRUS images. Our study is a first step to gather knowledge on TRUS lesion visibility.

The aim of this retrospective observer study was to determine the proportion of MR suspicious lesions that are visible on TRUS.

6.2 Patients and methods

6.2.1 Patient selection

Data in this study was collected retrospectively from the data of the Radboudumc within the ongoing Prostate Cancer Molecular Medicine (PCMM) project. The PCMM project is a multi-center study focusing on prostate cancer detection. The inclusion criteria for the PCMM study were patients with localized prostate cancer confirmed by biopsy who were scheduled for radical prostatectomy in our institution. The Institutional Review Board approved the study, and all patients gave their written informed consent.

Between December 2010 and August 2013, 48 consecutive PCMM patients diagnosed with prostate cancer at our centre were included. Fourteen patients did not have a TRUS or prostatectomy. In the remaining 34 patients, a total of 56 lesions were prospectively detected on mp-MR imaging. For those 56 lesions, prostatectomy results were available.

6.2.2 MR imaging

In all patients mp-MR imaging was performed according to the ESUR guidelines⁸⁵ using a 3T MR-scanner (MAGNETOM Trio or Skyra; Siemens, Erlangen, Germany) either with a pelvic phased-array coil or a combination of an endorectal and pelvic phased-array coil.

The mp-MR imaging protocol included anatomical T2-weighted images in axial, coronal, and sagittal planes. Axial DWI was acquired and apparent diffusion coefficient (ADC) maps were automatically calculated. Dynamic contrast-enhanced (DCE)-MR images were obtained using a gadolinium-based contrast agent.

One expert radiologist with 20 years of experience in prostate MR image interpretation evaluated the images, using structured PIRADS reporting.^{85,169,170} To assess the final score a 'dominant sequence weighting' was used, being DWI for peripheral zone and T2-weighted imaging for transition zone.

6.2.3 TRUS imaging

The PCMM project involved collecting TRUS images for study purposes. TRUS images were collected after MR imaging and the performing physician was aware of the MR results. The TRUS images were acquired on a Toshiba Aplio XG/Aplio 500 machine (Toshiba Medical Systems, Japan) using a 4D end-firing transrectal transducer (Toshiba PVT-681MV; Toshiba Medical Systems, Japan) containing an internal, automatically tiltable convex element producing wedge shaped 3D volumes. The 3D grey-scale TRUS images of the prostate were acquired with a scanning angle of 70°/90° and an acquisition rate of 0.1/0.2 volumes per second. The 3D raw image data was exported from the US machine and converted from a polar to a Cartesian representation with an isotropic voxel size of 0.2 mm.

6.2.4 Histopathology

After radical prostatectomy, prostate specimens were uniformly processed and entirely submitted for histological investigations. After histological staining, all specimens were

evaluated by one of two expert urological pathologists, one with 20 years of experience and one with 8 years of experience. The entire tumour volume was outlined on each step section. Each individual tumour was graded according to the 2005 International Society of Urological Pathology Modified Gleason Grading System³⁶ and staged according to the 2002 TNM classification.

6.2.5 Observer experiment

The anonymized mp-MR images and grey-scale TRUS images were shown retrospectively in identical order to 5 observers, who analysed the images independently. The PIRADS scores of all MR lesions were visible. Observers were aware that patients were scheduled for radical prostatectomy, but did not have knowledge of the pathology outcomes. The observers varied in expertise: 2 observers were researchers with experience in prostate image analysis and MR-TRUS fusion biopsies; 1 observer was a urologist performing MR-TRUS fusion biopsies; and 2 observers were radiologists experienced in prostate MR imaging, one performing MR-TRUS fusion biopsies, the other radiologist had no experience in prostate ultrasound.

All observers were asked to determine the visibility of prostate lesions on pre-recorded 3D TRUS images using an interactive in-house developed tool installed on a desktop in a lit office. Each of them had to perform cognitive fusion of MR and TRUS images. Three orthogonal views of the TRUS images were presented, and the observers had the possibility to translate and rotate the TRUS images around the three axes to allow cognitive fusion. Scrolling, zooming, and window levelling could be adjusted manually to optimize visibility.

The observers were asked to mark the centre of the location of all 56 lesions on TRUS (example shown in Figure 6.1). All readers assigned a 5-point visibility score to each of the lesions (1: definitely not visible; 2: probably not visible; 3: uncertain; 4: probably visible; 5: definitely visible). If the prostate could not be fully displayed due to restrictions of the TRUS probe, the observer could pick a sixth option 'out of view'.

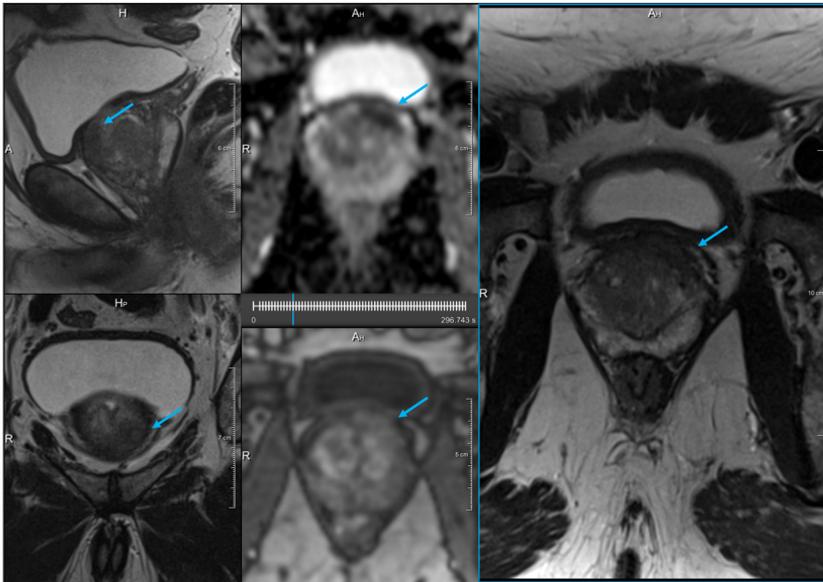
6.2.6 Data analysis

Statistical proportion analysis was performed to determine the amount of lesions visible, subdivided into PIRADS score and index lesions (i.e. most aggressive lesions) only.

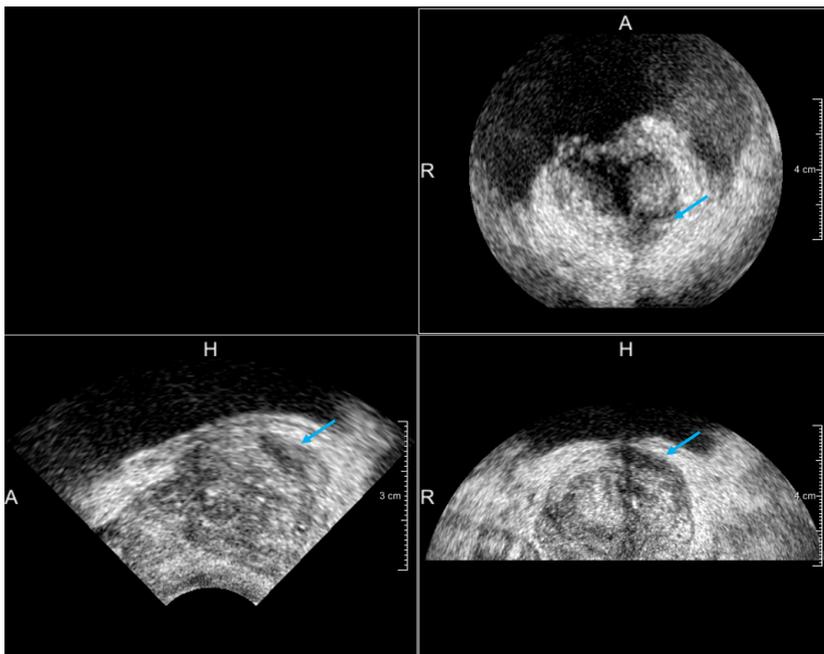
The proportion of visible lesions for different PIRADS assessments was determined including the 95% confidence intervals. A lesion was considered visible if at least three of the five observers scored a 4 or 5 on the 5-point visibility scale.

The observer variability of the tumour location on TRUS was determined by calculating the distance to the mean location as pointed out by the observers. A small distance is likely to be an indication for a good localization of the lesion on TRUS during biopsy.

The averaged localization distances are grouped according to PIRADS and visibility score. An analysis of variance (ANOVA) is performed to determine significance.



(a)



(b)

Figure 6.1: (a) Multiparametric MR images showing a PIRADS 5 lesion (indicated by the blue arrow). (b) Corresponding ultrasound image. Visibility score of the lesion was 5 for all observers.

Table 6.1: Summary of patient demographics.

Parameter	Value
No. of patients	34
Median age (y)	63 (50 – 70)
Median PSA (ng/mL)	8.0 (2.5 – 30.0)
Median Gleason score	7 (4 – 9)
Clinical stage	
- T2	22
- T3	12

Each MR lesion was correlated to the pathology outcomes by means of visual inspection of the corresponding prostatectomy specimen and Gleason scores were noted. The pathology outcomes were grouped by visibility of the lesion on TRUS images to investigate whether TRUS visibility correlates with Gleason score.

Differences were considered to be significant when $p < 0.05$. Statistical analyses were performed with Matlab (The Mathworks, Inc., Nattick, MA, version 7.14.0).

6.3 Results

MR and TRUS images were collected in 34 patients. They had a median age of 63 years and a median PSA of 8.0 ng/mL (Table 6.1). In total, 56 lesions were detected on the mp-MR images. PIRADS 5 was present in 61%, PIRADS 4 in 14%, PIRADS 3 in 5% and PIRADS 2 in 20% (Table 6.2). Of the PIRADS 2 lesions, 55% was not the most suspicious (index) lesion.

Of all lesions, 43% (24/56) were assessed as visible (score 4 or 5) on TRUS by at least 3 observers. When only index lesions were taken into account, 56% (19/34) were visible. Of the PIRADS 4 and 5 lesions, 55% (23/42) were visible on TRUS. For PIRADS 5 lesions this was 62% (21/34). One of the PIRADS 4 lesions was ‘out of view’ according to 4 of the 5 observers, and therefore also considered ‘invisible’. The results and 95% confidence intervals are provided in Table 6.2 and Figure 6.2.

The MR detected lesions were predominantly located in the peripheral zone (47/56). Of these lesions 47% (22/47) were visible on TRUS. Of the remaining nine transition zone lesions two (22%) were visible on TRUS.

The overall localization variability of lesions, expressed as the distance to the mean location, on TRUS varied from 0.4 – 18.7 mm (mean 4.9 ± 3.2 mm), when averaged between the observers the range was 0.4 – 8.6 mm. Larger distances corresponded to a lesion considered not visible by one or more observers, the localization variability for the visible lesions was 2.1 mm. Boxplots showing the averaged distances per lesion grouped according to their PIRADS classification and mean visibility score are shown in Figure 6.3. Visibility score shows a strong correlation with the distance, i.e. visible lesions have a lower variability. An ANOVA showed a significant difference ($p = 0.016$) for the localization variability grouped according to mean visibility score, but not for PIRADS classification ($p = 0.378$).

Table 6.2: Distribution of PIRADS scores for MR lesions and visibility per PIRADS score.

PI-RADS	Amount	Number visible	Visibility(95% CI)
1	0	0	-
2	11	1	9.1% (1.6 – 37.7%)
3	3	0	0.0% (0.0 – 56.2%)
4	8	2	25.0% (7.2 – 59.1%)
5	34	21	61.8% (45.0 – 76.1%)
Index lesion	34	19	55.9% (39.5 – 71.1%)
All	56	24	42.9% (30.1 – 55.9%)

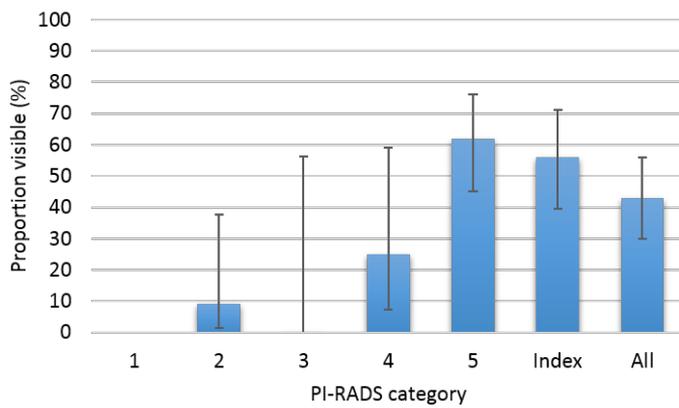


Figure 6.2: Tumour visibility on TRUS according to PIRADS score, with additional categories for index and all lesions. Proportion (%) including 95% confidence intervals is shown as error bars.

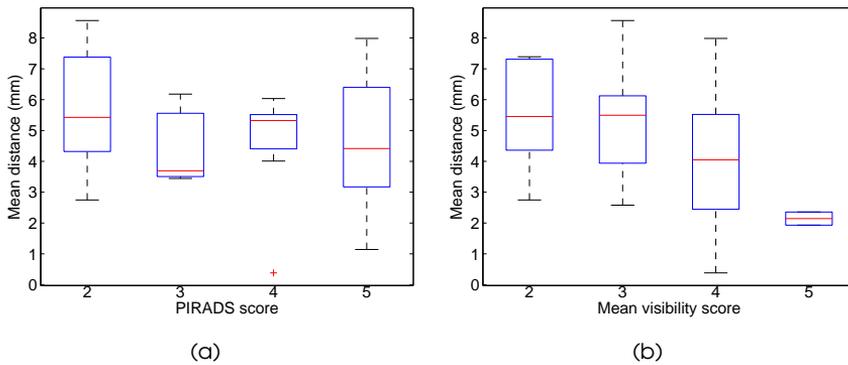


Figure 6.3: Mean distances of the tumour location on ultrasound grouped according to (a) PIRADS classification and (b) mean visibility score.

Table 6.3: Distribution of Gleason scores (GS) grouped according to the visibility of the tumour on TRUS.

	Negative	GS 4	GS 5	GS 6	GS 7		GS 8	GS 9
					3 + 4	4 + 3		
Visible	2	0	2	6	7	5	0	2
Invisible	12	1	4	4	4	3	2	2
Total	14	1	6	10	11	8	2	4

The distribution of Gleason scores for visible and invisible tumours is shown in Table 6.3 and summarized in Figure 6.4. Of the TRUS visible tumours, 58% (14/24) were Gleason 7 or higher on prostatectomy and 83% (20/24) had a Gleason 6 or higher (see Figure 6.4). Of the lesions that were not visible on TRUS, this was 34% (11/32) and 47% (15/32), respectively. Of the TRUS invisible lesions, 38% (12/32) were negative on prostatectomy specimen, for the visible tumours this was only 8% (2/24).

6.4 Discussion

In our study we found that 43% of the MR detected lesions were considered visible on TRUS. In PIRADS 4 and 5 lesions this was the case in 55%. For the PIRADS 5 lesions the TRUS visibility increased to 62%. Thus more than half of the potential biopsy targets can be visible on TRUS when using the information from mp-MR imaging. For these cases and especially the PIRADS 5 cases, any targeted TRUS guided biopsy method will benefit from TRUS lesion visibility, increasing the chance of obtaining a representative biopsy.

To our knowledge, our study is the first to investigate the visibility of prostate lesions on TRUS with prior knowledge of mp-MR images. There are publications on the incidence of hypo-, hyper-, and isoechoic lesions in TRUS guided biopsies, and also on targeted biopsies based on ultrasound appearance.^{59,171–173} Hypoechoic areas have a 17 – 57%

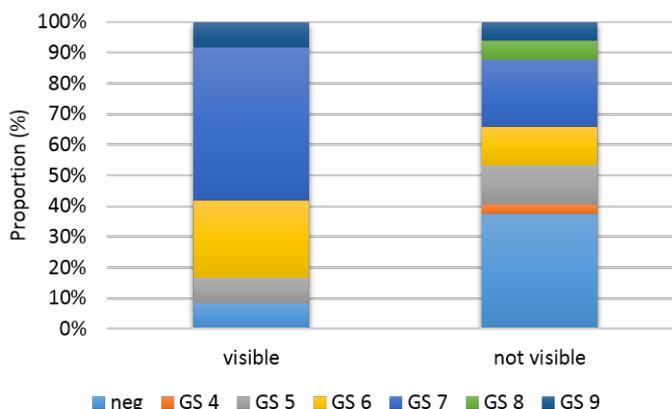


Figure 6.4: Distribution of the pathology outcomes for lesions that were visible and not visible on TRUS images.



chance of being cancer.²³ Targeting all hypoechoic nodules will therefore result in a relatively low cancer detection rate, so it is important to know which are suspicious. Our results show that it may be possible to use prior knowledge of mp-MR imaging for selecting the hypoechoic lesions that require biopsy while indicating other hypoechoic areas that may be ignored. However, further research is required to determine if this is indeed possible. Also, more radiologists with different levels of expertise should then be included to investigate how this affects the results.

The location of the tumour on TRUS was well reproducible between observers. When averaged between observers, distances to the mean location per lesion varied between 0.4 – 8.6 mm. Most of the distances were well below the clinically significant tumour size (diameter of 10 mm). Larger distances were seen if an observer scored a 1 or 2 for visibility on TRUS. The observers agreed significantly better on the location of the visible lesions. The visible lesions may thus be accurately targeted with MR-TRUS fusion biopsy.

More than half of the TRUS visible tumours corresponded to Gleason 7 or higher, indicating that these contain a Gleason 4 or 5 component. Only one third of the invisible lesions had Gleason 7 or higher, and the remaining one third was negative on prostatectomy. Therefore, we can conclude that intermediate- and high-grade prostate cancer is better visible on TRUS images compared to low-grade prostate cancer. Our data included two Gleason 8 lesions, which were not visible on TRUS. A potential explanation for this TRUS invisibility might be that both lesions were Gleason 3 + 5 = 8. Also, one of them was not suspicious on mp-MR imaging (PIRADS 2), the other one was scored as PIRADS 5.

The ability to predict the TRUS visibility from MR suspiciousness would allow these lesions to be targeted with regular TRUS devices without fusion, or enhance the accuracy of cognitive or computer-assisted fusion systems. The visible lesions may be targeted under (direct) TRUS guidance and thus are less dependent on the registration accuracy. For the lesions that are not visible on TRUS, one can consider an in-bore MR guided biopsy or a computer-assisted MR-TRUS fusion system (depending on the size of the lesion¹³⁰).

Our results are in line with a recent study where fusion biopsy is investigated including TRUS suspicion.¹⁶⁸ In that study it was shown that TRUS visibility facilitates targeted biopsies leading to a higher detection rate of significant cancer compared to systematic TRUS guided biopsies. MR and TRUS images were assessed independently from each other and cancer suspiciousness was determined on a 3-point scale. MR suspicion correlated with TRUS suspicion and combining both will help to select the most suspicious lesions. Ukimura *et al.*¹⁶⁸ did not look at the distribution among Gleason scores, for which we show that TRUS visible lesions are also more aggressive than TRUS invisible lesions.

A limitation of our study is that it has a selection bias; the data only contains patients who are scheduled for a prostatectomy. This thus does not represent the patient population with elevated PSA referred to detect their significant cancer. We can therefore

not draw a conclusion on overall US visibility for a regular clinical biopsy cohort, which may include smaller, lower-grade tumours and benign conditions. The number of lesions visible on TRUS may in this population be slightly lower. Also, the observers were aware of patients being scheduled for prostatectomy and had knowledge of the PIRADS scores. Another limitation is the small number of patients, thus this study needs to be confirmed by other studies with higher number of patients. Nonetheless, the results are promising and significant.

The observers were provided with pre-recorded 3D TRUS images. Although they were able to scroll through the prostate volume, they could not handle the probe themselves and assess 'live' images. The TRUS images of the prostate often contain artefacts around urethra and bladder, which might be reduced when moving the probe during TRUS examination. In some cases a lesion might not be visible due to TRUS artefacts, especially if it is located in the anterior part of the prostate. A lesion that is not visible on the pre-recorded images may be visualized better during 'live' TRUS. The proportion of visible tumours might then slightly increase.

In conclusion, we have shown that more than half of the lesions detected on mp-MR imaging were visible on TRUS, for PIRADS 5 this was almost two thirds. TRUS lesion visibility may help to improve finding the correct target location during MR guided TRUS biopsy (both cognitive and computational fusion). Also, TRUS visible lesions appeared to be more aggressive than invisible lesions; more than half of the visible lesions contain a Gleason 4 component or higher.

7 – MR-TRUS fusion biopsy

Wendy J. M. van de Ven, Wulphert Venderink, J. P. Michiel Sedelaar, Jeroen Veltman, Jelle O. Barentsz, Jurgen J. Fütterer, Erik B. Cornel, Henkjan J. Huisman

Original title: MR targeted TRUS prostate biopsy using local reference augmentation – initial experience

Accepted for publication in: International Urology and Nephrology

Abstract

Purpose: To evaluate MR targeted TRUS prostate biopsy using a novel local reference augmentation method.

Patients and methods: Tracker based MR-TRUS fusion was applied using local reference augmentation. In contrast to conventional whole gland fusion, local reference augmentation focuses the highest registration accuracy to the region surrounding the lesion to be biopsied. Pre-acquired multi-parametric MR images (mpMRI) were evaluated using PIRADS classification. T2-weighted MR images were imported on an ultrasound machine to allow for MR-TRUS fusion. Biopsies were targeted to the most suspicious lesion area identified on mpMRI. Each target was biopsied 1 – 5 times. For each biopsied lesion the diameter, PIRADS and Gleason scores, visibility during fusion, and representativeness were recorded.

Results: Included were 23 consecutive patients with 25 MR suspicious lesions, of which 11 patients had a previous negative TRUS guided biopsy and 12 were biopsy naïve. The cancer detection rate was 64% (Gleason score ≥ 6). Biopsy was negative (i.e. no Gleason score) in 7 patients confirmed by follow-up in all of them (up to 18 months). After MR-TRUS fusion, 88% of the lesions could be visualized on TRUS. The cancer detection rate increases with increasing lesion size, being 73% for lesions larger than 10 mm.

Conclusion: Tracker based MR-TRUS fusion biopsy with local reference augmentation is feasible, especially for lesions with an MR maximum diameter of at least 10 mm or PIRADS 5 lesions. If this is not the case, we recommend in-bore MR guided biopsy.

7.1 Introduction

A PSA test followed by systematic (on average 12 core) transrectal ultrasound (TRUS) guided biopsy (USgBx) is the currently internationally accepted diagnostic procedure to detect prostate cancer and determine patient management.²⁸ TRUS cannot localize malignant tissue and is merely used to guide systematic biopsies. USgBx has a low sensitivity (40%),^{30,60,61} causing three problems: 1) significant cancers can be missed or underestimated; 2) there is unnecessary overtreatment due to overdiagnosis;^{62,64,98} and 3) it may lead to repeat biopsies inducing increased infection rates.¹⁷⁴ Therefore, multi-parametric MR imaging and MR guided biopsy might be a better alternative.

Multi-parametric MR imaging (mpMRI) has recently emerged as a diagnostic technique that can accurately localize significant cancer in the prostate.^{75,76} In-bore MR guided MR biopsy (MRgMRBx) has been shown to 1) reduce the detection of low-risk cancer; and 2) increase the detection rate of intermediate and high-risk cancer, while using fewer cores.¹⁰⁴ However, the associated cost, relative complexity, and inconvenience of MRgMRBx may prevent widespread adaptation in clinical practice. An alternative biopsy method for MR guided biopsy would be welcome.

MR guided TRUS fusion biopsy (MRgUSBx) has recently emerged.^{107,115,125} This allows to combine the high accuracy of mpMRI with the ease and accessibility of TRUS. However, for 95% correct Gleason grading, a 1.9 mm accurate spatial registration of MR and US is required.¹³⁰ Most MRgUSBx devices do not achieve this accuracy in practice (3 – 6 mm^{116,125}). Accuracy can be slightly increased by taking one or more additional cores.¹⁷⁵

Two MRgUSBx strategies can be distinguished: cognitive and computational fusion. The fastest and simplest form of computational fusion is tracker based rigid registration, using an electro-magnetic (EM)-tracker.^{111,112} An EM-tracker attached to a TRUS probe tracks its position and orientation allowing to link a live TRUS image to a prerecorded MR image. We previously performed a phantom study on EM-tracker registration and estimated the registration accuracy in 3D to be 5 – 7 mm.¹⁷⁶ Current rigid MR-TRUS fusion protocols focus on optimizing accuracy for the entire gland volume. Due to prostate deformation, the registration accuracy can never be optimal within the whole gland. By restricting the registration to the partial gland volume surrounding the lesion, a more consistent and possibly better registration accuracy can be achieved within this partial volume containing the lesion. The EM-tracker approach we use in our study allows to do this quickly, which, combined with visual feedback, can lead in a few iterations to an augmented, focal match of TRUS and MR imaging. We propose a novel protocol to augment the accuracy locally by selecting reference landmarks on both MR and TRUS images that are close to the biopsy target,¹⁷⁷ which we refer to as local reference augmentation in analogy to all-weather aircraft landing systems.

The aim of this study is to evaluate our novel EM-tracker MR-TRUS fusion biopsy protocol using local reference augmentation in regular clinical practice. To our knowledge, this is the first report on a locally optimized MR-TRUS fusion biopsy method. We will

explore the capability of sampling mpMRI suspicious lesions and get insight into the representativeness of the biopsy result. Additionally, we will determine the proportion of tumors confidently visible on TRUS after fusion.

7.2 Patients and methods

7.2.1 Patient population

Inclusion criteria for our study were patients scheduled for MRgUSBx who had an mpMRI showing a lesion scored as PIRADS ≥ 4 , or PIRADS 3 lesion with additional clinical suspicion (e.g. unusually high PSA, persistent rising PSA). Biopsy was performed at the Radboudumc (Nijmegen, The Netherlands) or at the ZGT (Hengelo, The Netherlands). The study was approved by the Institutional Review Board of the Radboudumc for MR lesions > 9 mm, and all included Radboudumc patients gave their written informed consent. The requirement to obtain Institutional Review Board approval was waived at ZGT as MRgUSBx was their regular clinical procedure in prostate cancer diagnosis. Our data set contains all patients included at the Radboudumc and ZGT between September 2013 and October 2014.

7.2.2 Multi-parametric magnetic resonance imaging

Prostate imaging mpMRI sequences were compliant to the ESUR guidelines⁸⁵ and included three orthogonal T2-weighted, diffusion weighted, and dynamic contrast enhanced (DCE) series. Apparent diffusion coefficient (ADC) maps were calculated by the scanner. DCE used a gadolinium-based contrast agent. Preferentially, we also added a 3D T2-weighted sequence with an isotropic resolution of 1 mm for MRgUSBx. Images of the entire prostate gland and seminal vesicles were obtained using a 3 Tesla MRI scanner (MAGNETOM Trio or Skyra; Siemens, Erlangen, Germany) with either a pelvic phased-array coil or a combination of an endorectal and pelvic phased-array coil.

Several prostate radiologists prospectively evaluated the mpMRI in a regular clinical setting, using structured reporting with the ESUR standardized PIRADS classification.⁸⁵ The location of each lesion was stored on an in-house developed mpMRI analysis, viewing and reporting workstation (ProCAD).¹³⁵ All mpMRI evaluations were discussed in a consensus meeting and adapted if necessary.

7.2.3 Biopsy procedure

An Aplio 500 (Toshiba Medical Systems, Japan) ultrasound device with an end-firing transrectal transducer (PVT-781VT; Toshiba Medical Systems, Japan) was used for the MRgUSBx. Previously obtained T2-weighted MR images were uploaded to the ultrasound device. The original mpMRI including PIRADS scores were displayed on our mpMRI workstation, available during the fusion procedure. For a peripheral zone lesion, the biopsy target was the darkest lesion region on ADC, for the transition zone it was the most suspicious area on the T2-weighted series. The MR target location was first identified on

the workstation displaying the mpMRI and then re-located on the uploaded T2-weighted image.

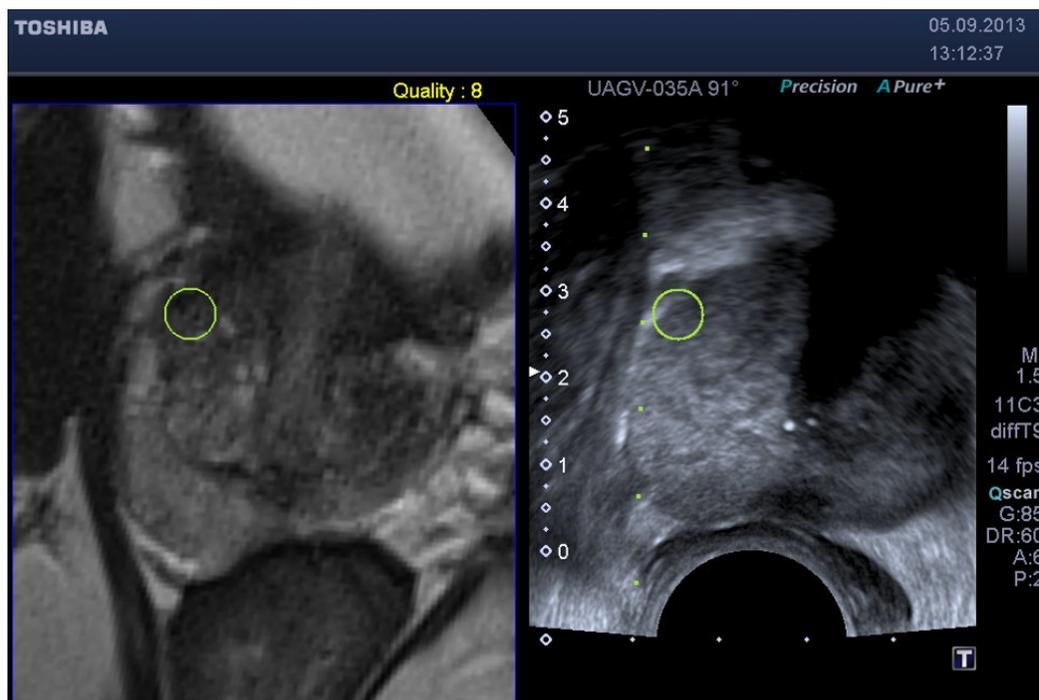
Patients were positioned in the left lateral position for biopsy, similar to USgBx. The TRUS probe was inserted rectally with gel. A needle guide was placed onto the transducer. The ultrasound machine had a SmartFusion option that includes an EM position sensor attached to the TRUS transducer to spatially correlate imported 3D MR images and US in real-time. The SmartFusion EM-tracker based fusion is a two-step process. First, the US scanning orientation is matched to a variable MR image reformatted orientation by manually selecting the best matching reformatting angle. Secondly, the correct anatomical 3D position is linked by selecting the same reference anatomical landmark in both images. During the biopsy procedure, the live US and the pre-acquired transversal T2-weighted images were shown simultaneously, allowing MR image guidance (example shown in Figure 7.1). The accuracy of the EM-based method was enhanced by our novel local reference augmentation, i.e. the reference landmark used for synchronizing 3D position was selected close to the target location as identified on MR. The MR identified lesion location is then re-located on ultrasound using the fused image display. Visible mismatch was minimized by repeating the landmark selection, compensating for landmark localization errors or patient movement. In case the lesion was visible on TRUS after initial fusion, the biopsy was targeted to the TRUS location. Note that visibility in this respect means that lesions become visible on ultrasound only during the MR targeting fusion procedure. They are much less visible on ultrasound as such without the aid of fusion. Each mpMRI detected target was biopsied 1 – 5 times. MR-TRUS fusion screenshots were stored during the biopsy to record the exact needle core location as part of the procedure to assess the representativeness.

7.2.4 Histopathology

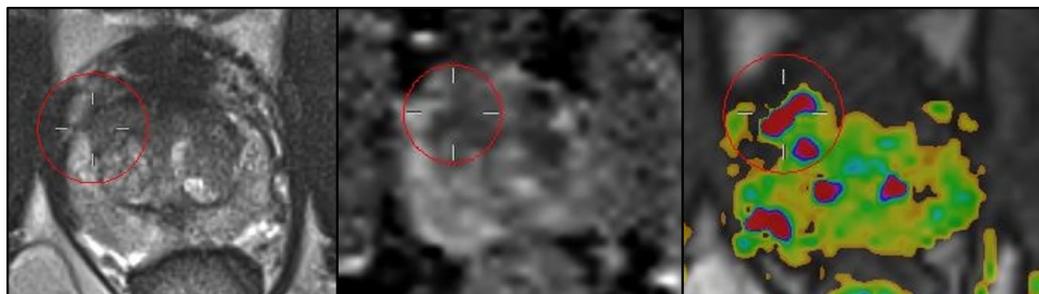
Similar to all prostate biopsy procedures, all biopsy core specimens were examined by one of two specialized urogenital pathologists and graded according to the 2005 International Society of Urological Pathology Modified Gleason Grading System.³⁶ For stratification of biopsy data into significant and insignificant cancer we applied the criteria for MRgMRBx as published by Pokorny *et al.*¹⁰⁴ In short, lesions with a Gleason score ≥ 7 in at least one of the MRgUSBx cores were defined as being clinically significant, as well as high-volume Gleason 3 + 3 (i.e. tumor length > 6 mm or more than 2 positive cores). Low-volume Gleason 3 + 3 or Gleason scores < 6 were considered clinically insignificant, and lesions for which no Gleason score could be determined were considered negative. The cancer detection rate was based on lesions with Gleason score ≥ 6 . The pathology results were correlated to the MR-TRUS fusion biopsy images and the original mpMRI study.

7.2.5 Biopsy evaluation

A urologist in consultation with a radiologist evaluated the biopsy. The biopsy was considered representative if the patient was not scheduled for an immediate MRgMRBx



(a)



(b)

Figure 7.1: (a) Screenshot of the Toshiba Aplio 500 during MRgUSBx. The green circle indicates the target as reported on mpMRI, projected on the US image after fusion. The dotted green line indicates trajectory along which the needle will shoot in the prostate (to be moved slightly for correct targeting in this screenshot). (b) The corresponding mpMRI with from left to right the transversal T2-weighted image, ADC map, and DCE image. These images were displayed using ProCAD and were available during the fusion procedure.

Table 7.1: Summary of patient characteristics.

Parameter	All patients, $n = 23$			
	Mean	SD	Median	Range
Age (y)	63	6.4	65	51 – 75
PSA (ng/mL)	10.3	6.2	8.9	2.9 – 29.3

re-biopsy. As part of the radiological quality control procedure, all mpMRI studies that did not have significant cancer after MRgUSBx were re-evaluated by two expert prostate radiologists in consensus. Furthermore, follow-up results of patients were collected.

7.2.6 Data analysis

As an indication of feasibility, the cancer detection rate and number of non-representative biopsies were analyzed. Earlier research indicated that PIRADS and Gleason score, as well as visibility and lesion size had an effect upon the detection rate, and therefore we also performed subgroup analyses. Statistical proportion analysis was performed to determine the cancer detection rate for each (sub)group. Three different size groups were created (0 – 10 mm, 11 – 20 mm, and ≥ 20 mm). Finally, the mean number of cores taken per lesion was determined for each size group.

7.3 Results

Between September 2013 and October 2014, 23 consecutive patients with 25 mpMRI suspicious lesions underwent MRgUSBx and were included (two patients had two lesions). Table 7.1 summarizes the general characteristics of the included patients. Eleven patients had at least one previous negative TRUS biopsy session, one patient had a previous negative MRgMRBx one week before MRgUSBx (but representativeness of MRgMRBx was uncertain), and the other 11 patients were biopsy naïve. The prospective mpMRI scores were: 3 PIRADS 3 lesions, 9 PIRADS 4 lesions, and 13 PIRADS 5 lesions. Most of the mpMRI suspicious lesions were located in the peripheral zone (20/25).

All MRgUSBx were considered representative, none needed an immediate re-biopsy. Table 7.2 shows the results of the prostate biopsies. In summary, the median number of targeted cores taken per lesion was 2 (range 1 – 5). Cancer (Gleason score ≥ 6) was detected in 16 of the 25 lesions (64%), and 16 of 23 patients (70%). Two patients had a second lesion with Gleason score ≥ 6 . MRgUSBx was negative in 7 patients: 2 had a PIRADS 5 lesion, 4 had a PIRADS 4 lesion, and 1 had a PIRADS 3 lesion. Patients with negative MRgUSBx were referred to active surveillance based on PSA or follow-up mpMRI after 3 – 6 months.

The cancer detection rates per PIRADS score are shown in Table 7.3. The cancer detection rate of the PIRADS 5 lesions was 77%, of PIRADS 4 this was 44%, and of the PIRADS 3 lesions 67%. Pathological biopsy outcomes per PIRADS score are shown in

Table 7.2: Results of prostate biopsies.

Parameter	Value
No. of patients/lesions	23/25
No. of patients/lesions with cancer (GS \geq 6)	16/16
Total no. of cores	64
No. of positive cores (GS \geq 6)	28
Mean primary Gleason grade	3.19 \pm 0.39
Mean secondary Gleason grade	3.25 \pm 0.43
Mean Gleason score (GS)	6.43 \pm 0.50
No. of GS 3 + 3	9 (of which 4 were clinically significant)
No. of GS 3 + 4	4
No. of GS 4 + 3	3

Table 7.3: Cancer detection rates per PIRADS score and TRUS lesion visibility, including 95% confidence intervals (CI).

Category	No. of lesions	No. of lesions with any cancer	Proportion (95% CI) any cancer	No. of lesions with significant cancer	Proportion (95% CI) significant cancer
PIRADS 3	3	2	67% (20 – 94%)	2	67% (20 – 94%)
PIRADS 4	9	4	44% (19 – 73%)	3	33% (12 – 65%)
PIRADS 5	13	10	77% (49 – 93%)	6	46% (23 – 71%)
TRUS visible	22	14	64% (43 – 80%)	10	45% (27 – 65%)
TRUS invisible	3	2	67% (20 – 94%)	1	33% (6 – 80%)
All	25	16	64% (44 – 80%)	11	44% (27 – 68%)

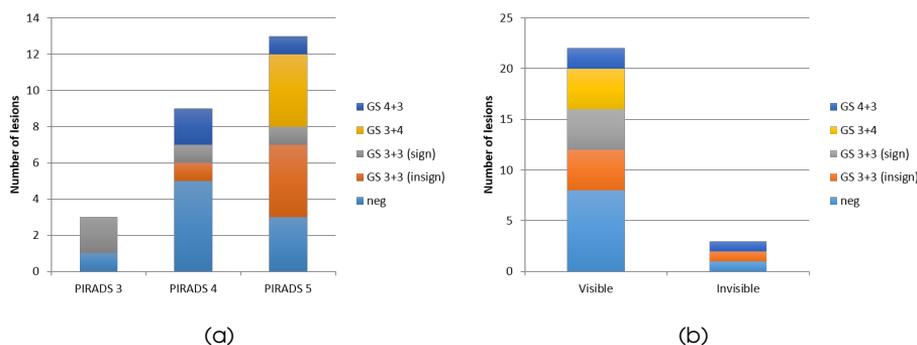
**Figure 7.2:** The number of lesions detected with targeted MRgUSBx according to (a) the PIRADS score on mpMRI, and (b) the visibility of the lesion on TRUS.

Table 7.4: Biopsy outcomes grouped according to lesion size on mpMRI.

Largest diameter	No. of lesions	Mean no. of cores (range)	Cancer (GS \geq 6) detection rate per lesion (95% CI)	Cancer (GS \geq 6) detection rate per core (95% CI)
0 – 10 mm	10	2.4 (2 – 3)	50% (24 – 76%)	33% (18 – 53%)
11 – 20 mm	11	2.5 (1 – 5)	64% (35 – 85%)	44% (28 – 63%)
> 20 mm	4	2.8 (2 – 4)	100% (45 – 100%)	73% (43 – 91%)

Figure 7.2(a). Clinically significant lesions were present in 46%, 33%, and 67% of the PIRADS 5, 4, and 3 lesions, respectively.

During the biopsy procedure, 23 of the lesions (88%) could be visualized on TRUS after image registration. For TRUS visible lesions, biopsies were targeted to the location as visible on TRUS. The cancer detection rate of the TRUS visible lesions was 64% and that of the TRUS invisible lesions 67% (see Table 7.3). For clinically significant cancer this changes to 45% and 33% for TRUS visible and invisible lesions, respectively. The pathological outcomes for TRUS visibility are shown in Figure 7.2(b).

In Table 7.4 the lesions are grouped according to their size. The cancer detection rate is higher for the larger lesions, on both lesion and core basis. For lesions larger than 10 mm, the cancer detection rate is 73% (Gleason score \geq 6). Also, slightly more cores are taken for larger lesions.

The follow-up of the mpMRI suspicious patients with a negative or insignificant MRgUSBx outcome was collected and results are shown in Table 7.5. In summary, follow-up results showed that 3 of 7 patients with negative MRgUSBx had stable or decreasing PSA after 6 – 18 months and one patient is in active surveillance. For the remaining three: one had negative USgBx after 12 months, one had negative MRgMRBx after 12 months, and one showed a PIRADS 2 lesion on follow-up mpMRI. For the five patients with insignificant MRgUSBx: one patient was lost to follow-up, one patient has decreasing PSA, one patient is scheduled for biopsy, and two are still in active surveillance.

7.4 Discussion

Prostate cancer (Gleason score \geq 6) was detected in 64% of the lesions biopsied, and in 70% of the patients. All biopsies were representative showing that our novel local reference augmented method is feasible in clinical practice. During MR-TRUS fusion, 88% of the lesions could be visualized on TRUS alone, allowing targeted biopsies to be optimized using live TRUS guidance. The cancer detection rate increases with increasing tumor size.

The representativeness of the mpMRI suspicious, but negative MRgUSBx was confirmed by follow-up; i.e. none of the seven negative MRgUSBx patients revealed clinically significant pathology. The detection rate for clinically significant cancer (44%) was lower than the 65% shown by Pokorny *et al.*¹⁰⁴ for MRgMRBx. Three reasons can be pointed out for this difference: 1) different patient population between studies; 2) difference in biopsy technique; and 3) difference in expertise of the radiologist(s). In Pokorny *et al.*¹⁰⁴

Table 7.5: Re-evaluation of original mpMRI and follow-up results for negative and clinically insignificant GS 3 + 3 outcomes.

Biopsy outcome	PSA (ng/mL)	Original PIRADS	PZ/TZ	Re-evaluated PIRADS	Re-evaluation comments	Follow-up results
Negative						
	23	5	PZ	2*	Negative MRgMRBx one month earlier.	Still in active surveillance.
	16	5	PZ	5	Biopsy may not have been representative.	Stable PSA after 6 months and mpMRI is unchanged.
	6	4	TZ	4	Biopsy results were considered acceptable during re-evaluation of mpMRI.	Increasing PSA to 8.4 and now PIRADS 5 lesion on mpMRI after 12 months; MRgMRBx was negative.
	9.7	4	PZ	4	Biopsy may not have been representative.	Stable PSA after 6 months.
	3.9	4	PZ	4	Negative biopsy outcome is acceptable.	PSA increased to 5.1, but USgBx was negative after 12 months.
	6.1	4	TZ	3*	Biopsy outcome prostatitis is acceptable.	PSA decreased to 3.9 after 6 months.
	7.3	3	PZ	2*	Negative biopsy outcome is acceptable.	After 12 months, mpMRI showed a PIRADS 2 lesion corresponding to prostatitis.
GS 3 + 3						
	13	5	PZ	4*	Biopsy was representative.	Lost to follow-up.
	6.4	5	PZ	5	Tumor volume in biopsy is small regarding the significant tumor visible on mpMRI.	PSA increased to 7.7 after 18 months, patient in active surveillance.
	9	4	PZ/TZ	3*	Biopsy was representative.	Decreasing PSA to 8.1 after 12 months.
GS 3 + 3 and negative (patients with more than one lesion)						
	11	5	PZ	5	Biopsy was representative.	Patient scheduled for biopsy.
		5	PZ	5	Biopsy may not have been representative, difficult location to target.	
	6.3	5	PZ	4*	Biopsy was representative.	Still in active surveillance.
		4	PZ	4	Small lesion, biopsy outcome may not have been representative.	

* Lesions that have been downgraded in re-evaluation of the original mpMRI

three expert radiologists in consensus evaluated the mpMRI, which in our study was done by the attending prostate radiologist. To investigate the third point, two expert radiologists in consensus re-evaluated the original mpMRIs with negative and clinically insignificant MRgUSBx. Table 7.5 shows that the original mpMRI assessment may indeed have overestimated tumor aggression: 43% (6/14) of the lesions were downgraded during retrospective re-evaluation by experts. This confirms that expertise is important. In case subsequent biopsy reveals no clinically significant cancer in PIRADS 4 and 5 lesions it is very important to re-evaluate the quality of the mpMRI, the reading, and the subsequent biopsy technique.

The original results of our locally optimized EM-based registration method are well in line with results of other EM-based systems, which have a cancer detection rate between 49 – 69%.^{111,112} Clinical studies with other MR-TRUS fusion systems, also show similar detection rates.^{111,112,128,129} However, patient populations differ quite a bit between the different studies, e.g. regarding the amount of patients with a previous negative biopsy or patients that were biopsy naïve.

We know from previous phantom studies that our EM-based registration method has a registration accuracy of about 5 mm.¹⁷⁶ Yet we were still able to achieve reasonable detection rates in the 0 – 10 mm category. The following items played a role. First, we enhanced the EM-based registration technique by locally optimizing fusion through the iterative selection of anatomical landmarks close to the target. Secondly, the number of biopsy cores was increased in case the performing physician was not certain about the biopsy taken. By taking more cores per target, the tumor hit-rate increases.¹⁷⁵ Thirdly, during the MRgUSBx we noticed that 88% of the targets became visible on TRUS images during MR-TRUS fusion. In case the targets become visible on TRUS, these can be more accurately targeted even if the registration is not optimal.¹⁶⁸ The TRUS visibility is often subtle and may very well depend on the quality of the ultrasound images.

The cancer detection rate increases with increasing lesion size, which might be an indication that the smaller lesions are harder to hit with MRgUSBx and might better be biopsied with MRgMRBx. For lesions larger than 10 mm diameter, our results show a cancer detection rate of 73%, approaching the results of MRgMRBx.

The main limitation of our study is the small number of patients. But sufficient to indicate that MR-TRUS fusion with local reference augmentation is feasible for targeting prostate biopsies. To make a good comparison with MRgMRBx more patients should be included in a non-inferiority trial setting. Then, similar patient groups can be compared and it can be determined whether MRgUSBx is non-inferior to MRgMRBx.

To summarize, MR-TRUS fusion biopsy using local reference augmentation seems a viable clinical alternative to MR guided biopsy for lesions with an mpMRI maximum diameter of at least 10 mm, or PIRADS 5 lesions. Smaller lesions may still require in-bore MR guided biopsy.



8 – Summary & Discussion

In this thesis, both clinical and technical requirements regarding MR-TRUS fusion for prostate biopsies have been investigated. This chapter provides a summary of the main results and conclusions, followed by a general discussion of these conclusions and some suggestions for further research, and finally a view on future perspectives.

8.1 Summary

In chapter 2, the results of a large clinical trial on MR guided TRUS fusion biopsy were discussed. This discussion is based on the recently published paper by Siddiqui *et al.*¹²⁸ They compared the results of MR-TRUS fusion biopsy with systematic TRUS guided biopsy. Its main findings are that MR-TRUS fusion biopsy outperforms systematic TRUS guided biopsy regarding the cancer detection rate of especially the aggressive cancers, avoiding detection of indolent cancers. However, implementation of MR-TRUS fusion biopsy techniques requires caution: good quality MR images and image interpretation is required; accurate segmentation and registration is essential for targeting tumor suspicious regions with MR-TRUS fusion guidance; and small lesions have a chance of being missed using this technique. The results show that any of several MR guided biopsy techniques has the potential to replace systematic TRUS guided prostate biopsies in the future. However, we conclude that further research is required to determine the threshold tumor size and to compare the accuracy of MR-TRUS fusion biopsy with that of direct in-bore MR guided biopsy.

The registration accuracy that is required for targeting the most aggressive tumor part with MR guided TRUS biopsy is assessed in chapter 3. This registration accuracy depends on the size of the most aggressive part, the tumor focal spot. Our population included 51 patients with 62 peripheral zone tumors. More than half of those tumors were heterogeneous, thus containing a high-grade tumor focal spot. A simulation experiment performed on the whole tumor population allowed to determine the required target registration error (TRE) given a requested hit-rate. The results of this simulation experiment showed that a technical registration accuracy of 1.9 mm is required for finding the highest Gleason grade component in 95% of the tumors in our population with MR guided TRUS biopsies. This is only a theoretical measure of accuracy, in clinical practice other factors like the correct placement of the biopsy gun and needle deflection will possibly lead to additional inaccuracies.

Chapter 4 describes a registration method with biomechanical regularization. A common approach for the registration of MR and TRUS images is the alignment of cross-sectional prostate contours. This surface-based registration does not control internal prostate deformation. By extending such a surface-based registration method with biomechanical modeling, internal deformation of the prostate can be simulated. Initial evaluation of the registration accuracy of the biomechanical regularized method compared to a regular surface-based registration method is done for MR-MR registration. MR images before and after insertion of a needle guide were collected from six patients scheduled for in-bore MR guided biopsy. Manual segmentation was followed by a mesh-

ing step and subsequently the biomechanical modeling of prostate deformation. The registration accuracy was determined by calculating the TRE for 45 anatomical landmarks. The median TRE of a surface-based registration with biomechanical regularization was 1.88 mm, which was significantly better than 2.61 mm without biomechanical regularization. Therefore, biomechanical modeling has the potential to improve the accuracy of multimodal prostate registration when comparing it to regular surface-based registration.

In chapter 5, the biomechanical modeling constrained surface-based registration method was developed further. To be able to apply the method presented in chapter 4 to MR-TRUS registration, some adaptations had to be made. First of all, an initial rigid alignment of MR and TRUS images is required. Simulation convergence was also improved by better conditioning of the mesh model, and the parameter settings for meshing and simulation were automated. Manual intervention is only required for prostate segmentation. MR and TRUS images were collected from ten patients. Again, anatomical landmarks were used for determining the registration accuracy. The median TRE of a surface-based registration with biomechanical regularization was 2.76 mm. This was significantly better than the median TRE of 3.47 mm for regular surface-based registration without biomechanical regularization. Biomechanical finite element modeling has the potential to improve the accuracy of multimodal prostate registration and can help to improve the effectiveness of MR guided TRUS biopsy procedures.

MR guided TRUS fusion biopsies can benefit from the visibility of potential prostate lesions. Visible lesions can be targeted under TRUS guidance. For biopsying 'invisible' lesions an accurate registration algorithm is required. To have a better understanding of the visibility of prostate cancer on TRUS images using prior knowledge of MRI, we determined the proportion of lesions that are visible on TRUS in chapter 6. Multiparametric (mp)-MR images from 34 patients were collected and assessed according to the PI-RADS guidelines. In total, 56 lesions were detected and scored on mp-MRI. Five observers were asked to determine the visibility of each of the prostate lesions on 3D TRUS images and assign a visibility score on a 5-point scale. Our results showed that 43% of all MR lesions were considered visible by the majority of the observers. Of the PI-RADS 4 and 5 lesions, 55% were visible on TRUS and for merely PI-RADS 5 this increased to 62%. For clinical application, this means that more than half of the potential biopsy targets are visible on TRUS images when using the information from mp-MRI. For these cases and especially the PI-RADS 5 cases (of which almost two thirds were visible) MR guided TRUS fusion biopsy will benefit from TRUS lesion visibility. For the lesions that are not visible during fusion biopsy, an accurate registration algorithm or an in-bore MR biopsy is required to target the lesion.

In chapter 7, the clinical feasibility of a MR-TRUS fusion biopsy system was tested. Toshiba's Smart Fusion algorithm is based on electro-magnetic (EM)-tracking of the TRUS probe. It is a two-step process: first the image plane orientation is matched, then the in-plane position is linked by selecting the same reference landmark in both images. Because this is a rigid registration technique which does not correct for prostate deformations,

it is estimated to have a registration accuracy of 5 mm. The accuracy can be optimized locally by enhancing the method with local reference augmentation, i.e. the reference landmark is selected close to the biopsy target. Initial results are based on 23 patients with 25 MR suspicious lesions. The cancer detection rate is 64%. The cancer detection rate increases with increasing lesion size, being 73% for lesions larger than 10 mm. Biopsy was negative in 7 patients and follow-up remained negative in all of them. Our results show that MR-TRUS fusion biopsy with local reference augmentation is feasible in clinical practice, especially for the larger lesions.

8.2 General discussion

The optimal prostate cancer diagnostic strategy would involve low morbidity and low cost to reliably identify cancers that present potential harm to the patient. It would also minimize unnecessary biopsies or other invasive procedures in patients who do not have harmful cancers, decreasing invasiveness and the number of biopsy cores in particular. Furthermore, it is important to correctly determine the cancer aggressiveness and reduce overtreatment. If an indolent cancer exists that requires no immediate treatment, diagnosing cancer would cause potential psychological harm and unnecessary treatments with their associated costs and morbidity. The current diagnostic pathway needs improvements to approach this ideal.

At the moment, a PSA test will be followed by a systematic TRUS guided biopsy to make a definite diagnosis of prostate cancer. However, a PSA test has limited specificity and sensitivity, and a systematic TRUS biopsy can miss the tumor or wrongly diagnose the aggressiveness. In this era, where many men receive a PSA test, diagnostics need to be improved. Also, if screening becomes applicable, an effective diagnostic pathway needs to be established.

An MR guided approach has proven to be able to solve many of the issues of systematic TRUS guided biopsies as currently used in clinical practice. MRI can help to detect and localize tumors requiring treatment. Guidelines have been developed to standardize prostate MRI. In-bore MR guided MR biopsies can accurately target potential lesions with less cores. The cancer detection rate of MR guided MR biopsies is much higher than systematic TRUS guided biopsies, especially for the clinically significant tumors. MRI has a high negative predictive value and the number of biopsies can be reduced significantly. Furthermore, an MR guided approach is a potentially more cost-effective than TRUS guided biopsies. A drawback is that clinical use of MR guided MR biopsies is restricted by its limited availability and relative complexity. MR guided TRUS biopsy is potentially a more accessible and practical solution and can help to reduce the increasing workload of MRI and thus provide a faster diagnostic path to the patient.

The work described in this thesis tries to provide an answer on whether MR guided TRUS biopsy is a viable alternative. Several groups already compared MR guided TRUS biopsies to systematic TRUS biopsies. Different commercially available systems have been explored as well as different study populations. Although the numbers may be slightly

different, all of them show an increased detection rate of especially significant tumors compared to systematic TRUS biopsies. There are many advantages of MR guided TRUS biopsies over the systematic TRUS biopsies. Among these are the targeted approach, reduction of biopsy cores, and more accurate Gleason grading. So yes, MR guided TRUS biopsy certainly is a viable alternative to systematic TRUS guided biopsies. However, the remaining question is whether it is also a viable alternative to direct in-bore MR guided biopsies. Several challenges exist though, and some of them have been addressed in this thesis.

First of all, caution is required before embarking on immediate large-scale implementation of MRI-guided biopsy techniques for men with suspected prostate cancer. An experienced MRI radiologist is crucial for obtaining good biopsy samples, as optimal acquisition and standardized interpretation of mp-MR images is essential. Acquisition and interpretation of the mp-MR images requires skills that can only be obtained by good training and experience. Minimal requirements for prostate mp-MR image acquisition and standardization for reporting (PI-RADS) have recently been published. This will help to improve the general reliability of the techniques. However, this holds for both MR-TRUS fusion biopsies as well as in-bore MR guided biopsies.

The success-rate of MR guided TRUS biopsies is highly depending on the registration accuracy. We have shown that for correctly grading 95% of the tumors, a technical registration accuracy of 1.9 mm is required. This is the theoretical threshold on the TRE to actually hit the most aggressive part of the tumor by taking only one biopsy core. The probability of hitting the tumor will increase when 2 or 3 cores will be taken, which is also usually done with in-bore MR guided biopsies. The volume of (the most aggressive part of) the tumor plays an important role in the hit-rate as well. Larger tumors have a higher probability of being hit and could therefore be successfully targeted with a less accurate registration method. This is the case with in-bore MR guided biopsies as well. However, in clinical practice there are more factors than just the registration accuracy that influence the success-rate of the fusion biopsy. These are for instance the correct placement of the biopsy gun and needle deflection, which both have a role in the success-rate of in-bore MR guided biopsies as well.

Many different registration methods have been described, some of them are implemented in clinical systems. However, most of them are likely to not reach the accuracy of 1.9 mm. The major challenge in MR-TRUS registration is compensating for prostate deformation. Rigid registration methods are relatively easy and fast, but ignore shape differences and are therefore not very accurate in general. Non-rigid methods do correct for differences in prostate shapes between the two modalities. These methods are more complex, but also more accurate. However, the outcomes are not always physically plausible. We explored the possibility of extending a non-rigid surface-based method with biomechanical modeling. Soft-tissue properties are incorporated and prostate deformation is simulated. The results show that biomechanical modeling can improve the registration accuracy of a non-rigid registration method. The possibilities need to be

explored further, but improvements to the current systems should be feasible. A possible suggestion for future work is to consider elastography as enhancement for the biomechanical model. This may provide non-uniform elastic properties that better characterize the prostate.

The current clinically available MR guided TRUS biopsy systems not only differ in implemented registration algorithms, but also in clinical usability and required manual input. The relatively easy-to-use systems are usually less accurate than the more advanced systems. However, the complex methods require a longer time for computing the registration results. Some systems require manual segmentation, which is a time-consuming task, while other systems are more automated and less operator-dependent. The different systems may have different learning curves, so experience of the operating physician plays an important role as well.

In clinical practice, it will be convenient if the registration procedure is easy and fast to use. This may be accompanied with a lack in accuracy. However, this does not necessarily mean that these systems cannot be successful in clinical practice. It is important that the operating physician is aware of the accuracy of the system. In case the system is not able to accurately register the smaller lesions, one should consider to proceed to in-bore biopsies immediately. The larger lesions, on the other hand, may be successfully targeted with an easy and fast MR guided TRUS biopsy system.

A lack in registration accuracy may be partly resolved by tumor visibility on TRUS images. More than half of the tumors are actually visible on TRUS images if one knows where to look based on prior knowledge of MRI. The visible lesions can be accurately targeted under TRUS guidance, thereby less depending on the registration accuracy. Visible lesions may even be targeted using cognitive fusion, where the physician performing the biopsy reviews the lesion on MRI and aims the biopsy needle at the appropriate prostate area on TRUS. We correlated TRUS visibility to PI-RADS, but more research is required for better identification of TRUS visible lesions. MR characteristics of the lesions that can be visualized on TRUS should be determined. The PI-RADS scores of the different modalities of mp-MRI can be addressed separately, peripheral and transition zone tumors may behave differently on TRUS images, Gleason grades could be taken as ground truth, lesion size might play an important role, etc. Knowing what type of lesions are visible will help decide which technique can be used best for targeted prostate biopsies.

In our study, we looked at tumor visibility on common grey-scale TRUS images. Other ultrasound modalities are emerging and may have potential in prostate cancer imaging. Contrast-enhanced, Doppler, and/or elastography have shown to be able to increase the cancer detection rate when compared to non-targeted systematic biopsies. When combining several modalities and thus using multiparametric TRUS imaging, prostate cancer image visibility might be improved. Potentially, computer-aided detection (CAD) might also help to enhance possible prostate lesions on TRUS. These are some suggestions for future research, which is required to find out if there may be a potential role for any of these techniques.

Finally, we explored the feasibility of a clinical MR-TRUS fusion biopsy system. The implemented EM-based rigid registration method has an accuracy of about 5 mm. This makes the method fast and relatively easy to use, which is very convenient in regular clinical practice. By enhancing the method with local reference augmentation, the accuracy around the target can be optimized. We started off with biopsying only the relatively large and aggressive tumors, to be sure to take representative biopsies. We noticed that quite some tumors are visible after fusion. Combining computational with cognitive fusion seems to work well in clinical practice, especially if tumors are visible on TRUS images. Also the larger lesions may very well be targeted using fusion biopsies. The patient group we studied is relatively small, but our results show that the system is feasible in clinical practice. More data should be collected to give a clear indication of the success-rate of MR-TRUS fusion biopsy and compare this with in-bore MR guided biopsy. The correlation between success-rate and tumor size should be determined.

Some other systems work similarly as the one we tested, but there are also systems that are much more complex. Although the registration method will then be much more accurate, the system itself is less user friendly. Cumbersome devices and manual segmentation make these systems less suitable in clinical practice. Each fusion system has its own advantages and disadvantages, which should be considered carefully. One should be aware of possible shortcomings, e.g. less accurate fusion systems may lead to a lower cancer detection rate compared to more accurate systems. Future studies should provide more data and compare the different biopsy methods. It should be figured out how fusion biopsies can be used best and what methodology is optimal for clinical practice.

To summarize, MR guided TRUS biopsy may certainly be a viable alternative to systematic TRUS guided biopsy. But can it be a viable alternative to in-bore MR guided biopsy as well? In this work, several technical and clinical issues have been addressed. From our results, it can be concluded that MR guided TRUS biopsy has the potential to be a viable alternative to in-bore MR guided biopsy. Among other studies, we have shown that the cancer detection rate of MR guided TRUS biopsies correlates to PI-RADS score, and that PI-RADS 5 lesions may very well be biopsied using fusion. Also, the relatively large tumors (diameter ≥ 10 mm) can be successfully targeted with MR guided TRUS biopsy. Besides, aggressive tumors have a higher chance of being visible on TRUS images using prior knowledge of MR appearance, thereby facilitating targeted biopsy. Of course, the characteristics of lesions that may be successfully biopsied with fusion depend on the accuracy of the fusion system. Therefore, further research is required to determine the exact lesion characteristics for each fusion system to allow successful biopsy.

8.3 Future perspectives

Any of several MR guided biopsy techniques can be a viable alternative to the current systematic TRUS guided biopsies. This will certainly happen in the near future, thereby changing the current diagnostic pathway for prostate cancer diagnosis. Current clinically available MR-TRUS fusion biopsy systems can still be improved and more tools may

become available. Ideally, MRI will get an important role in clinical practice, making screening for prostate cancer more feasible.

How would all of this change the diagnostic pathway? If prostate cancer screening would be introduced, an initial selection will probably still be based on a PSA test. A pre-biopsy MRI will then subsequently follow for the men with an elevated PSA level. The MRI scans need to be assessed according to the PI-RADS guidelines, ideally in a double reading setting. As the number of scans will increase dramatically, CAD may potentially assist the radiologist. The results of MRI will then help to decide whether the patient should proceed to prostate biopsy. Based on the lesion characteristics, a certain targeted biopsy technique will be advised. Larger and visible lesions, in particular, will be suitable for MR guided TRUS biopsy. A large part of the lesions requiring biopsy can therefore be successfully targeted with MR guided TRUS biopsy, the remaining lesions need to be biopsied directly in the MR scanner. Radiologists and urologists should work together to determine whether biopsy results are representative. Lesions that have been unsuccessfully biopsied using either biopsy technique, but are still suspicious for being cancer, should be re-biopsied in the MR scanner. The biopsy results will then help the attending physician to make a treatment decision.

The combination of MR guided TRUS biopsies and direct in-bore MR guided MR biopsies may be a more cost-effective solution than the systematic TRUS guided biopsies, or an MR only approach. Advantages of both TRUS and MRI will be combined. The targeted strategy will improve cancer detection and correctly determining the cancer aggressiveness, providing patients with a clear answer. Overdiagnosis and overtreatment will be reduced, improving quality of life.

8.4 Closing remarks

In my opinion, the clinical pathway as described above would be a great improvement to current clinical practice. Of course, there are several challenges still remaining and further research should provide more solutions. The work described in this thesis is a good basis for future studies, and will thereby contribute to incorporation of MR guided TRUS prostate biopsies into clinical practice, with the final goal of improved patient care.

APPENDICES



Nederlandse samenvatting

In dit proefschrift zijn zowel klinische als technische aspecten beschreven die betrekking hebben op MR-echo fusie voor prostaat bipten. Hieronder volgt een samenvatting van de belangrijkste resultaten en conclusies.

In hoofdstuk 2 zijn de bevindingen van een grootschalige klinische studie van Siddiqui *et al.*¹²⁸ naar MR-echo fusie bipten besproken. Daarin zijn de resultaten van MR-echo fusie biopsie vergeleken met systematische echo geleide biopsie. De belangrijkste bevindingen zijn dat MR-echo fusie biopsie beter is dan systematische echo geleide biopsie wat betreft kanker detectie van met name agressieve tumoren, waarbij detectie van indolente tumoren wordt vermeden. Men dient echter voorzichtig te zijn met de toepassing van MR-echo fusie biopsie: ten eerste is een goede kwaliteit MRI noodzakelijk, alsmede een juiste beoordeling van de beelden. Nauwkeurige segmentatie en registratie is essentieel voor het gericht bipten van de tumor onder MR-echo geleide. Met name kleine tumoren hebben een kans om te worden gemist met deze techniek. De resultaten laten zien dat verschillende MR-echo fusie biopsie technieken de potentie hebben om systematische echo geleide bipten in de toekomst te vervangen. Verder onderzoek is nodig om te bepalen wat de minimale tumor grootte is waarbij fusie biopsie mogelijk is. Ook moet de nauwkeurigheid van MR-echo fusie biopsie worden vergeleken met die van in-bore MR geleide biopsie.

De registratie nauwkeurigheid die vereist is om het meest agressieve tumor gedeelte te raken met MR geleide echo biopsie is beschreven in hoofdstuk 3. Deze registratie nauwkeurigheid is afhankelijk van de grootte van het meest agressieve deel van de tumor. Onze populatie bestond uit 51 patiënten met 62 perifere zone tumoren. Meer dan de helft van deze tumoren waren heterogeen, wat wil zeggen dat deze een hoog-gradig tumor gedeelte bevatten. Een simulatie-experiment is uitgevoerd op de gehele tumor populatie om de minimaal vereiste registratie nauwkeurigheid in te schatten voor een bepaalde hit-rate. Voor het vinden van de hoogste Gleason graad in 95% van de tumoren met MR-echo fusie bipten, is een registratie nauwkeurigheid van 1,9 mm nodig. Dit is slechts de theoretische mate van nauwkeurigheid. In de kliniek spelen ook andere factoren een rol. De plaatsing van de naaldgeleider en de afbuiging van de naald kunnen bijvoorbeeld leiden tot extra onnauwkeurigheden.

Hoofdstuk 4 beschrijft een registratiemethode gebaseerd op biomechanische modellering. Een veel voorkomende aanpak voor de registratie van MR en echo beelden is het zo goed mogelijk op elkaar passen van prostaat contouren. Deze contour-gebaseerde registratie methode houdt geen rekening met interne vervormingen van de prostaat. Door deze methode uit te breiden met biomechanische modellering, kunnen interne vervormingen van de prostaat worden gesimuleerd. Een eerste schatting van de registratie nauwkeurigheid van deze biomechanisch-geregulariseerde methode wordt gedaan met MR-MR registratie. Dit wordt vergeleken met een reguliere contour-gebaseerde registratie methode. MR beelden zijn gemaakt voorafgaand en na inbrenging van een naaldgeleider en zijn verzameld van zes patiënten die gepland waren voor een MR-geleide biopsie. Na handmatige segmentatie werd de prostaat in kleine elementjes verdeeld. Daarna volgde

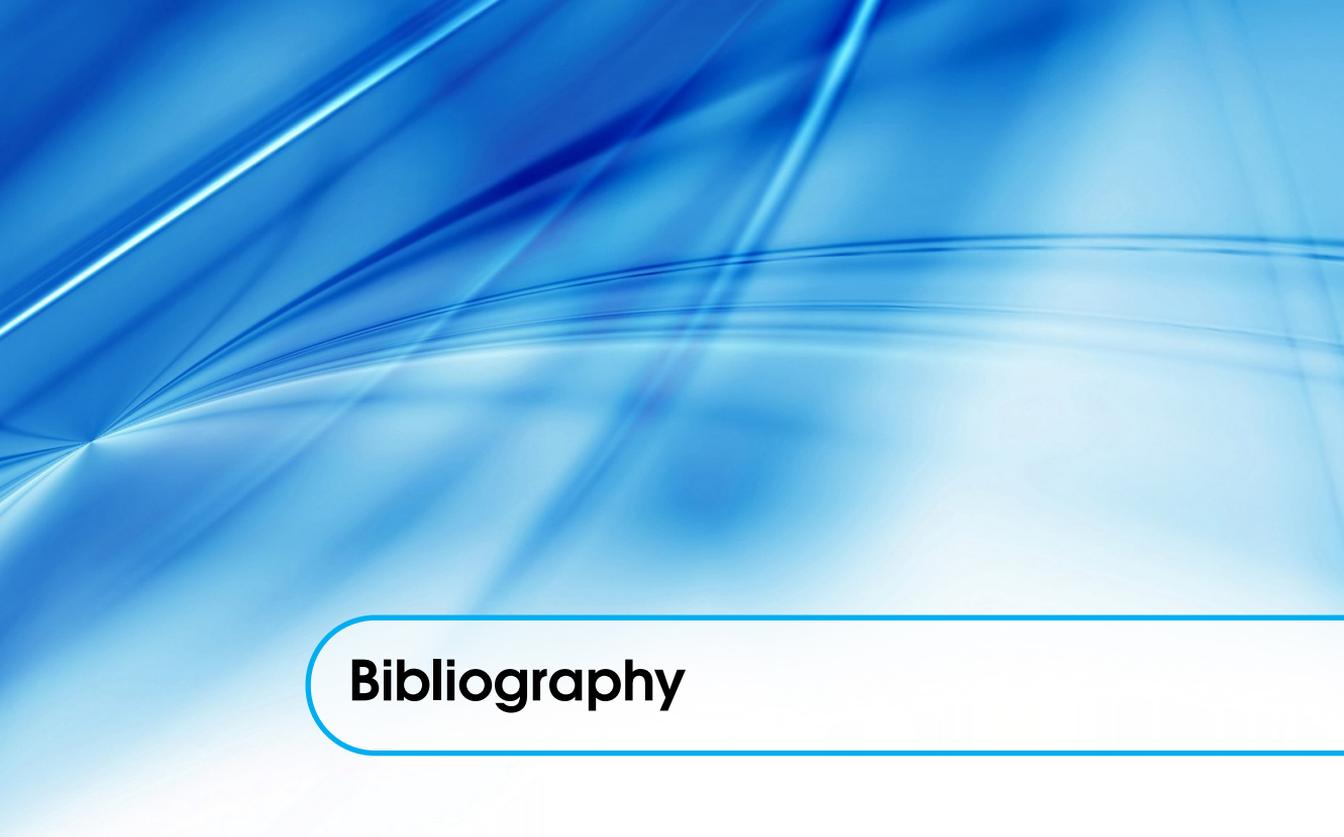
de biomechanische modellering van de vervorming van de prostaat. De nauwkeurigheid is bepaald door het berekenen van de registratiefout van 45 anatomische referentiepunten. De mediane fout van de biomechanische modelleringsmethode was 1,88 mm. Deze was significant beter dan 2,61 mm zonder biomechanische modellering. Biomechanische modellering heeft dus de potentie om de nauwkeurigheid van multimodale prostaat registratie te verbeteren.

In hoofdstuk 5 is de registratie methode zoals beschreven in hoofdstuk 4 verder ontwikkeld. Voor toepassing op MR-echo registratie zijn een aantal aanpassingen noodzakelijk. Allereerst is een initiële rigide registratie van MR en echo beelden vereist. Verder is de simulatie convergentie verbeterd door een betere conditionering van het model en zijn de parameterinstellingen voor de simulatie geautomatiseerd. Handmatige interventie is hierdoor alleen nog nodig voor de segmentatie van de prostaat. MR en echo beelden van tien patiënten zijn verzameld. Ook hier zijn anatomische referentiepunten gebruikt om de registratie nauwkeurigheid te bepalen. De mediaan van de biomechanische modelleringsmethode was 2,76 mm. Dit was significant beter dan de mediaan van 3,47 mm voor de reguliere registratie methode. Biomechanische modellering biedt de mogelijkheid om de nauwkeurigheid van multimodale prostaat registratie te verbeteren en kan helpen om de effectiviteit van MR-echo fusie biopsie te verbeteren.

MR geleide echo fusie biopsie kan verbeteren indien potentiële prostaat tumoren zichtbaar zijn op echo. Zichtbare tumoren kunnen gericht worden geprikt onder echo geleiding, terwijl voor onzichtbare tumoren een nauwkeurige registratie is vereist. Om meer te weten te komen over de zichtbaarheid van prostaatkanker op echo beelden met voorkennis van MRI, hebben we het aantal tumoren dat zichtbaar is op echo onderzocht in hoofdstuk 6. Multiparametrische MR beelden van 34 patiënten zijn verzameld en beoordeeld volgens de PI-RADS richtlijnen. In totaal zijn 56 tumoren op MRI gedetecteerd en beoordeeld. Vijf waarnemers zijn gevraagd om de zichtbaarheid van deze tumoren op 3D echo beelden te bepalen volgens een 5-puntsschaal. Onze resultaten laten zien dat 43% van alle MR tumoren voor de meerderheid van de waarnemers zichtbaar was. Van de PI-RADS 4 en 5 tumoren was 55% zichtbaar op echo en voor PI-RADS 5 zelfs 62%. Voor klinische toepassing betekent dit dat meer dan de helft van de tumoren zichtbaar is op echo beelden met voorkennis van multiparametrische MRI. Voor deze gevallen en in het bijzonder de PI-RADS 5 gevallen (waarvan bijna tweederde zichtbaar was) kan MR-echo fusie biopsie profiteren van zichtbaarheid op echo. Voor tumoren die niet zichtbaar zijn tijdens fusie biopsie is een nauwkeurige registratie methode of MR geleide biopsie nodig om gericht te kunnen biopsieren.

In hoofdstuk 7 wordt de klinische haalbaarheid van een MR-echo fusie biopsie systeem beschreven. De Smart Fusion methode van Toshiba is gebaseerd op het elektromagnetisch volgen van de echo transducer. Het proces bestaat uit twee stappen: eerst wordt de oriëntatie van de beelden gelijk gelegd, daarna wordt de exacte positie verbonden door middel van anatomische referentiepunten. Omdat dit een rigide registratietechniek is die niet gecorrigeerd wordt voor prostaat vervormingen, wordt de registratie

nauwkeurigheid geschat op ongeveer 5 mm. De nauwkeurigheid kan lokaal worden geoptimaliseerd door de methode te verbeteren met lokale referentie vergroting, dat wil zeggen dat het referentiepunt zo dicht mogelijk bij het doel wordt gekozen. De eerste resultaten zijn gebaseerd op 23 patiënten met 25 MR verdachte gebieden. Kanker is gedetecteerd in 64% van de verdachte gebieden. Voor tumoren groter dan 10 mm neemt dit zelfs toe tot 73%. Biopsie was negatief in 7 patiënten en follow-up bleef negatief in alle 7. Onze resultaten laten zien dat MR-TRUS fusie biopsie met de lokale referentie vergroting uitvoerbaar is in de kliniek, zeker voor de grotere tumoren.



Bibliography

- [1] H. Gray. *Anatomy of the human body*. Lea & Febiger, Philadelphia, Pennsylvania USA, 20th edition, 1918.
- [2] J. E. McNeal. The zonal anatomy of the prostate. *Prostate*, 2:35–49, 1981.
- [3] J. E. McNeal, E. A. Redwine, F. S. Freiha, and T. A. Stamey. Zonal distribution of prostatic adenocarcinoma. correlation with histologic pattern and direction of spread. *Am J Surg Pathol*, 12:897–906, 1988.
- [4] A. M. De Marzo, E. A. Platz, S. Sutcliffe, J. Xu, H. Grönberg, C. G. Drake, Y. Nakai, W. B. Isaacs, and W. G. Nelson. Inflammation in prostate carcinogenesis. *Nat Rev Cancer*, 7:256–269, 2007.
- [5] J. Ferlay, D. M. Parkin, and E. Steliarova-Foucher. Estimates of cancer incidence and mortality in Europe in 2008. *Eur J Cancer*, 46:765–781, 2010.
- [6] V. Nelen. Epidemiology of prostate cancer. In *Prostate Cancer*, volume 175 of *Recent Results in Cancer Research*, chapter 1, pages 1–8. Springer Berlin Heidelberg, 2007.
- [7] R. Siegel, J. Ma, Z. Zou, and A. Jemal. Cancer statistics, 2014. *CA Cancer J Clin*, 64:9–29, 2014.
- [8] J. Ferlay, H. R. Shin, F. Bray, D. Forman, C. Mathers, and D. M. Parkin. Estimates of worldwide burden of cancer in 2008: GLOBOCAN 2008. *Int J Cancer*, 127:2893–2917, 2010.
- [9] E. D. Crawford. Epidemiology of prostate cancer. *Urology*, 62:3–12, 2003.
- [10] P. T. Scardino, R. Weaver, and M. A. Hudson. Early detection of prostate cancer. *Hum Pathol*, 23:211–222, 1992.
- [11] P. Tenke, J. Horti, P. Balint, and B. Kovacs. Prostate cancer screening. In *Prostate Cancer*, volume 175 of *Recent Results in Cancer Research*, chapter 5, pages 65–81. Springer Berlin Heidelberg, 2007.
- [12] A. M. D. Wolf, R. C. Wender, R. B. Etzioni, I. M. Thompson, A. V. D’Amico, R. J. Volk, D. D. Brooks, C. Dash, I. Guessous, K. Andrews, C. DeSantis, R. A. Smith, and American Cancer Society Prostate Cancer Advisory Committee. American Cancer Society guideline for the early detection of prostate cancer: update 2010. *CA Cancer J Clin*, 60:70–98, 2010.
- [13] Integraal Kankercentrum Nederland (IKNL). URL <http://www.cijfersoverkanker.nl>.
- [14] N. B. DeLongchamps, A. Singh, and G. P. Haas. The role of prevalence in the diagnosis of prostate cancer. *Cancer Control*, 13:158–168, 2006.
- [15] M. Sánchez-Chapado, G. Olmedilla, M. Cabeza, E. Donat, and A. Ruiz. Prevalence of prostate cancer and prostatic intraepithelial neoplasia in Caucasian Mediterranean males: an autopsy study. *Prostate*, 54: 238–247, 2003.
- [16] J. E. Johansson, O. Andrén, S. O. Andersson, P. W. Dickman, L. Holmberg, A. Magnuson, and H. O. Adami. Natural history of early, localized prostate cancer. *JAMA*, 291:2713–2719, 2004.
- [17] W. J. Catalona, D. S. Smith, T. L. Ratliff, K. M. Dodds, D. E. Coplen, J. J. Yuan, J. A. Petros, and G. L. Andriole. Measurement of prostate-specific antigen in serum as a screening test for prostate cancer. *N Engl J Med*, 324:1156–1161, 1991.
- [18] K. Lin, R. Lipsitz, T. Miller, S. Janakiraman, and U.S. Preventive Services Task Force. Benefits and harms of prostate-specific antigen screening for prostate cancer: an evidence update for the U.S. Preventive Services Task Force. *Ann Intern Med*, 149:192–199, 2008.
- [19] E. D. Crawford, E. P. DeAntoni, R. Etzioni, V. C. Schaefer, R. M. Olson, C. A. Ross, and The Prostate Cancer Education Council. Serum prostate-specific antigen and digital rectal examination for early detection of prostate cancer in a national community-based program. *Urology*, 47:863–869, 1996.

- [20] K. Mistry and G. Cable. Meta-analysis of prostate-specific antigen and digital rectal examination as screening tests for prostate carcinoma. *J Am Board Fam Pract*, 16:95–101, 2003.
- [21] H. Watanabe, H. Kato, T. Kato, M. Morita, and M. Tanaka. Diagnostic application of ultrasonotomography to the prostate. *Nihon Hinyokika Gakkai Zasshi*, 59:273–279, 1968.
- [22] H. Watanabe. History and applications of transrectal sonography of the prostate. *Urol Clin North Am*, 16: 617–622, 1989.
- [23] S. W. T. P. J. Heijmink, H. van Moerkerk, L. A. L. M. Kiemeney, J. A. Witjes, F. Frauscher, and J. O. Barentsz. A comparison of the diagnostic performance of systematic versus ultrasound-guided biopsies of prostate cancer. *Eur Radiol*, 16:927–938, 2006.
- [24] J. Raja, N. Ramachandran, G. Munneke, and U. Patel. Current status of transrectal ultrasound-guided prostate biopsy in the diagnosis of prostate cancer. *Clin Radiol*, 61:142–153, 2006.
- [25] K. K. Hodge, J. E. McNeal, M. K. Terris, and T. A. Stamey. Random systematic versus directed ultrasound guided transrectal core biopsies of the prostate. *J Urol*, 142:71–75, 1989.
- [26] J. C. Presti. Prostate biopsy: current status and limitations. *Rev Urol*, 9:93–98, 2007.
- [27] T. A. Stamey. Making the most out of six systematic sextant biopsies. *Urology*, 45:2–12, 1995.
- [28] O. Ukimura, J. A. Coleman, A. de la Taille, M. Emberton, J. I. Epstein, S. J. Freedland, G. Giannarini, A. S. Kibel, R. Montironi, G. Ploussard, M. J. Roobol, V. Scattoni, and J. S. Jones. Contemporary role of systematic prostate biopsies: indications, techniques, and implications for patient care. *Eur Urol*, 63: 214–230, 2013.
- [29] M. Baumann, P. Mozer, V. Daanen, and J. Troccaz. Prostate biopsy tracking with deformation estimation. *Med Image Anal*, 16:562–576, 2012.
- [30] K. A. Roehl, J. A. V. Antenor, and W. J. Catalona. Serial biopsy results in prostate cancer screening study. *J Urol*, 167:2435–2439, 2002.
- [31] C. S. Stewart, B. C. Leibovich, A. L. Weaver, and M. M. Lieber. Prostate cancer diagnosis using a saturation needle biopsy technique after previous negative sextant biopsies. *J Urol*, 166:86–92, 2001.
- [32] F. Sano, H. Terao, T. Kawahara, Y. Miyoshi, T. Sasaki, K. Noguchi, Y. Kubota, and H. Uemura. Contrast-enhanced ultrasonography of the prostate: various imaging findings that indicate prostate cancer. *BJU Int*, 107:1404–1410, 2011.
- [33] M. Brock, C. von Bodman, R. J. Palisaar, B. Löppenberg, F. Sommerer, T. Deix, J. Noldus, and T. Eggert. The impact of real-time elastography guiding a systematic prostate biopsy to improve cancer detection rate: a prospective study of 353 patients. *J Urol*, 187:2039–2043, 2012.
- [34] D. J. Rosario, J. A. Lane, C. Metcalfe, J. L. Donovan, A. Doble, L. Goodwin, M. Davis, J. W. F. Catto, K. Avery, D. E. Neal, and F. C. Hamdy. Short term outcomes of prostate biopsy in men tested for cancer by prostate specific antigen: prospective evaluation within ProtecT study. *BMJ*, 344:d7894, 2012.
- [35] D. F. Gleason. Classification of prostatic carcinomas. *Cancer Chemother Rep*, 50:125–128, 1966.
- [36] J. I. Epstein, W. C. Allsbrook, M. B. Amin, L. L. Egevad, and ISUP Grading Committee. The 2005 International Society of Urological Pathology (ISUP) consensus conference on Gleason grading of prostatic carcinoma. *Am J Surg Pathol*, 29:1228–1242, 2005.
- [37] P. A. Humphrey. Gleason grading and prognostic factors in carcinoma of the prostate. *Mod Pathol*, 17: 292–306, 2004.

- [38] P. C. Albertsen, J. A. Hanley, and J. Fine. 20-year outcomes following conservative management of clinically localized prostate cancer. *JAMA*, 293:2095–2101, 2005.
- [39] M. Borre, B. Nerstrøm, and J. Overgaard. The natural history of prostate carcinoma based on a Danish population treated with no intent to cure. *Cancer*, 80:917–928, 1997.
- [40] J. Hugosson and G. Aus. Natural course of localized prostate cancer. a personal view with a review of published papers. *Anticancer Res*, 17:1441–1448, 1997.
- [41] M. A. Dall’Era, P. C. Albertsen, C. Bangma, P. R. Carroll, H. B. Carter, M. R. Cooperberg, S. J. Freedland, L. H. Klotz, C. Parker, and M. S. Soloway. Active surveillance for prostate cancer: a systematic review of the literature. *Eur Urol*, 62:976–983, 2012.
- [42] L. Klotz, L. Zhang, A. Lam, R. Nam, A. Mamedov, and A. Loblaw. Clinical results of long-term follow-up of a large, active surveillance cohort with localized prostate cancer. *J Clin Oncol*, 28:126–131, 2010.
- [43] L. Budäus, M. Bolla, A. Bossi, C. Cozzarini, J. Crook, A. Widmark, and T. Wiegel. Functional outcomes and complications following radiation therapy for prostate cancer: a critical analysis of the literature. *Eur Urol*, 61:112–127, 2012.
- [44] J. D. Hall, J. C. Boyd, M. C. Lippert, and D. Theodorescu. Why patients choose prostatectomy or brachytherapy for localized prostate cancer: results of a descriptive survey. *Urology*, 61:402–407, 2003.
- [45] J. Hegarty, P. V. Beirne, E. Walsh, H. Comber, T. Fitzgerald, and M. Wallace Kazer. Radical prostatectomy versus watchful waiting for prostate cancer. *Cochrane Database Syst Rev*, page CD006590, 2010.
- [46] F. Peinemann, U. Grouven, L. G. Hemkens, C. Bartel, H. Borchers, M. Pinkawa, A. Heidenreich, and S. Sauerland. Low-dose rate brachytherapy for men with localized prostate cancer. *Cochrane Database Syst Rev*, page CD008871, 2011.
- [47] R. Raaijmakers, B. G. Blijenberg, J. A. Finlay, H. G. Rittenhouse, M. F. Wildhagen, M. J. Roobol, and F. H. Schröder. Prostate cancer detection in the prostate specific antigen range of 2.0 to 3.9 ng/ml: value of percent free prostate specific antigen on tumor detection and tumor aggressiveness. *J Urol*, 171:2245–2249, 2004.
- [48] I. M. Thompson, D. K. Pauler, P. J. Goodman, C. M. Tangen, M. S. Lucia, H. L. Parnes, L. M. Minasian, L. G. Ford, S. M. Lippman, E. D. Crawford, J. J. Crowley, and C. A. Coltman. Prevalence of prostate cancer among men with a prostate-specific antigen level ≤ 4.0 ng per milliliter. *N Engl J Med*, 350:2239–2246, 2004.
- [49] A. N. Vis, R. F. Hoedemaeker, M. Roobol, T. H. van der Kwast, and F. H. Schröder. Tumor characteristics in screening for prostate cancer with and without rectal examination as an initial screening test at low PSA (0.0-3.9 ng/ml). *Prostate*, 47:252–261, 2001.
- [50] I. M. Thompson, D. P. Ankerst, C. Chi, M. S. Lucia, P. J. Goodman, J. J. Crowley, H. L. Parnes, and C. A. Coltman. Operating characteristics of prostate-specific antigen in men with an initial PSA level of 3.0 ng/ml or lower. *JAMA*, 294:66–70, 2005.
- [51] G. L. Andriole, E. D. Crawford, R. L. Grubb, S. S. Buys, D. Chia, T. R. Church, M. N. Fouad, E. P. Gelmann, P. A. Kvale, D. J. Reding, J. L. Weissfeld, L. A. Yokochi, B. O’Brien, J. D. Clapp, J. M. Rathmell, T. L. Riley, R. B. Hayes, B. S. Kramer, G. Izmirlian, A. B. Miller, P. F. Pinsky, P. C. Prorok, J. K. Gohagan, C. D. Berg, and the PLCO Project Team. Mortality results from a randomized prostate-cancer screening trial. *N Engl J Med*, 360:1310–1319, 2009.

- [52] F. H. Schröder, J. Hugosson, M. J. Roobol, T. L. J. Tammela, S. Ciatto, V. Nelen, M. Kwiatkowski, M. Lujan, H. Lilja, M. Zappa, L. J. Denis, F. Recker, A. Berenguer, L. Määtänen, C. H. Bangma, G. Aus, A. Villers, X. Rebillard, T. van der Kwast, B. G. Blijenberg, S. M. Moss, H. J. de Koning, A. Auvinen, and the ERSPC Investigators. Screening and prostate-cancer mortality in a randomized European study. *N Engl J Med*, 360:1320–1328, 2009.
- [53] F. H. Schröder, J. Hugosson, M. J. Roobol, T. L. J. Tammela, S. Ciatto, V. Nelen, M. Kwiatkowski, M. Lujan, H. Lilja, M. Zappa, L. J. Denis, F. Recker, A. Páez, L. Määtänen, C. H. Bangma, G. Aus, S. Carlsson, A. Villers, X. Rebillard, T. van der Kwast, P. M. Kujala, B. G. Blijenberg, U.-H. Stenman, A. Huber, K. Taari, M. Hakama, S. M. Moss, H. J. de Koning, A. Auvinen, and the ERSPC Investigators. Prostate-cancer mortality at 11 years of follow-up. *N Engl J Med*, 366:981–990, 2012.
- [54] M. Djulbegovic, R. J. Beyth, M. M. Neuberger, T. L. Stoffs, J. Vieweg, B. Djulbegovic, and P. Dahm. Screening for prostate cancer: systematic review and meta-analysis of randomised controlled trials. *BMJ*, 341:c4543, 2010.
- [55] M. J. Roobol, M. Kerkhof, F. H. Schröder, J. Cuzick, P. Sasieni, M. Hakama, U. H. Stenman, S. Ciatto, V. Nelen, M. Kwiatkowski, M. Lujan, H. Lilja, M. Zappa, L. Denis, F. Recker, A. Berenguer, M. Ruutu, P. Kujala, C. H. Bangma, G. Aus, T. L. J. Tammela, A. Villers, X. Rebillard, S. M. Moss, H. J. de Koning, J. Hugosson, and A. Auvinen. Prostate cancer mortality reduction by prostate-specific antigen-based screening adjusted for nonattendance and contamination in the European Randomised Study of Screening for Prostate Cancer (ERSPC). *Eur Urol*, 56:584–591, 2009.
- [56] S. J. Otto, P. J. van Leeuwen, J. W. Hoekstra, J. W. Merckelbach, J. H. M. Blom, F. H. Schröder, M. J. Roobol, and H. J. de Koning. Blinded and uniform causes of death verification in cancer screening: a major influence on the outcome of a prostate cancer screening trial? *Eur J Cancer*, 46:3061–3067, 2010.
- [57] F. H. Schröder, H. B. Carter, T. Wolters, R. C. N. van den Bergh, C. Gosselaar, C. H. Bangma, and M. J. Roobol. Early detection of prostate cancer in 2007. Part 1: PSA and PSA kinetics. *Eur Urol*, 53:468–477, 2008.
- [58] A. E. Pelzer, A. Tewari, J. Bektic, A. P. Berger, F. Frauscher, G. Bartsch, and W. Horninger. Detection rates and biologic significance of prostate cancer with PSA less than 4.0 ng/mL: observation and clinical implications from Tyrol screening project. *Urology*, 66:1029–1033, 2005.
- [59] B. Spajic, H. Eupic, D. Tomas, G. Stimac, B. Kruslin, and O. Kraus. The incidence of hyperechoic prostate cancer in transrectal ultrasound-guided biopsy specimens. *Urology*, 70:734–737, 2007.
- [60] M. Norberg, L. Egevad, L. Holmberg, P. Sparén, B. J. Norlén, and C. Busch. The sextant protocol for ultrasound-guided core biopsies of the prostate underestimates the presence of cancer. *Urology*, 50:562–566, 1997.
- [61] M. K. Terris. Sensitivity and specificity of sextant biopsies in the detection of prostate cancer: preliminary report. *Urology*, 54:486–489, 1999.
- [62] R. Kvåle, B. M. Iler, R. Wahlqvist, S. D. Fosså, A. Berner, C. Busch, A. E. Kyrдалen, A. Svindland, T. Viset, and O. J. Halvorsen. Concordance between Gleason scores of needle biopsies and radical prostatectomy specimens: a population-based study. *BJU Int*, 103:1647–1654, 2009.
- [63] M. Noguchi, T. A. Stamey, J. E. McNeal, and C. M. Yemoto. Relationship between systematic biopsies and histological features of 222 radical prostatectomy specimens: lack of prediction of tumor significance for men with nonpalpable prostate cancer. *J Urol*, 166:104–109, 2001.
- [64] A. Rajinikanth, M. Manoharan, C. T. Soloway, F. J. Civantos, and M. S. Soloway. Trends in Gleason score: Concordance between biopsy and prostatectomy over 15 years. *Urology*, 72:177–182, 2008.

- [65] S. Tomioka, H. Nakatsu, N. Suzuki, S. Murakami, O. Matsuzaki, and J. Shimazaki. Comparison of Gleason grade and score between preoperative biopsy and prostatectomy specimens in prostate cancer. *Int J Urol*, 13:555–559, 2006.
- [66] H. Hricak, G. C. Dooks, J. E. McNeal, A. S. Mark, M. Marotti, A. Avallone, M. Pelzer, E. C. Proctor, and E. A. Tanagho. MR imaging of the prostate gland: normal anatomy. *AJR Am J Roentgenol*, 148:51–58, 1987.
- [67] N. L. Robertson, M. Emberton, and C. M. Moore. MRI-targeted prostate biopsy: a review of technique and results. *Nat Rev Urol*, 10:589–597, 2013.
- [68] F. V. Coakley and H. Hricak. Radiologic anatomy of the prostate: a clinical approach. *Radiol Clin North Am*, 38:15–30, 2000.
- [69] M. R. Engelbrecht, H. J. Huisman, R. J. F. Laheij, G. J. Jager, G. J. L. H. van Leenders, C. A. Hulsbergen-van de Kaa, J. J. M. C. H. de la Rosette, J. G. Blickman, and J. O. Barentsz. Discrimination of prostate cancer from normal peripheral zone and central gland tissue by using dynamic contrast-enhanced MR imaging. *Radiology*, 229:248–254, 2003.
- [70] R. Bammer. Basic principles of diffusion-weighted imaging. *Eur J Radiol*, 45:169–184, 2003.
- [71] T. W. J. Scheenen, D. W. J. Klomp, S. A. Röhl, J. J. Fütterer, J. O. Barentsz, and A. Heerschap. Fast acquisition-weighted three-dimensional proton MR spectroscopic imaging of the human prostate. *Magn Reson Med*, 52:80–88, 2004.
- [72] A. Sciarra, J. Barentsz, A. Bjartell, J. Eastham, H. Hricak, V. Panebianco, and J. A. Witjes. Advances in magnetic resonance imaging: How they are changing the management of prostate cancer. *Eur Urol*, 59:962–977, 2011.
- [73] J. J. Fütterer, S. W. T. P. J. Heijmink, T. W. J. Scheenen, J. Veltman, H. J. Huisman, P. Vos, C. A. Hulsbergen-van de Kaa, J. A. Witjes, P. F. M. Krabbe, A. Heerschap, and J. O. Barentsz. Prostate cancer localization with dynamic contrast-enhanced MR imaging and proton MR spectroscopic imaging. *Radiology*, 241:449–458, 2006.
- [74] N. B. Delongchamps, M. Rouanne, T. Flam, F. Beuvon, M. Liberatore, M. Zerbib, and F. Cornud. Multiparametric magnetic resonance imaging for the detection and localization of prostate cancer: combination of T2-weighted, dynamic contrast-enhanced and diffusion-weighted imaging. *BJU Int*, 107:1411–1418, 2011.
- [75] K. Kitajima, Y. Kaji, Y. Fukabori, K. Yoshida, N. Suganuma, and K. Sugimura. Prostate cancer detection with 3 T MRI: Comparison of diffusion-weighted imaging and dynamic contrast-enhanced MRI in combination with T2-weighted imaging. *J Magn Reson Imaging*, 31:625–631, 2010.
- [76] A. Tanimoto, J. Nakashima, H. Kohno, H. Shinmoto, and S. Kuribayashi. Prostate cancer screening: The clinical value of diffusion-weighted imaging and dynamic MR imaging in combination with T2-weighted imaging. *J Magn Reson Imaging*, 25:146–152, 2007.
- [77] N. M. deSouza, S. F. Riches, N. J. Vanas, V. A. Morgan, S. A. Ashley, C. Fisher, G. S. Payne, and C. Parker. Diffusion-weighted magnetic resonance imaging: a potential non-invasive marker of tumour aggressiveness in localized prostate cancer. *Clin Radiol*, 63:774–782, 2008.
- [78] T. Hambrock, D. M. Somford, H. J. Huisman, I. M. van Oort, J. A. Witjes, C. A. Hulsbergen-van de Kaa, T. Scheenen, and J. O. Barentsz. Relationship between apparent diffusion coefficients at 3.0-T MR imaging and Gleason grade in peripheral zone prostate cancer. *Radiology*, 259:453–461, 2011.
- [79] Y. Itou, K. Nakanishi, Y. Narumi, Y. Nishizawa, and H. Tsukuma. Clinical utility of apparent diffusion coefficient (ADC) values in patients with prostate cancer: can ADC values contribute to assess the aggressiveness of prostate cancer? *J Magn Reson Imaging*, 33:167–172, 2011.

- [80] S. Verma, A. Rajesh, H. Morales, L. Lemen, G. Bills, M. Delworth, K. Gaitonde, J. Ying, R. Samartunga, and M. Lamba. Assessment of aggressiveness of prostate cancer: correlation of apparent diffusion coefficient with histologic grade after radical prostatectomy. *AJR Am J Roentgenol*, 196:374–381, 2011.
- [81] H. K. Lim, J. K. Kim, K. A. Kim, and K.-S. Cho. Prostate cancer: apparent diffusion coefficient map with T2-weighted images for detection – a multireader study. *Radiology*, 250:145–151, 2009.
- [82] J. J. Fütterer, M. R. Engelbrecht, H. J. Huisman, G. J. Jager, C. A. Hulsbergen-van de Kaa, J. A. Witjes, and J. O. Barentsz. Staging prostate cancer with dynamic contrast-enhanced endorectal MR imaging prior to radical prostatectomy: experienced versus less experienced readers. *Radiology*, 237:541–549, 2005.
- [83] L. Dickinson, H. U. Ahmed, C. Allen, J. O. Barentsz, B. Carey, J. J. Fütterer, S. W. Heijmink, P. J. Hoskin, A. Kirkham, A. R. Padhani, R. Persad, P. Puech, S. Punwani, A. S. Sohaib, B. Tombal, A. Villers, J. van der Meulen, and M. Emberton. Magnetic resonance imaging for the detection, localisation, and characterisation of prostate cancer: recommendations from a European consensus meeting. *Eur Urol*, 59:477–494, 2011.
- [84] G. J. Kelloff, P. Choyke, D. S. Coffey, and P. C. I. W. G. . Challenges in clinical prostate cancer: role of imaging. *AJR Am J Roentgenol*, 192:1455–1470, 2009.
- [85] J. O. Barentsz, J. Richenberg, R. Clements, P. Choyke, S. Verma, G. Villeirs, O. Rouvière, V. Logager, J. J. Fütterer, and European Society of Urogenital Radiology. ESUR prostate MR guidelines 2012. *Eur Radiol*, 22:746–757, 2012.
- [86] J. G. R. Bomers and J. O. Barentsz. Standardization of multiparametric prostate MR imaging using PI-RADS. *Biomed Res Int*, 2014:431680, 2014.
- [87] L. M. Johnson, B. Turkbey, W. D. Figg, and P. L. Choyke. Multiparametric MRI in prostate cancer management. *Nat Rev Clin Oncol*, 11:346–353, 2014.
- [88] M. C. Roethke, T. H. Kuru, S. Schultze, D. Tichy, A. Kopp-Schneider, M. Fenchel, H.-P. Schlemmer, and B. A. Hadaschik. Evaluation of the ESUR PI-RADS scoring system for multiparametric MRI of the prostate with targeted MR/TRUS fusion-guided biopsy at 3.0 Tesla. *Eur Radiol*, 24:344–352, 2014.
- [89] A. B. Rosenkrantz, S. Kim, R. P. Lim, N. Hindman, F.-M. Deng, J. S. Babb, and S. S. Taneja. Prostate cancer localization using multiparametric MR imaging: comparison of Prostate Imaging Reporting and Data System (PI-RADS) and Likert scales. *Radiology*, 269:482–492, 2013.
- [90] D. Portalez, P. Mozer, F. Cornud, R. Renard-Penna, V. Misrai, M. Thoulouzan, and B. Malavaud. Validation of the European Society of Urogenital Radiology scoring system for prostate cancer diagnosis on multiparametric magnetic resonance imaging in a cohort of repeat biopsy patients. *Eur Urol*, 62:986–996, 2012.
- [91] L. Schimmöller, M. Quentin, C. Arsov, R. S. Lanzman, A. Hiester, R. Rabenalt, G. Antoch, P. Albers, and D. Blondin. Inter-reader agreement of the ESUR score for prostate MRI using in-bore MRI-guided biopsies as the reference standard. *Eur Radiol*, 23:3185–3190, 2013.
- [92] S. D. Herman, A. C. Friedman, P. D. Radecki, and D. F. Caroline. Incidental prostatic carcinoma detected by MRI and diagnosed by MRI/CT-guided biopsy. *AJR Am J Roentgenol*, 146:351–352, 1986.
- [93] J. Haffner, L. Lemaitre, P. Puech, G.-P. Haber, X. Leroy, J. S. Jones, and A. Villers. Role of magnetic resonance imaging before initial biopsy: comparison of magnetic resonance imaging-targeted and systematic biopsy for significant prostate cancer detection. *BJU Int*, 108:E171–E178, 2011.
- [94] T. Hambrock, D. M. Somford, C. Hoeks, S. A. W. Bouwense, H. Huisman, D. Yakar, I. M. van Oort, J. A. Witjes, J. J. Fütterer, and J. O. Barentsz. Magnetic resonance imaging guided prostate biopsy in men with repeat negative biopsies and increased prostate specific antigen. *J Urol*, 183:520–527, 2010.

- [95] C. M. A. Hoeks, M. G. Schouten, J. G. R. Bomers, S. P. Hoogendoorn, C. A. Hulsbergen-van de Kaa, T. Hambrock, H. Vergunst, J. P. M. Sedelaar, J. J. Fütterer, and J. O. Barentsz. Three-Tesla magnetic resonance-guided prostate biopsy in men with increased prostate-specific antigen and repeated, negative, random, systematic, transrectal ultrasound biopsies: Detection of clinically significant prostate cancers. *Eur Urol*, 62:902–909, 2012.
- [96] S. H. Lee, M. S. Chung, J. H. Kim, Y. T. Oh, K. H. Rha, and B. H. Chung. Magnetic resonance imaging targeted biopsy in men with previously negative prostate biopsy results. *J Endourol*, 26:787–791, 2012.
- [97] Y. Watanabe, A. Terai, T. Araki, M. Nagayama, A. Okumura, Y. Amoh, T. Ishimori, M. Ishibashi, S. Nakashita, and Y. Dodo. Detection and localization of prostate cancer with the targeted biopsy strategy based on ADC map: A prospective large-scale cohort study. *J Magn Reson Imaging*, 35:1414–1421, 2012.
- [98] T. Hambrock, C. Hoeks, C. Hulsbergen-van de Kaa, T. Scheenen, J. Fütterer, S. Bouwense, I. van Oort, F. Schröder, H. Huisman, and J. Barentsz. Prospective assessment of prostate cancer aggressiveness using 3-T diffusion-weighted magnetic resonance imaging-guided biopsies versus a systematic 10-core transrectal ultrasound prostate biopsy cohort. *Eur Urol*, 61:177–184, 2012.
- [99] D. Beyersdorff, A. Winkel, B. Hamm, S. Lenk, S. A. Loening, and M. Taupitz. MR imaging-guided prostate biopsy with a closed MR unit at 1.5 T: initial results. *Radiology*, 234:576–581, 2005.
- [100] K. Engelhard, H. P. Hollenbach, B. Kiefer, A. Winkel, K. Goeb, and D. Engehausen. Prostate biopsy in the supine position in a standard 1.5-T scanner under real time MR-imaging control using a MR-compatible endorectal biopsy device. *Eur Radiol*, 16:1237–1243, 2006.
- [101] T. Franiel, C. Stephan, A. Erbersdobler, E. Dietz, A. Maxeiner, N. Hell, A. Huppertz, K. Miller, R. Strecker, and B. Hamm. Areas suspicious for prostate cancer: MR-guided biopsy in patients with at least one transrectal US-guided biopsy with a negative finding – multiparametric MR imaging for detection and biopsy planning. *Radiology*, 259:162–172, 2011.
- [102] M. Roethke, A. G. Anastasiadis, M. Lichy, M. Werner, P. Wagner, S. Kruck, C. D. Claussen, A. Stenzl, H. P. Schlemmer, and D. Schilling. MRI-guided prostate biopsy detects clinically significant cancer: analysis of a cohort of 100 patients after previous negative TRUS biopsy. *World J Urol*, 30:213–218, 2012.
- [103] N. Arumainayagam, H. U. Ahmed, C. M. Moore, A. Freeman, C. Allen, S. A. Sohaib, A. Kirkham, J. van der Meulen, and M. Emberton. Multiparametric MR imaging for detection of clinically significant prostate cancer: A validation cohort study with transperineal template prostate mapping as the reference standard. *Radiology*, 268:761–769, 2013.
- [104] M. R. Pokorny, M. de Rooij, E. Duncan, F. H. Schröder, R. Parkinson, J. O. Barentsz, and L. C. Thompson. Prospective study of diagnostic accuracy comparing prostate cancer detection by transrectal ultrasound-guided biopsy versus magnetic resonance (MR) imaging with subsequent MR-guided biopsy in men without previous prostate biopsies. *Eur Urol*, 66:22–29, 2014.
- [105] M. de Rooij, S. Crienen, J. A. Witjes, J. O. Barentsz, M. M. Rovers, and J. P. Grutters. Cost-effectiveness of magnetic resonance (MR) imaging and MR-guided targeted biopsy versus systematic transrectal ultrasound-guided biopsy in diagnosing prostate cancer: A modelling study from a health care perspective. *Eur Urol*, 66:430–436, 2014.
- [106] T. Penzkofer and C. M. Tempny-Afdhal. Prostate cancer detection and diagnosis: the role of MR and its comparison with other diagnostic modalities – a radiologist’s perspective. *NMR Biomed*, 27:3–15, 2014.
- [107] I. Kaplan, N. E. Oldenburg, P. Meskill, M. Blake, P. Church, and E. J. Holupka. Real time MRI-ultrasound image guided stereotactic prostate biopsy. *Magn Reson Imaging*, 20:295–299, 2002.

- [108] F. Cornud, L. Brolis, N. B. Delongchamps, D. Portalez, B. Malavaud, R. Renard-Penna, and P. Mozer. TRUS-MRI image registration: a paradigm shift in the diagnosis of significant prostate cancer. *Abdom Imaging*, 38:1447–1463, 2013.
- [109] J. K. Logan, S. Rais-Bahrami, B. Turkbey, A. Gomella, H. Amalou, P. L. Choyke, B. J. Wood, and P. A. Pinto. Current status of magnetic resonance imaging (MRI) and ultrasonography fusion software platforms for guidance of prostate biopsies. *BJU Int*, 114:641–652, 2014.
- [110] C. M. Moore, N. L. Robertson, N. Arsanious, T. Middleton, A. Villers, L. Klotz, S. S. Taneja, and M. Emberton. Image-guided prostate biopsy using magnetic resonance imaging-derived targets: a systematic review. *Eur Urol*, 63:125–140, 2013.
- [111] P. Puech, O. Rouvière, R. Renard-Penna, A. Villers, P. Devos, M. Colombel, M.-O. Bitker, X. Leroy, F. Mège-Lechevallier, E. Comperat, A. Ouzzane, and L. Lemaitre. Prostate cancer diagnosis: Multiparametric MR-targeted biopsy with cognitive and transrectal US-MR fusion guidance versus systematic biopsy—prospective multicenter study. *Radiology*, 268:461–469, 2013.
- [112] N. B. Delongchamps, M. Peyromaure, A. Schull, F. Beuvon, N. Bouazza, T. Flam, M. Zerbib, N. Muradyan, P. Legman, and F. Cornud. Prebiopsy magnetic resonance imaging and prostate cancer detection: Comparison of random and targeted biopsies. *J Urol*, 189:493–499, 2013.
- [113] S. Xu, J. Kruecker, B. Turkbey, N. Glossop, A. K. Singh, P. Choyke, P. Pinto, and B. J. Wood. Real-time MRI-TRUS fusion for guidance of targeted prostate biopsies. *Comput Aided Surg*, 13:255–264, 2008.
- [114] T. E. Byrne. A review of prostate motion with considerations for the treatment of prostate cancer. *Med Dosim*, 30:155–161, 2005.
- [115] O. Ukimura, N. Hirahara, A. Fujihara, T. Yamada, T. Iwata, K. Kamoi, K. Okihara, H. Ito, T. Nishimura, and T. Miki. Technique for a hybrid system of real-time transrectal ultrasound with preoperative magnetic resonance imaging in the guidance of targeted prostate biopsy. *Int J Urol*, 17:890–893, 2010.
- [116] A. K. Singh, J. Kruecker, S. Xu, N. Glossop, P. Guion, K. Ullman, P. L. Choyke, and B. J. Wood. Initial clinical experience with real-time transrectal ultrasonography-magnetic resonance imaging fusion-guided prostate biopsy. *BJU Int*, 101:841–845, 2008.
- [117] R. Narayanan, J. Kurhanewicz, K. Shinohara, E. D. Crawford, A. Simoneau, and J. S. Suri. MRI-ultrasound registration for targeted prostate biopsy. In *IEEE Int Symp Biomedical Imaging*, pages 991–994, 2009.
- [118] J. Mitra, Z. Kato, R. Martí, A. Oliver, X. Lladó, D. Sidibé, S. Ghose, J. C. Vilanova, J. Comet, and F. Meriaudeau. A spline-based non-linear diffeomorphism for multimodal prostate registration. *Med Image Anal*, 16:1259–1279, 2012.
- [119] S. Martin, M. Baumann, V. Daanen, and J. Troccaz. MR prior based automatic segmentation of the prostate in TRUS images for MR/TRUS data fusion. In *IEEE Int Symp Biomedical Imaging*, pages 640–643, 2010.
- [120] A. Fedorov, K. Tuncali, F. M. Fennessy, J. Tokuda, N. Hata, W. M. Wells, R. Kikinis, and C. M. Tempany. Image registration for targeted MRI-guided transperineal prostate biopsy. *J Magn Reson Imaging*, 36: 987–992, 2012.
- [121] V. V. Karnik, A. Fenster, J. Bax, D. W. Cool, L. Gardi, I. Gyacskov, C. Romagnoli, and A. D. Ward. Assessment of image registration accuracy in three-dimensional transrectal ultrasound guided prostate biopsy. *Med Phys*, 37:802–813, 2010.
- [122] Y. Hu, T. Carter, H. Ahmed, M. Emberton, C. Allen, D. Hawkes, and D. Barratt. Modelling prostate motion for data fusion during image-guided interventions. *IEEE Trans Med Imaging*, 30:1887–1900, 2011.

- [123] R. Alterovitz, K. Goldberg, J. Pouliot, I.-C. J. Hsu, Y. Kim, S. M. Noworolski, and J. Kurhanewicz. Registration of MR prostate images with biomechanical modeling and nonlinear parameter estimation. *Med Phys*, 33:446–454, 2006.
- [124] A. Bharatha, M. Hirose, N. Hata, S. K. Warfield, M. Ferrant, K. H. Zou, E. Suarez-Santana, J. Ruiz-Alzola, A. D’Amico, R. A. Cormack, R. Kikinis, F. A. Jolesz, and C. M. Tempny. Evaluation of three-dimensional finite element-based deformable registration of pre- and intraoperative prostate imaging. *Med Phys*, 28:2551–2560, 2001.
- [125] Y. Hu, H. U. Ahmed, Z. Taylor, C. Allen, M. Emberton, D. Hawkes, and D. Barratt. MR to ultrasound registration for image-guided prostate interventions. *Med Image Anal*, 16:687–703, 2012.
- [126] B. A. Hadaschik, T. H. Kuru, C. Tulea, P. Rieker, I. V. Popeneciu, T. Simpfendorfer, J. Huber, P. Zogal, D. Teber, S. Pahernik, M. Roethke, P. Zamecnik, W. Roth, G. Sakas, H.-P. Schlemmer, and M. Hohenfellner. A novel stereotactic prostate biopsy system integrating pre-interventional magnetic resonance imaging and live ultrasound fusion. *J Urol*, 186:2214–2220, 2011.
- [127] T. Miyagawa, S. Ishikawa, T. Kimura, T. Suetomi, M. Tsutsumi, T. Irie, M. Kondoh, and T. Mitake. Real-time virtual sonography for navigation during targeted prostate biopsy using magnetic resonance imaging data. *Int J Urol*, 17:855–860, 2010.
- [128] M. M. Siddiqui, S. Rais-Bahrami, H. Truong, L. Stamatakis, S. Vourganti, J. Nix, A. N. Hoang, A. Walton-Diaz, B. Shuch, M. Weintraub, J. Kruecker, H. Amalou, B. Turkbey, M. J. Merino, P. L. Choyke, B. J. Wood, and P. A. Pinto. Magnetic resonance imaging/ultrasound-fusion biopsy significantly upgrades prostate cancer versus systematic 12-core transrectal ultrasound biopsy. *Eur Urol*, 64:713–719, 2013.
- [129] G. A. Sonn, E. Chang, S. Natarajan, D. J. Margolis, M. Macairan, P. Lieu, J. Huang, F. J. Dorey, R. E. Reiter, and L. S. Marks. Value of targeted prostate biopsy using magnetic resonance-ultrasound fusion in men with prior negative biopsy and elevated prostate-specific antigen. *Eur Urol*, 65:809–815, 2013.
- [130] W. J. M. van de Ven, C. A. Hulsbergen-van de Kaa, T. Hambrock, J. O. Barentsz, and H. J. Huisman. Simulated required accuracy of image registration tools for targeting high-grade cancer components with prostate biopsies. *Eur Radiol*, 23:1401–1407, 2013.
- [131] A. Jemal, F. Bray, M. M. Center, J. Ferlay, E. Ward, and D. Forman. Global cancer statistics. *CA Cancer J Clin*, 61:69–90, 2011.
- [132] M. Aihara, T. M. Wheeler, M. Otori, and P. T. Scardino. Heterogeneity of prostate cancer in radical prostatectomy specimens. *Urology*, 43:60–67, 1994.
- [133] E. T. Ruijter, C. A. van de Kaa, J. A. Schalken, F. M. Debruyne, and D. J. Ruijter. Histological grade heterogeneity in multifocal prostate cancer. Biological and clinical implications. *J Pathol*, 180:295–299, 1996.
- [134] S. Kadoury, P. Yan, S. Xu, N. Glossop, P. Choyke, B. Turkbey, P. Pinto, B. Wood, and J. Kruecker. Realtime TRUS/MRI fusion targeted-biopsy for prostate cancer: A clinical demonstration of increased positive biopsy rates. In *Prostate Cancer Imaging. Computer-Aided Diagnosis, Prognosis, and Intervention*, volume 6367 of *Lect Notes Comput Sci*, pages 52–62, 2010.
- [135] H. Huisman and P. Vos. MRCAD for daily clinical analysis of prostate MR. *Kitware Source*, 13:14–15, 2010.
- [136] J. I. Epstein. An update of the Gleason grading system. *J Urol*, 183:433–440, 2010.
- [137] J. H. Kim, J. K. Kim, B. W. Park, N. Kim, and K. S. Cho. Apparent diffusion coefficient: prostate cancer versus noncancerous tissue according to anatomical region. *J Magn Reson Imaging*, 28:1173–1179, 2008.

- [138] T. Tamada, T. Sone, Y. Jo, S. Toshimitsu, T. Yamashita, A. Yamamoto, D. Tanimoto, and K. Ito. Apparent diffusion coefficient values in peripheral and transition zones of the prostate: comparison between normal and malignant prostatic tissues and correlation with histologic grade. *J Magn Reson Imaging*, 28:720–726, 2008.
- [139] A. Oto, A. Kayhan, Y. Jiang, M. Tretiakova, C. Yang, T. Antic, F. Dahi, A. L. Shalhav, G. Karczmar, and W. M. Stadler. Prostate cancer: differentiation of central gland cancer from benign prostatic hyperplasia by using diffusion-weighted and dynamic contrast-enhanced MR imaging. *Radiology*, 257:715–723, 2010.
- [140] C. Sato, S. Naganawa, T. Nakamura, H. Kumada, S. Miura, O. Takizawa, and T. Ishigaki. Differentiation of noncancerous tissue and cancer lesions by apparent diffusion coefficient values in transition and peripheral zones of the prostate. *J Magn Reson Imaging*, 21:258–262, 2005.
- [141] X. Chai, M. van Herk, J. B. van de Kamer, M. C. C. M. Hulshof, P. Remeijer, H. T. Lotz, and A. Bel. Finite element based bladder modeling for image-guided radiotherapy of bladder cancer. *Med Phys*, 38:142–150, 2011.
- [142] Z. A. Taylor, M. Cheng, and S. Ourselin. High-speed nonlinear finite element analysis for surgical simulation using graphics processing units. *IEEE Trans Med Imaging*, 27:650–663, 2008.
- [143] M. M. Center, A. Jemal, J. Lortet-Tieulent, E. Ward, J. Ferlay, O. Brawley, and F. Bray. International variation in prostate cancer incidence and mortality rates. *Eur Urol*, 61:1079–1092, 2012.
- [144] R. Siegel, D. Naishadham, and A. Jemal. Cancer statistics, 2012. *CA Cancer J Clin*, 62:10–29, 2012.
- [145] J.-L. Campos-Fernandes, L. Bastien, N. Nicolaiew, G. Robert, S. Terry, F. Vacherot, L. Salomon, Y. Allory, D. Vordos, A. Hoznek, R. Yiou, J. J. Patard, C. C. Abbou, and A. de la Taille. Prostate cancer detection rate in patients with repeated extended 21-sample needle biopsy. *Eur Urol*, 55:600–606, 2009.
- [146] W. J. M. van de Ven, Y. Hu, J. O. Barentsz, N. Karssemeijer, D. Barratt, and H. J. Huisman. Surface-based prostate registration with biomechanical regularization. In *Medical Imaging*, volume 8671 of *Proceedings of the SPIE*, page 86711R, 2013.
- [147] F. Ritter, T. Boskamp, A. Homeyer, H. Laue, M. Schwier, F. Link, and H.-O. Peitgen. Medical image analysis: A visual approach. *IEEE Pulse*, 2:60–70, 2011.
- [148] H. Si. *Tetgen - a quality tetrahedral mesh generator and three-dimensional Delaunay triangulator*, 2006. URL <http://tetgen.berlios.de>.
- [149] F. Heckel, O. Konrad, H. Karl Hahn, and H.-O. Peitgen. Interactive 3D medical image segmentation with energy-minimizing implicit functions. *Comput Graph*, 35:275–287, 2011.
- [150] I. T. Young and L. J. van Vliet. Recursive implementation of the Gaussian filter. *Signal Processing*, 44:139–151, 1995.
- [151] T. Boehler, D. van Straaten, S. Wirtz, and H.-O. Peitgen. A robust and extendible framework for medical image registration focused on rapid clinical application deployment. *Comput Biol Med*, 41:340–349, 2011.
- [152] J. R. Shewchuk. Tetrahedral mesh generation by Delaunay refinement. In *Proceedings of the SCG*, pages 86–95, 1998.
- [153] G. L. Miller, D. Talmor, S.-H. Teng, and N. Walkington. A Delaunay based numerical method for three dimensions: generation, formulation, and partition. In *Proceedings of the STOC*, pages 683–692, 1995.
- [154] Z. A. Taylor, O. Comas, M. Cheng, J. Passenger, D. J. Hawkes, D. Atkinson, and S. Ourselin. On modelling of anisotropic viscoelasticity for soft tissue simulation: numerical solution and GPU execution. *Med Image Anal*, 13:234–244, 2009.

- [155] R Development Core Team. *R: A Language and Environment for Statistical Computing*. R Foundation for Statistical Computing, Vienna, Austria, 2011. URL <http://www.R-project.org/>.
- [156] J. Pinheiro, D. Bates, S. DebRoy, D. Sarkar, and R Development Core Team. *nlme: Linear and Nonlinear Mixed Effects Models*, 2011. R package version 3.1-101.
- [157] W. J. M. van de Ven and J. O. Barentsz. Prostate cancer: MRI/US-guided biopsy – a viable alternative to TRUS-guidance. *Nat Rev Urol*, 10:559–560, 2013.
- [158] S. Klein, U. A. van der Heide, I. M. Lips, M. van Vulpen, M. Staring, and J. P. W. Pluim. Automatic segmentation of the prostate in 3D MR images by atlas matching using localized mutual information. *Med Phys*, 35:1407–1417, 2008.
- [159] S. Ghose, A. Oliver, R. Martí, X. Lladó, J. C. Vilanova, J. Freixenet, J. Mitra, D. Sidibé, and F. Meriaudeau. A survey of prostate segmentation methodologies in ultrasound, magnetic resonance and computed tomography images. *Comput Methods Programs Biomed*, 108:262–287, 2012.
- [160] G. Litjens, R. Toth, W. van de Ven, C. Hoeks, S. Kerkstra, B. van Ginneken, G. Vincent, G. Guillard, N. Birbeck, J. Zhang, R. Strand, F. Malmberg, Y. Ou, C. Davatzikos, M. Kirschner, F. Jung, J. Yuan, W. Qiu, Q. Gao, P. E. Edwards, B. Maan, F. van der Heijden, S. Ghose, J. Mitra, J. Dowling, D. Barratt, H. Huisman, and A. Madabhushi. Evaluation of prostate segmentation algorithms for MRI: The PROMISE12 challenge. *Med Image Anal*, 18:359–373, 2014.
- [161] Y. Chi, J. Liang, and D. Yan. A material sensitivity study on the accuracy of deformable organ registration using linear biomechanical models. *Med Phys*, 33:421–433, 2006.
- [162] Y. Kim, B. Ahn, J. W. Lee, K. H. Rha, and J. Kim. Local property characterization of prostate glands using inhomogeneous modeling based on tumor volume and location analysis. *Med Biol Eng Comput*, 51:197–205, 2013.
- [163] J. Chappelow, B. N. Bloch, N. Rofsky, E. Genega, R. Lenkinski, W. DeWolf, and A. Madabhushi. Elastic registration of multimodal prostate MRI and histology via multiattribute combined mutual information. *Med Phys*, 38:2005–2018, 2011.
- [164] E. Gibson, C. Crukley, M. Gaed, J. A. Gómez, M. Moussa, J. L. Chin, G. S. Bauman, A. Fenster, and A. D. Ward. Registration of prostate histology images to ex vivo MR images via strand-shaped fiducials. *J Magn Reson Imaging*, 36:1402–1412, 2012.
- [165] A. Walton Diaz, A. N. Hoang, B. Turkbey, C. W. Hong, H. Truong, T. Sterling, S. Rais-Bahrami, M. M. Siddiqui, L. Stamatakis, S. Vourganti, J. Nix, J. Logan, C. Harris, M. Weintraub, C. Chua, M. J. Merino, P. Choyke, B. J. Wood, and P. A. Pinto. Can magnetic resonance-ultrasound fusion biopsy improve cancer detection in enlarged prostates? *J Urol*, 190:2020–2025, 2013.
- [166] P. Mozer, M. Rouprêt, C. Le Cossec, B. Granger, E. Comperat, A. de Gorski, O. Cussenot, and R. Renard-Penna. First round of targeted biopsies with magnetic resonance imaging/ultrasound-fusion images compared to conventional ultrasound-guided trans-rectal biopsies for the diagnosis of localised prostate cancer. *BJU Int*, 115:50–57, 2015.
- [167] N. B. Delongchamps, A. Lefèvre, N. Bouazza, F. Beuvon, P. Legman, and F. Cornud. Detection of significant prostate cancer with magnetic resonance targeted biopsies – should transrectal ultrasound-magnetic resonance imaging fusion guided biopsies alone be a standard of care? *J Urol*, 193:1198–1204, 2015.
- [168] O. Ukimura, A. Marien, S. Palmer, A. Villers, M. Aron, A. L. de Castro Abreu, S. Leslie, S. Shoji, T. Matsugasumi, M. Gross, P. Dasgupta, and I. S. Gill. Trans-rectal ultrasound visibility of prostate lesions identified by magnetic resonance imaging increases accuracy of image-fusion targeted biopsies. *World J Urol*, 33:1669–1676, 2015.

- [169] J. C. Weinreb, J. O. Barentsz, P. L. Choyke, F. Curnud, M. A. Haider, K. J. Macura, D. Margolis, M. D. Schnall, F. Shtern, C. M. Tempany, H. C. Thoeny, and S. Verma. PI-RADS Pirads Imaging – Reporting and Data System: 2015, Version 2. *Eur Urol*, 69:16–40, 2016.
- [170] J. O. Barentsz, J. C. Weinreb, S. Verma, H. C. Thoeny, C. M. Tempany, F. Shtern, A. R. Padhani, D. Margolis, K. J. Macura, M. A. Haider, F. Curnud, and P. L. Choyke. Synopsis of the PI-RADS v2 guidelines for multiparametric prostate magnetic resonance imaging and recommendations for use. *Eur Urol*, 69:41–49, 2016.
- [171] N. E. Fleshner, M. O’Sullivan, C. Premdass, and W. R. Fair. Clinical significance of small (less than 0.2 cm³) hypoechoic lesions in men with normal digital rectal examinations and prostate-specific antigen levels less than 10 ng/mL. *Urology*, 53:356–358, 1999.
- [172] R. Onur, P. J. Littrup, J. E. Pontes, and F. J. Bianco, Jr. Contemporary impact of transrectal ultrasound lesions for prostate cancer detection. *J Urol*, 172:512–514, 2004.
- [173] G. Sperandeo, M. Sperandeo, M. Morcaldi, E. Caturelli, L. Dimitri, and A. Camagna. Transrectal ultrasonography for the early diagnosis of adenocarcinoma of the prostate: a new maneuver designed to improve the differentiation of malignant and benign lesions. *J Urol*, 169:607–610, 2003.
- [174] B. Ehdaie, E. Vertosick, M. Spaliviero, A. Giallo-Uvino, Y. Taur, M. O’Sullivan, J. Livingston, J. Eastham, P. Scardino, and K. Touijer. The impact of repeat biopsies on infectious complications in men with prostate cancer on active surveillance. *J Urol*, 191:660–664, 2014.
- [175] P. R. Martin, D. W. Cool, C. Romagnoli, A. Fenster, and A. D. Ward. Magnetic resonance imaging-targeted, 3D transrectal ultrasound-guided fusion biopsy for prostate cancer: Quantifying the impact of needle delivery error on diagnosis. *Med Phys*, 41:073504, 2014.
- [176] W. J. M. van de Ven, S. Rinsma, N. Karssemeijer, J. O. Barentsz, and H. J. Huisman. Electro-magnetic tracker-based fusion for image-guided TRUS prostate biopsy. In *European Congress of Radiology*, 2014.
- [177] W. J. M. van de Ven, J. P. M. Sedelaar, J. J. Fütterer, and H. J. Huisman. Focally targeted magnetic resonance imaging guided transrectal ultrasound biopsy of the prostate with an ultrasound machine that has electromagnetic tracking fusion. In *Annual Meeting of the Radiological Society of North America*, 2014.



Publications

Papers in international journals

W. J. M. van de Ven, W. Venderink, J. P. M. Sedelaar, J. Veltman, J. O. Barentsz, J. J. Fütterer, E. B. Cornel, and H. J. Huisman. MR targeted TRUS prostate biopsy using local reference augmentation – initial experience. *International Urology and Nephrology*, in press.

W. J. M. van de Ven, J. P. M. Sedelaar, M. M. G. van der Leest, C. A. Hulsbergen - van de Kaa, J. O. Barentsz, J. J. Fütterer, and H. J. Huisman. Visibility of prostate cancer on transrectal ultrasound during fusion with multiparametric magnetic resonance imaging for prostate biopsy. *Clinical Imaging*, 40(4):745–750, 2016.

W. J. M. van de Ven, Y. Hu, J. O. Barentsz, N. Karssemeijer, D. Barratt, and H. J. Huisman. Biomechanical modeling constrained surface-based image registration for prostate MR guided TRUS biopsy. *Medical Physics*, 42(5):2470–2481, 2015.

M. R. Pokorny, **W. J. M. van de Ven**, J. O. Barentsz, and L. C. Thompson. Reply to Yaalini Shanmugabavan, Stephanie Guillaumier and Hashim U. Ahmed's Letter to Editor re: Morgan R. Pokorny, Maarten de Rooij, Earl Duncan, et al. Prospective study of diagnostic accuracy comparing prostate cancer detection by transrectal ultrasound-guided biopsy versus magnetic resonance (MR) imaging with subsequent MR-guided biopsy in men without previous prostate biopsies. *Eur Urol* 2014;66:22-9. *European Urology*, 67(3):e54–e55, 2015.

G. J. S. Litjens, R. Toth, **W. J. M. van de Ven**, C. M. A. Hoeks, S. Kerkstra, B. van Ginneken, G. Vincent, G. Guillard, N. Birbeck, J. Zhang, R. Strand, F. Malmberg, Y. Ou, C. Davatzikos, M. Kirschner, F. Jung, J. Yuan, W. Qiu, Q. Gao, P. E. Edwards, B. Maan, F. van der Heijden, S. Ghose, J. Mitra, J. A. Dowling, D. Barratt, H. J. Huisman, and A. Madabhushi. Evaluation of prostate segmentation algorithms for MRI: the PROMISE12 challenge. *Medical Image Analysis*, 18(2):359–373, 2014.

W. J. M. van de Ven and J. O. Barentsz. Prostate cancer: MRI/US-guided biopsy – a viable alternative to TRUS-guidance. *Nature Reviews Urology*, 10(10):559–560, 2013.

W. J. M. van de Ven, C. A. Hulsbergen - van de Kaa, T. Hambroek, J. O. Barentsz, and H. J. Huisman. Simulated required accuracy of image registration tools for targeting high-grade cancer components with prostate biopsies. *European Radiology*, 23(5):1401–1407, 2013.

D. F. Stegeman, **W. J. M. van de Ven**, G. A. van Elswijk, R. Oostenveld, and B. U. Kleine. The α -motoneuron pool as transmitter of rhythmicities in cortical motor drive. *Clinical Neurophysiology*, 121(10):1633–1642, 2010.

Papers in conference proceedings

W. J. M. van de Ven, Y. Hu, N. Karssemeijer, J. O. Barentsz, D. Barratt, and H. J. Huisman. Surface-based prostate registration with biomechanical regularization. In *Medical Imaging: Image-Guided Procedures, Robotic Interventions, and Modeling*, volume 8671 of Proceedings of the SPIE, page 86711R, 2013.

G. J. S. Litjens, O. A. Debats, **W. J. M. van de Ven**, N. Karssemeijer, and H. J. Huisman. A pattern recognition approach to zonal segmentation of the prostate on MRI. In *Medical Image Computing and Computer-Assisted Intervention*, volume 7511 of Lecture Notes in Computer Science, pages 413–420, 2012.

W. J. M. van de Ven, G. J. S. Litjens, J. O. Barentsz, T. Hambrock, and H. J. Huisman. Required accuracy of MR-US registration for prostate biopsies. In *MICCAI Workshop: Prostate Cancer Imaging. Image Analysis and Image-Guided Interventions*, volume 6963 of Lecture Notes in Computer Science, pages 92–99, 2011.

Abstracts in conference proceedings

W. J. M. van de Ven, J. P. M. Sedelaar, J. J. Fütterer, and H. J. Huisman. Focally targeted magnetic resonance imaging guided transrectal ultrasound biopsy of the prostate with an ultrasound machine that has electromagnetic tracking fusion. In *Annual Meeting of the Radiological Society of North America*, 2014.

W. J. M. van de Ven, S. Rinsma, N. Karssemeijer, J. O. Barentsz, and H. J. Huisman. Electromagnetic tracker-based fusion for image-guided TRUS prostate biopsy. In *European Congress of Radiology*, 2014.

W. J. M. van de Ven, N. Karssemeijer, J. O. Barentsz, and H. J. Huisman. Image registration for prostate MR guided biopsy using automated biomechanical modeling. In *Annual Meeting of the Radiological Society of North America*, 2013.

W. J. M. van de Ven, J. -P. van Basten, B. J. de Kruif, P. Dunias, and F. P. Wieringa. In-vivo breed spectrum diffuse spectrometrie – een verkenning naar verbeteringen voor onderscheid van de neurovasculaire bundel tijdens robot-prostatectomie (RALP). In *Najaarsvergadering NVU*, volume 18, number 6 of Nederlands Tijdschrift voor Urologie, page 159, 2010.

W. J. M. van de Ven, B. U. Kleine, G. A. van Elswijk, R. Oostenveld, and D. F. Stegeman. The α -motoneuron pool as transmitter of rhythmicities in cortical motor drive. In *XVIII Congress of the International Society of Electrophysiology and Kinesiology*, 2010.

J. P. van Dijk, **W. J. M. van de Ven**, and D. F. Stegeman. Evaluating the motor unit number index (MUNIX) as a measure for motor unit loss. In *XVIII Congress of the International Society of Electrophysiology and Kinesiology*, 2010.

D. F. Stegeman, G. A. van Elswijk, **W. J. M. van de Ven**, and B. U. Kleine. The three frequencies: the α -motoneuron pool as transmitter of rhythmicities in cortico-spinal motor drive. In *International Workshop and Conference on Human Reflexes: Wiring and Firing of Motoneurons*, 2009.



Dankwoord

Als laatste wil ik graag iedereen bedanken die heeft geholpen bij het tot stand brengen van dit proefschrift. Een aantal van jullie wil ik persoonlijk noemen.

Dr. Huisman, beste Henkjan, als co-promotor ben jij degene geweest die de dagelijkse begeleiding gedurende mijn promotie op zich heeft genomen. Tijdens onze wekelijkse besprekingen hebben we vele discussies gehad en probeerde je me weer te prikkelen als ik even vastzat. Tussen alle ProCAD zaken en subsidie aanvragen had je gelukkig ook nog tijd om mijn artikelen kritisch te bekijken. Dit zorgde ervoor dat het net weer wat scherper op papier kwam. We hebben geleerd dat technici en klinici toch echt een andere blik hebben en dat de klinische artikelen een andere aanpak vereisen. Gelukkig zijn alle artikelen inmiddels geaccepteerd. Bedankt dat je achter me stond en in mijn promotie bent blijven geloven.

Prof. Karssemeijer, beste Nico, als promotor was je iets minder betrokken bij de dagelijkse begeleiding. Toch hebben we regelmatig besproken hoe het met mijn promotie ging. Jouw kennis en ervaring heeft me zeker verder geholpen, met name bij de technische verhalen. Jouw kritische blik liet me vaak weer kritisch nadenken over wat ik aan het doen was. Je bent specialist op het gebied van de mammografie, maar was ook altijd geïnteresseerd in mijn onderzoek. Ook wil ik je ontzettend bedanken voor je hulp en steun met de laatste loodjes.

Prof. Barentsz, beste Jelle, als tweede promotor heb jij ook een belangrijke rol gespeeld tijdens mijn promotie. Zonder jouw kennis en ervaring was dit proefschrift niet geweest zoals het nu is. Als expert op het gebied van de prostaat MRI wil jij altijd het beste voor de patiënt. Het was niet altijd makkelijk om je te overtuigen van het nut van MR-TRUS fusie. Ondanks dat je het vaak enorm druk had, nam je de toch de tijd om kritisch naar met name de klinische context van mijn artikelen te kijken. Je wist er vaak toch weer een paar details uit te pikken die nog niet helemaal klopte, waardoor het verhaal sterker werd. Bedankt voor je inbreng.

Beste Dr. Fütterer en Dr. Sedelaar, bedankt voor jullie hulp bij het opzetten van de klinische studie naar MR-TRUS fusie biopten. Jullie klinische ervaring was hierbij onmisbaar. Ook waardeer ik jullie snelle reacties op de artikelen waar we samen aan gewerkt hebben.

Beste Dr. Cornel en Dr. Veltman, jullie hebben ervoor gezorgd dat onze studie naar MR-TRUS fusie biopten werd uitgebreid naar het ZGT. Op deze manier hebben we er een multi-center studie van kunnen maken en hebben we de data wat sneller kunnen verzamelen. Bedankt voor jullie hulp en medewerking.

Wulphert, bedankt dat je mijn paranimf wilt zijn. Daarnaast ook bedankt voor de samenwerking tijdens de MR-TRUS fusie studie. Zonder jouw hulp was het voor mij een stuk moeilijker geworden om het laatste artikel van mijn proefschrift af te ronden. Ik wens je veel succes met de voortzetting van de fusie biopten.

Marloes, Christina en Thomas, als co-auteurs hebben jullie natuurlijk ook een belangrijke bijdrage geleverd aan dit proefschrift. Bedankt voor jullie medewerking en tijd.

Dean Barratt and Yipeng Hu, thank you for your collaboration and giving me the opportunity to visit UCL in London. Your experience in applying biomechanical modeling to MR-TRUS fusion helped me getting started. Thanks for your contribution to some of the papers in this thesis.

I would like to thank Toshiba for providing us with the newest ultrasound equipment. Special thanks to Dr. Christoph Simm, Tetsuya Yoshida, Richard Stavenuiter, Daniella de Bok, Fred Bijvoet, and Jan Arkesteijn for all their help and contributions related to the prostate ultrasound and fusion biopsies.

Geert en Oscar, binnen DIAG waren wij de enige promovendi op het gebied van de prostaat. We hadden te maken met dezelfde frustraties, maar delen gelukkig ook leuke dingen en zijn natuurlijk lange tijd kamergenoten geweest. Geert, bedankt dat je mijn paranimf wilt zijn. Daarnaast wil ik je, samen met Michael, Sven, en Sjoerd, bedanken voor de hulp met MeVisLab en ProCAD.

Ik wil ook graag alle andere leden van de prostaatwerkgroep bedanken voor de discussies tijdens onze tweewekelijkse bijeenkomst.

Gisèle, Esther en Siebren, bedankt dat jullie me hebben geholpen met het opnemen van de prostaat echo's.

Denise, bedankt voor je hulp met de prostaat echo's. Ook alle laboranten op de echo bedankt voor het vrij maken van de juiste echokamer als ik jullie weer eens tijdens een lunchpauze lastig kwam vallen.

Marijke en Manita, zonder jullie was het inplannen van de wetenschaps-echo's een stuk lastiger geweest.

Solange en Leonie, bedankt voor jullie hulp.

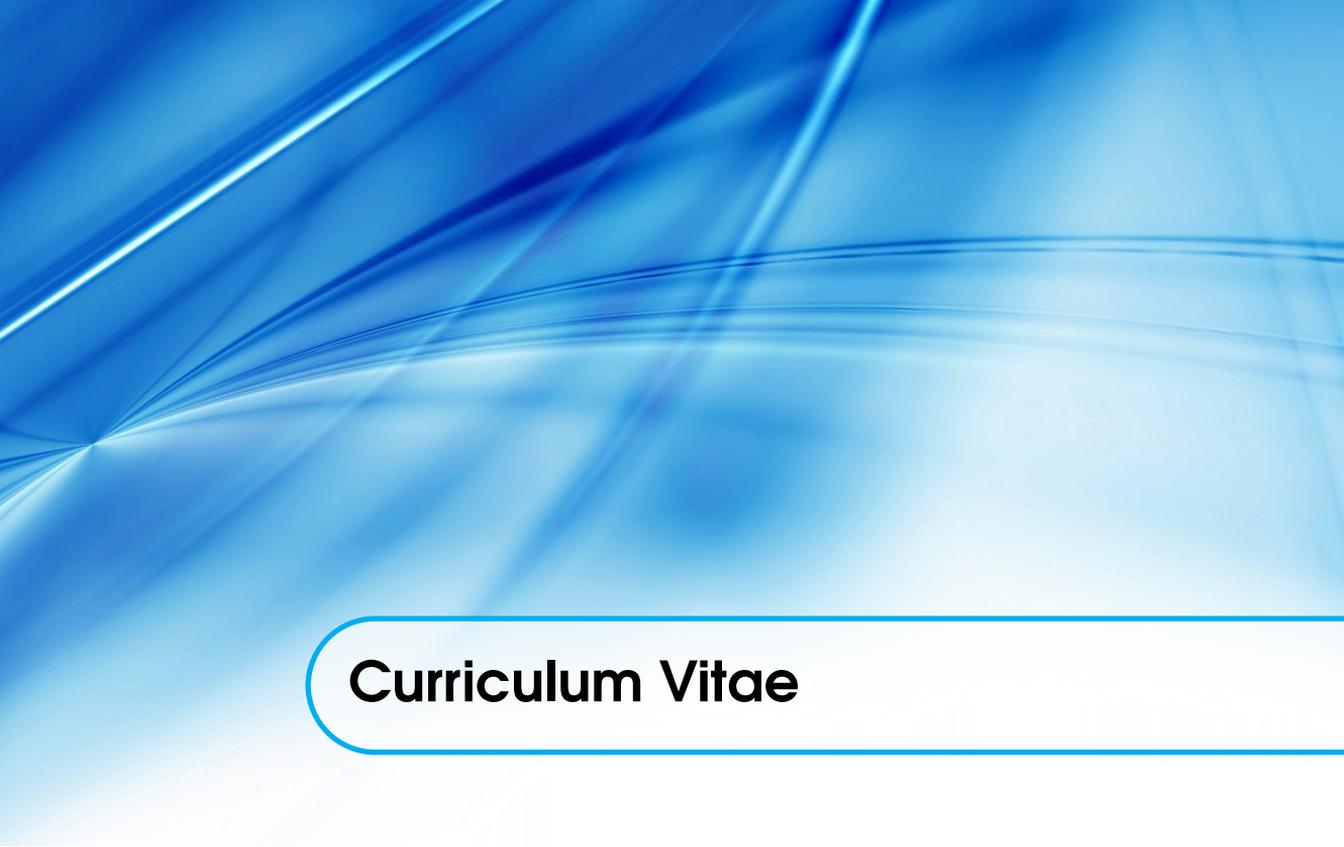
Daarnaast wil ik natuurlijk ook alle onderzoekers binnen DIAG bedanken. Het was een gezellige omgeving waar naast onderzoek ook ruimte was voor sociale en sportieve activiteiten. Met het DIAG team "Runtime error" hebben we meerdere malen aan de zevenheuvelenloop meegedaan. Ook de borrels, feestjes en natuurlijk de DIAG weekenden waren erg gezellig. De vroege vogels onder ons begonnen de dag goed met een lekkere kop koffie. De volgende namen mogen ook zeker niet ontbreken in dit dankwoord: Albert, Clarisa, Colin, Geert, Jan, Jan-Jurre, Leticia, Mark, Michiel, Oscar, Pragnya, Rashindra, Rick, Rieneke, Sarah en Steven, bedankt!

Rick, bedankt voor het ontwerpen van de kaft van mijn proefschrift.

Amy, ik ben blij om jou als zus te hebben. Vorig jaar heb je netjes je master behaald, iets waarop je heel trots kunt zijn. Inmiddels heb je ook een leuke baan als study director gevonden. Ik wens jou en Rick een mooie toekomst samen.

Lieve pap en mam, heel erg bedankt voor alles. Jullie hebben mij en Amy altijd gesteund en de mogelijkheid gegeven om te gaan studeren. Zonder jullie was ik nooit geweest waar ik nu ben.

Als laatste natuurlijk Bart. De laatste loodjes waren niet altijd even makkelijk, maar opgeven was geen optie. Het heeft wat langer geduurd dan gepland, maar nu is het boekje dan toch eindelijk af. Bedankt voor jouw steun en liefde. Ik hou van je!



Curriculum Vitae

Wendy van de Ven was born in Oss, The Netherlands, on June 3th 1987 and grew up in Heesch. She obtained her VWO diploma (pre-university education) from the Maaslandcollege in Oss in 2005. That same year she started studying Natural Sciences at the Radboud University in Nijmegen. She obtained her Bachelor of Science degree in 2008 and continued with the Master Natural Sciences, with a specialization in Biophysics. During her studies she performed a major research internship at the department of Neurology, Clinical Neurophysiology unit of the Radboud University Medical Center, Nijmegen. The project focussed on the transmission of cortical motor drive and motor unit loss. She finished her Master with a minor research internship at TNO Science and Industry, Medical in Eindhoven. There she worked on in vivo differentiation of the prostate capsule from the neurovascular bundles by diffuse reflectance spectrometry. In August 2010, she graduated cum laude and obtained the Master of Science degree.



Wendy started her PhD project at the Diagnostic Image Analysis Group (DIAG) of the department of Radiology and Nuclear Medicine, Radboud University Medical Center, Nijmegen in November 2010. Her research was about MR-TRUS fusion for prostate biopsies. Both technical and clinical requirements have been investigated. Part of the project was in collaboration with the Centre for Medical Image Computing at University College London, which she visited during her PhD. The results of her PhD research are described in this thesis.

From November 2014, Wendy continued working in DIAG as a project leader on an international multicenter clinical trial regarding MR-TRUS fusion prostate biopsies. The project was in collaboration with Toshiba Medical Systems. The main objective was to determine the clinical effectiveness of MR guided TRUS biopsies in comparison with in-bore MR guided biopsies.

Wendy is employed at ASML in Eindhoven since March 2015. There she is working as a design engineer on on-product overlay at the Applications department.

